NTNU
Norwegian University of
Science and Technology

Iron Uptake in the Cyanobacteria Synechococcus sp. PCC7002

Erland Årstøl

Biotechnology
Submission date: January 2017
Supervisor: Martin Frank Hohmann-Marriott, IBT

Norwegian University of Science and Technology
Department of Biotechnology and Food Science

Abstract

Cyanobacteria are important primary producers in marine and freshwater-environments. Their photosynthetic apparatus requires a relatively large amount of iron, and growth has been shown to be limited by iron availability in certain areas, particularly in southern oceans.

In this thesis I have examined genes related to iron uptake in the marine cyanobacterial model organism *Synechococcus sp. PCC 7002.* This organism has seen increased popularity as a model organism in recent years, but little work has been done on the mechanisms behind iron uptake.

Prior work has shown that Synechococcus 7002 produces siderophores, low-molecular weight molecules with high affinity for iron. I used sequence information to propose a biosynthetic pathway for synechobactin, the siderophore produced by *Synechococcus 7002*. Two of the genes in the siderophore-operon, coding for a transporter (*sidF*) and an esterase/lipase (*sidH*) were chosen for further analysis through the creation of deletion mutants. The mutants were characterized by growth studies and absorption spectra. Additionally, the chromeazurol S-assay was used to check the spread of siderophores in solid media. ΔSidH showed increased spread of siderophores compared to the wild type, a result that supports *sidH*'s hypothesized role in attaching fatty acid tails on synechobactin, thereby anchoring the siderophores in the cell membrane. The results for ΔSidF are more uncertain, with a phenotype similar to ΔSidH, most likely due to downstream effects of the deletion mutation. Growth studies and absorption spectra support the role of the genes in iron uptake.

Cytochrome C_M is potentially involved in pili-mediated iron reduction, converting insoluble Fe(III) to bio-available Fe(II). A deletion mutant was characterized by growth studies and whole cell absorption spectra, showing a clear phenotypic difference from the wildtype when cultured at both iron-replete conditions and under iron stress. While the data appears to support a role in iron uptake, the phenotypic response of the deletion mutant under iron-replete conditions indicates a complex role in Fe(III)-reduction.

The FutABC-transporter has a role in the uptake of Fe(III) in the model organism *Synechocystis 6803*, but its role in *Synechococcus 7002* is not clear. Growth studies and absorption spectra of a *futB* deletion mutant showed slower growth and lower pigment production than the wild type when grown under iron limitation. However, as similar

phenotypic responses were observed for growth both under Fe(III) and Fe(II), the exact role of FutABC in Synechococcus 7002 remains uncertain.

Sammendrag

Cyanobakterier (blågrønnbakterier) er viktige primærprodusenter i marine- og ferskvanns-miljøer. Deres fotosyntetiske apparat krever relativt store mengder jern. Cyanobakteriers vekst har vist seg å være jern-begrenset i visse områder, spesielt i sørlige hav.

I denne oppgaven har jeg undersøkt et knippe gener relatert til jernopptak i den marine modellorganismen *Synechococcus sp. Strain PCC 7002*. Denne organismen har økt i popularitet som modellorganisme de siste årene, men lite arbeid har blitt gjort på mekanismene bak jernopptak.

Tidligere arbeid har påvist at *Synechococcus 7002* produserer sideroforer, små molekyler med høy affinitet til jern. I denne oppgaven brukte jeg database-informasjon om sekvenshomologi til å foreslå en modell av biosyntesen til synechobactin, sideroforen *Synechococcus 7002* produserer. To av genene i siderofor-operonet, som koder for en transporter (*sidF)* og en esterase/lipase (*sidH)*, ble utvalgt for skapelsen av delesjonsmutanter. Disse ble brukt i vekstudier og absorpsjonspektra, samt brukt i overlegg-kromazurol S-assayet, hvor spredningen av sideroforer i fast medium kan analyseres. Delesjonsmutanten Δ*SidH* ga økt siderofor-spredning sammenlignet med villtype. Resulatet støtter hypotesen om at SidH er involvert i å sette fettsyrehaler på synechobactin, som forankrer sideroforene til cellemembranen. Resultatene var mer tvetydige for ΔSidF, hvor fenotypen var nær identisk med ΔSidH, mest sannsynlig grunnet nedstrømseffekter av delesjonen. Vekststudier og absorpsjonsspekter understøtter hypotesen om genenes rolle i jernopptak.

Cytokromet C_M ble undersøkt for en potensiell rolle i reduktivt jernopptak gjennom reduksjon av Fe(III) til Fe(II). En delesjonsmutant ble undersøkt ved vekststudier og full-celle absorpsjonsspektra under ulike jernforhold, og viser svekket vekst og pigmentproduksjon under vekst med og uten jern tilgjengelig. Resultatene støtter en rolle i jernopptak, men det fenotypiske avviket fra WT under jernrike forhold gjør denne konklusjonen usikker.

FutABC-transporteren har en rolle i opptak av Fe(III) i modellorganismen *Synechocystis 6803*, men transporterens rolle i *Synechococcus 7002* har ikke tidligere blitt undersøkt. Vekststudier viste saktere vekst enn villtype når en delesjonsmutant av *futB* ble kultivert under jernmangel. Dette resultatet gjaldt for vekst på både Fe(III) og Fe(II), et resultat som gjør at FutABCs rolle fortsatt er uavklart.

Acknowledgements

I would like to thank associate professor Martin F. Hohmann-Marriott for excellent supervision, guidance and encouragement during the project. PhD candidate Anne Ilse Maria Vogel has helped immensely with the laboratory work, and has been an invaluable sparring partner for both data analysis and the writing of this thesis. Their guidance has made working on the thesis both inspiring and enjoyable.

The assistance of professor emeritus Thor Bernt Melø was essential for conducting whole cell absorption spectra. His charitable guidance of someone who he had no obligation to help was much appreciated.

Working in the lab is social work. I'd like to thank Osasumwen Egharevba, Rahmi Lale, Gunvor Røkke, Jake Lamb, Anna Lødeng, Merethe Christensen Vadseth and all the members of the PhotoSynLab for being good company, as well as for assistance with various minor issues.

My deepest gratitude goes to Amanda Roland. She has patiently endured my rather unintelligible talk about "how green the circles are" and my evening excursions to take images. Her moral support and efforts to keep me motivated has been invaluable.

Table of contents

List of figures

List of tables

1 Introduction

Cyanobacteria are important primary producers in marine and freshwater environments. In addition to their ecological role, they have garnered interest as potentially useful for production of fine chemicals and biofuels. Model organisms for cyanobacteria have emerged that are capable of genetic transformation, in addition to having high biomass production from sunlight compared to plants (Lau et al. 2015).

Since 1990, the impact of iron concentrations for primary productivity in oceans has been intensely discussed. Martin's (1990) iron hypothesis posits that low availability of iron limits productivity in the oceans of the southern hemisphere. As a result of Martin's hypothesis, the artificial introduction of iron in marine environments has emerged as a possible way to alleviate climate change by sequestering carbon dioxide. The photosynthetic apparatus of cyanobacteria requires iron, rendering them iron hungry. Their iron uptake mechanisms therefore have implications both ecologically and for biotechnological applications.

In this master's thesis, I will explore the mechanics of iron uptake in the marine cyanobacteria *Synechococcus elongatus 7002 sp (*hereafter *Synechococcus 7002).* Fast doubling times and ease of transformation has made this species an increasingly popular model organism. It also holds relevance ecologically as it and close genetic relatives such as *Prochlorococcus* are significant global primary producers. Iron uptake in *Synechococcus 7002* has been little studied, and a model of iron uptake is yet to emerge. Clues to the genes involved can be garnered from what is known for the close genetic relative and model organism *Synechocystis sp. PCC6803 (*hereafter *Synechocystis 6803)* (Kranzler et al. 2012). However, *Synechocystis 6803* cannot produce siderophores, low-molecular weight iron chelators used in iron uptake in *Synechococcus 7002,* rendering such a comparison incomplete.

1.1 Goals of this thesis

The genetic basis of siderophore production in *Synechococcus* 7002 has not been previously explored, and will be a focus of this thesis. Using the available sequence data and bioinformatic analysis, I will propose a biosynthetic pathway for the production of siderophores in *Synechococcus 7002*. Two of the genes in the siderophore operon, a transporter and an esterase/lipase (*sidF* and *sidH)*, will be characterized through the creation

of deletion mutants. In addition to growth studies and whole cell absorption spectra, use of the overlay chrome azurol S-assay (O-CAS) will allow testing the function of the two mutants.

Besides the siderophore mutants, two additional genes thought to be used in iron uptake was chosen for study.

1. Cytochrome C_M is potentially involved in pilin-mediated iron reduction in *Synechococcus 7002*. While the physical properties of C_M fit the characteristics needed for iron reduction, this role has not been experimentally tested.
2. *futB* is thought to code for part of the FutABC Fe(III)-transporter in *Synechocystis 6803*, but the importance of this uptake mechanism has not been explored in *Synechococcus 7002*.

Using growth studies and whole cell absorption spectra on deletion mutants for these two genes, clues to their function can be garnered.

1.2 Structure of this thesis

This thesis investigates the role of four genes that are thought to be involved in different mechanisms of iron utilization in cyanobacteria. I will first give background information on *Synechococcus 7002* and the biological uptake of iron. I will then then detail the available research on *Synechococcus 7002* iron uptake, and present a bioinformatic analysis of the siderophore biosynthesis operon. From bioinformatic work and previous work, I will select four genes and state experimental research goals for each of them separately. The methods, results and discussion sections that follows will primarily be separated by experiment type (growth study, absorption spectra and O-CAS assay), and only secondarily separated by gene investigated. This solution, while pragmatic in terms of thesis structure, leads to the discussion of each gene to be discontinuous. I will therefore discuss the experimental data and highlight the impact of the findings for each gene separately in the conclusion section.

2 Background

In this chapter I will give background information concerning *Synechococcus 7002*, and the implications of the chemistry and ecology of iron for biological iron uptake. I will then present what is known about iron uptake in *Synechococcus 7002.* Siderophores will be described briefly as part of the ecology of iron in marine environments, but details of siderophore production in *Synechococcus 7002* will be considered separately in chapter 3.

2.1 The Cyanobacteria *Synechococcus* 7002

Synechococcus 7002 is an unicellular, euryhaline cyanobacteria that has in recent years been increasingly popular as a model organism for cyanobacteria (Ludwig and Bryant 2012). It has rapid doubling times (~6 hours) and natural transformability, as well as tolerance for high-light irradiation and high salt concentrations (Batterton and Van Baalen 1971; Nomura, Sakamoto, and Bryant 2006). The *Synechococcus 7002* genome has been sequenced and is publicly available (see http://www.ncbi.nlm.nih.gov/), but has not been fully annotated. Molecular techniques have been developed to enable high-level expression of endogenous proteins (Xu et al. 2011), making *Synechococcus* 7002 an attractive target for biotechnology applications.

Synechococcus 7002 was originally isolated from a mud sample in a Puerto Rico-fishery. The environment *Synechococcus 7002* was extracted from show variation in light intensity, temperature, nutrient availability and salinity (Ludwig and Bryant 2012b), indicating some flexibility for growth conditions. *Synechococcus 7002* has significant genetic homology and physiological similarities with the freshwater cyanobacteria model organism *Synechocystis 6803,* which allows inferring some genetic and functional relationships from research conducted on this organism.

Synechococcus 7002 grows photolithoautotrophically, gaining electrons from inorganic sources, carbon from CO_2, and energy from light (Ludwig and Bryant 2012b). It also has the capacity to grow on glycerol instead of CO_2 (Lambert and Stevens 1986). Cyanobacteria, including *Synechococcus 7002,* require an unusually high amount of iron, roughly ten-fold of non-photosynthetic prokaryotes, due to their photosynthetic apparatus containing many Fe-S proteins and cytochromes (Kranzler et al. 2012).

2.2 Iron in a biological context

2.2.1 Forms of iron

While iron is one of the most abundant elements on earth, the amount of bioavailable iron in marine environments is severely limited. In aqueous solutions, there are two relevant oxidation states, ferrous (Fe(II)) and ferric (Fe(III)) iron. Fe(II) is soluble at circumneutral pH, and is the preferred state for biological uptake. However, Fe(II) rapidly undergoes oxidation to Fe(III) in the presence of oxygen at circumneutral pH. Fe(III) is insoluble, and thus has significantly lower bioavailability (Saha et al. 2013). The consequence of the reactivity of free irons is that dissolved Fe-concentrations are low. Marine environments have concentrations of dissolved iron in the nano- to picomolar range (Kranzler et al. 2012).

Fe(III) can exist in several different forms. It precipitates as insoluble ferric oxyhydroxides, which has low bioavailability for microbes. Ferric iron can be kept soluble and bioavailable by complexation with organic molecules. This complexed form constitutes 99% of soluble Fe(III) in ocean and freshwater environments. These iron-binding organic molecules form two classes, L1 and L2. The L1 class binds strongly to Fe(III), and is thought be composed of siderophores, Fe-specific chelators (Kranzler et al. 2012). The L2 class has weaker binding to iron, and is thought to consist of degraded cellular debris with only incidental metal-binding qualities, forming a “ligand soup” in the upper layers of the oceans (Hunter and Boyd 2007).

2.2.2 Ecology of iron

For phytoplankton in general, iron requirements are 4-6 orders of magnitude higher than the extracellular environment, necessitating large energetic investments (Shaked and Lis 2012). The high iron requirements of phytoplankton lead to “the iron hypothesis” of John H. Martin (1990), suggesting that the productivity of southern oceans is limited by low availability of iron in many areas. Such areas, termed high-nitrate low-chlorophyll (HNLC) have lower productivity than might be expected from the level of other nutrients. Experiments with iron enrichment of HNLC-areas has shown significant increases in short term phytoplankton growth, but whether this constitutes a feasible method for long term carbon sequestration is not clear (Williamson et al. 2012).

2.2.3 Siderophores

Siderophores are biologically produced low-molecular weight (400-100kDA) compounds with high affinity for iron. They are excreted by a wide range of microbes under iron-limiting

conditions, enabling uptake of normally non-available Fe(III). Siderophores come in three different classes depending on the moiety that donates oxygen ligands: The catecholates, hydroxymates and mixed types (Saha et al. 2013). Siderophores are generally water-soluble and are, with a few lipid-bound exceptions, excreted into the environment. Each siderophore-producing organism may only produce one specific siderophore or a small number of different siderophores. However, many organisms have the potential to make use of xenosiderophores, siderophores synthesized by other microorganisms (Miethke and Marahiel 2007).

2.3 Synechococcus 7002 iron uptake

Iron uptake in *Synechococcus 7002* is currently little explored, and a full model of different iron uptake mechanisms is yet to emerge. In this subchapter, I will first consider what is known about regulation of iron uptake, and consider recent discoveries about the role of pili in reductive iron uptake. Furthermore, I will split the iron uptake mechanisms in play for *Synechococcus 7002* in two: Mechanisms that do or do not involve the production of siderophores. A comparison between *Synechococcus 7002* and *Synechocystis 6803* allows inferring some important iron uptake genes for non-siderophore mediated iron uptake. Details of siderophore production will be considered in chapter 3.

2.3.1 Regulation of iron homoestasis

High iron requirements for the photosynthetic apparatus renders the regulation of iron homoestasis crucial in cyanobacteria. Ferric uptake regulators (Fur) are the primary mechanism for regulation of iron uptake in cyanobacteria. These regulators are homodimers with both metal and DNA-binding sites that primarily act as transcriptional repressors when their metallic co-repressors are bound. Despite the name, many Fur-type repressors are involved with other conditions, such as oxidative stress (Ludwig et al. 2015). Fur-s can interact with a large number of genes and operons, ensuring a global response to varying iron levels. While Fur-type proteins for the most part act as repressors, they have also been shown to activate genes. In all, Fur-regulation ensures a response that varies from inducing iron uptake functions under iron limited conditions, to enabling iron storage mechanisms and utilizing iron-dependent proteins under conditions of sufficient iron (Lee and Helmann 2007).

In the *Synechococcus 7002* genome three *fur*-type genes exist. Transcription data of knockout mutants indicates that only one of them, SynPCC7002_A1649 (*fur)*, is involved in

upregulation of iron uptake-genes under iron deprivation (Ludwig et al. 2015). Transcriptome analysis of deletion mutants for *fur* shows significant upregulation of genes pertaining to biosynthesis of siderophores, Fe-transporters and non-Fe-utilizing variants of proteins.

The *fur*-knockout result is in agreement with a comparison of transcriptome levels between iron-limited and iron-replete growth of *Synechococcus 7002*, (Ludwig and Bryant 2012a), implicating *fur* as the main regulator of iron homeostasis in *Synechococcus 7002.*

In the laboratory environment, *Synechococcus 7002* is unlikely to experience iron deprivation unless this is explicitly intended by the researcher. However, conditions in marine environments have iron concentrations well below the ideal iron availability of *Synechococcus 7002*, meaning some degree of iron starvation is the norm. This means that Fur-proteins most of the time do not repress expression of iron-uptake genes, as iron levels are presumably low enough to warrant high-level production of iron-uptake proteins.

While growth rates have been shown to decrease under lowered iron concentration (Liu and Qiu 2012), the exact nature of the relationship between iron and growth is not clear. Previous work shows a significant increase in growth rates at certain low-level iron concentrations, and only a limited correlation between extracellular and intracellular iron levels (Wilhelm, Maxwell, and Trick 1996).

2.3.2 The role of pili in reductive iron uptake

Pili are hair-like appendages on the exterior of bacteria that have been implicated in iron uptake. The existence of electrically conducive pili that can reduce extracellular Fe(III)-oxides has been shown in several bacteria, and consequently pili are often called biological nanowire. *Synechocystis 6803* deletion mutants lacking the structural pili-gene *pilA1* show significantly reduced growth on iron oxides (Lamb et al. 2014). While there is experimental evidence for extracellular reduction of iron, the mechanism and components involved in this process remains unknown (Kranzler et al. 2011). *Synechococcus 7002* has genes appearing to code for structural pilin-protein. The role of *Synechococcus 7002's* homologue for the PilA1-gene in *Synechocystis 6803* is currently being investigated.

While the details of pili-mediated iron reduction are unknown, a hypothesis can be formed based on what is known of iron reduction processes in other organisms. Electrons used in the reduction of Fe(III) to Fe(II) stems from the bacterial metabolism. For model organisms such as *Geobacter* and *Schewanella*, that also have conductive pili, the electrons have been shown

to travel through the inner membrane and periplasm on a series of cytochromes with overlapping midpoint potentials (Bird, Bonnefoy, and Newman 2011).

A similar chain of cytochromes and other electron carriers can be hypothesized for *Synechococcus 7002* and *Synechocystis 6803*. Cytochrome C_M (herafter C_M) has been shown to undergo a one-electron redox reaction, with a midpoint potential at 151 ± 5 mV (Cho, Pakrasi, and Whitmarsh 2000). While a defined role in an electron transport chain is yet to be found for C_M, this midpoint potential would be suitable for reduction of Fe(III) to Fe(II). C_M in *Synechococcus 7002* has a 40,6% sequence similarity to the gene sll1359 in Synechocystis 6803, which show pilin characteristics (Lamb et al. 2014). C_M is also strongly upregulated by a factor of 20 under iron limitation conditions (Ludwig and Bryant 2012a). In sum, these factors make C_M a promising candidate to explore further for involvement in pili mediated iron reduction.

2.3.3 Lessons from *Synechocystis 6803* iron uptake*:* The futABC-transporter

Due to the small number of studies on iron uptake in *Synechococcus 7002*, considering the work done on the close genetic relative *Synechocystis 6803* is useful. I will give a short overview of this work, highlighting known differences between the two organisms. Crucially, *Synechocystis 6803* does not have genes for the biosynthesis of siderophores, which appear to play an important role in *Synechococcus 7002* iron uptake.

Kranzler et al. (2014) highlights reductive iron uptake as the most important mechanism for iron uptake in *Synechocystis 6803.* They suggest a model where, after transport through the outer membrane, Fe(III) is bound to the perisplasmic protein FutA2. From there, a still unidentified oxidase (ARTO) is involved in iron reduction, before Fe(II) is transported through the plasma membrane by the FeoB-transporter. In addition to this, the FutABC-transporter-complex is involved in the direct transport of Fe(III) through the plasma membrane. The relatively recent discovery of nanowires in *Synechocystis 6803* is not included in the model: How the nanowires eventually interacts with the components described by Kranzler et al. (2014) is not clear.

Work by Katoh et al. (2001) holds that the FutABC-transporter in *Synechocystis 6803* is composed of four parts forming an ABC-type transporter for Fe(III): The two periplasmic proteins FutA1 and FutA2, and the permease proteins FutB and FutC. Based on the similarity of deletion mutant phenotypes, it is likely that FutB and FutC are two parts of a transporter

protein. These deletion mutants show drastically lower Fe(III) uptake rates, with Fe(II) uptakes remaining at similar levels to the wild type.

The model described by Kranzler places heavy emphasis on the FeoB-protein as a transporter of Fe(II). However, there does not appear to be a homologous protein to FeoB in *Synechococcus 7002.* It is uncertain whether there is a separate Fe(II)-transporter in *Synechococcus 7002*, as it is a possibility that the production of siderophores renders such a Fe(II)-transport mechanism redundant.

The role and relative importance of the FutABC-transporter in *Synechococcus 7002*, a siderophore producing bacteria, is not yet established. Siderophores can bind Fe(III), and could conceivably facilitate iron uptake without need for the FutABC-transporter. The sequence homology for the four *FutABC-genes* between *Synechocystis 6803* and *Synechococcus 7002 r*anges between 52% and 65%. Whether FutBAC has a novel role or is part of a redundancy-mechanism for iron uptake is unknown. The genes for the *Synechococcus 7002* homologues for *FutABC* are upregulated under iron limitation. In *Synechococcus 7002, futA* and *futB* are upregulated respectively 8.13 and 8.63 times more than under iron-replete conditions, while *fuTB* is upregulated 1.55 times more (Ludwig and Bryant 2012a). The same relationship in terms of upregulation exists in *Synechocystis 6803* (Hernández-Prieto et al. 2012). It is unexpected that *futB* and *futC* appear not to be upregulated at the same rate under iron limitation, since they have been suggested to work as dimers. The error margins of the method used for *Synechococcus 7002* ensure that the authors recommend only considering transcription level difference of two-fold or more as significant (Ludwig and Bryant 2011), making it uncertain whether *futB* is upregulated at all. Deletion of *futB* seems make an ideal probe for exploring this topic, as it codes for the permease part of the FutABC-transporter. Without the permease subunit, the transporter as a whole should be nonfunctional.

2.3.4 Pigment production under iron stress in *Synechococcus 7002*

While a full overview of the pigments in *Synechococcus 7002* is beyond the scope of this thesis, it is worthwhile to consider how iron limitation influences the production of pigments. *Synechococcus 7002* produces a wide variety of different pigments, including chlorophyll a, phycobilins (Alvey et al. 2011) and the carotenoids β-carotene and six xanthophyll carotenoids (Zhu et al. 2010).

For cyanobacterial pigments in general, iron stress mainly influences photosystem I (PSI), which contains three iron-sulfur clusters. Iron stress can thus cause a reduction in PSI/PSII ratio, which may lead to oxidative damage due to the inability of PSI to handle the stream of electrons generated by photosystem II (PSII). This is counteracted by the induction of the protein isiA, which complexes with PSI and improves the light harvesting capability. This increased activity of PSI reduces the excitation pressure on PSII, and thus serves to reduce oxidative damage (La Rocca, Moro, and Rascio 2016).

In *Synechococcus sp. PCC 7942,* iron limitation is found to cause the induction of the isiA protein, which is associated with an increase in the relative amounts carotenoids compared to other pigments. IsiA likely has a carotenoid binding role, and works in a photoprotective manner (Ivanov et al. 2007). The increased ratio of carotenoids to chlorophyll can be used as an indicator of cell stress in cyanobacteria by measuring absorbance at 435nm (which is mainly composed of overlapping chlorophyll a and carotenoid absorption), and the absorbance peak at 680 nm which is contributed almost exclusively by chlorophyll a (Lamb et al. 2014).

3 Siderophores in *Synechococcus* 7002

In this chapter I will first briefly describe the work that has been done on characterizing the chemical properties of siderophores in *Synechococcus 7002*. I will then use sequence and transcription data to analyze the operon responsible for biosynthesis of siderophores. This will culminate in a proposed biosynthetic pathway for siderophores production, where two genes involved will be highlighted for further experimental study.

Under iron-limiting conditions *Synechococcus* 7002 produces three different amphiphilic siderophores, first discovered by Armstrong and Van Baalen (1979). These were later named synechobactin A-C, and determined to be hydroxamate-type siderophores, shown in figure 1. They are composed of a citric acid backbone connecting to a fatty acid tail by the second α-hydroxymate group on one side. The length of the fatty acid tail varies for the different types of synechobactin, and is presumed to enhance their affinity for the bacterial membrane (Ito and Butler 2005). While Ito and Butler described synechobactin A, B and C with fatty acid tails of $C_{12,}$ C_{10} and C_8 respectively, recent mass spectrometry work on *Synechococcus 7002* grown under iron limitation (Boiteau and Repeta 2015) show additional synechobactin molecules with side chain length of 11, 13 and 14 carbons. However, these variants seem to be less common, as they gave weaker mass spectrometry peaks. The variability in fatty acid chain length indicates a level of flexibility in the incorporation of fatty-acid tails, with a preference for even-numbered substrates.

Like many other Fe(III)-chelators, the Fe(III)-Synechobactin-complex appears to be photoreactive. Exposing Fe(III)-synechobactin A to light results in decarboxylation of the citrate group to a 3-ketoglutarate, while the iron remains bound to the siderophore (Ito and Butler 2005). Siderophores from other bacteria have been shown to take advantage of photoreduction to reduce Fe(III) to Fe(II) (Passananti et al. 2016; Barbeau et al. 2002), making this a likely mechanism for Fe(III)-reduction in *Synechococcus 7002.*

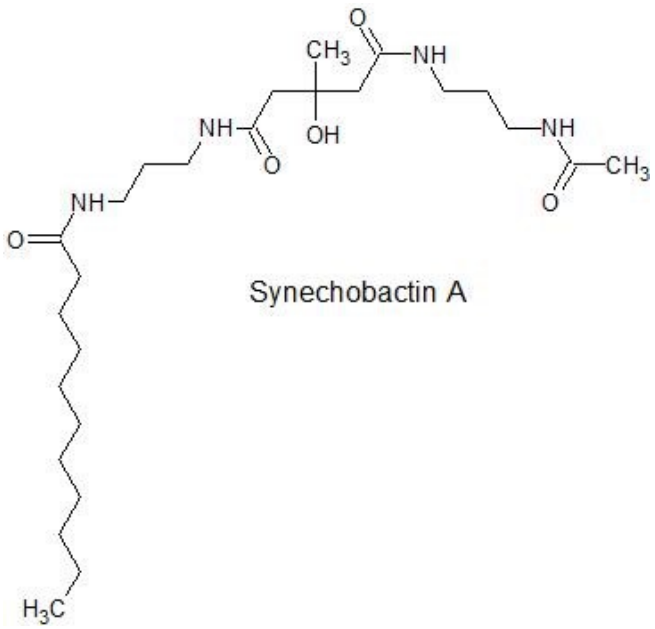

Figure 1: Structure of Synechobactin A, a citrate based molecule bound to two 1,3-diaminopropanes, with a fatty-acid moiety on one side. Synechobactin B, C, and other variants differ only in the length of this fatty acid moiety.

3.1.1 The siderophore operon in *Synechococcus 7002*

Literature search reveals that little work has been done on the genetic roots of biosynthesis of siderophores in *Synechococcus 7002*, with the annotation in Cyanobase (Fujisawa et al. 2014) of the genes involved coming from sequence homology and automated protein structure prediction.

There is a predicted operon on *Synechococcus 7002*'s pAQ7 plasmid, containing 8 genes presumably related to siderophore biosynthesis, shown in table 1. The role of this operon has been confirmed in unpublished work according to Balasubramanian et al. (2006). The genes, ranging from sidA to sidH (SYNPCC7002_G0025 to SYNPCC7002-G0018), are coregulated, and are predicted to have various functions in siderophore biosynthesis. Two different transcriptome analyses, one with deletion of the iron homeostasis regulator *fur* and one for iron limitation, indicate that these proteins are coregulated under Fe-limited conditions (Ludwig and Bryant 2012a; Ludwig et al. 2015).

Table 1: An overview of the genes in the siderophore operon and their presumptive functions. The information available is from Cyanobase, which bases the annotations on sequence homology and protein function prediction.

Gene	**Annotation**	**Extra annotation in cyanobase**
G0025 – SidA	2,4-diaminobutyrate 4-transaminase	
G0024 – SidB	L-2,4-diaminobutyrate decarboxylase	SidB
G0023 – SidC	Siderophore biosynthesis protein	
G0022 – SidD	Siderophore biosynthesis protein	IucB family – acetyl transferase
G0021 – SidE	siderophore biosynthesis protein	N-monooxygenase
G0020 – SidF	Mayor facilitator transport protein	
G0019 – SidG	Siderophore biosynthesis protein	IucA / IucC family
G0018 – SidH	Esterase/lipase	

3.1.2 Transcription levels in the siderophore operon

Microarray data from Ludwig and Bryant (2012a) give some insight into the regulation of the siderophore operon in *Synechococcus 7002*. Under iron deprived conditions, all 8 genes of the siderophore-operon are significantly upregulated. However, the degree of upregulation varies widely, as seen in table 2: The genes are close to the start of transcription are significantly more upregulated than the latter genes, as has been found to be the case for polycistronic operons (Lim, Lee, and Hussein 2011).

Table 2: Degree of upregulation under iron deprivation compared to standard conditions for genes in the siderophore operon, taken from Ludwig and Bryant (2012a).

Gene	Degree of upregulation
G0025 – SidA	284.05
G0024 – SidB	128.39
G0023 – SidC	151.72
G0022 – SidD	106.94
G0021 – SidE	91.89
G0020 – SidF	82.04
G0019 – SidG	54.48
G0018 – SidH	35.00

3.2 Bioinformatic dissection of siderophore synthesis in *Synechococcus 7002*

The annotation of the siderophores genes shown in table 1, in combination with knowledge of the biosynthesis of siderophores in other bacteria, allows making some hypotheses on the biosynthetic pathway of synechobactin. Biosynthesis of siderophores can be divided into polypeptides produced by nonribosomal peptide synthases (RPS) and those made by assembly of variants of amino acid-based diamides and dicarboxyl or tricarboxylic acids (Challis 2005). Based on the structure of synechobactin, it falls into the group of amino acid-based siderophores. Variants of this biosynthetic route have been described in a wide array of bacteria. One of them is in rhizobactin 1021, produced by the rhizobium *Sinorhizobium meliloti.* The structure of rhizobactin 1021 is very similar to the synechobactins, differing only by the type of fatty acid residue. Lynch et al. (2001) propose a biosynthetic pathway of rhizobactin 1021, based on sequence similarity to the well-established biosynthetic pathway for aerobactin, produced by *Escherichia coli*. The rhizobactin 1021 is hypothesized to be made by combining two 1,3-diaminopropane-molecules with citrate in a series of steps. The molecule 1,3-diaminopropane is itself synthesized from glutamic acid and aspartic B-semialdehyde. The final addition of the fatty acid moiety is done by a yet unknown mechanism.

Based on sequence homology and the annotation of genes in the *Synechococcus 7002* siderophore-operon, I hypothesize that synechobactin is made by essentially the same mechanism (figure 2) as has been proposed for rhizobactin 1021:

1. One carboxyl-group on glutamic acid is replaced by an amine group from aspartic-B-semialdehyde. Thus, L-2,4-diaminobutyric acid is produced along with 2-ketoglutaric acid. SidA is inferred from homology to be a 2,4-diaminobutyrate 4-transaminase, making it a reasonable candidate enzyme for this step.
2. Catalyzed by SidB, L-2,4-diaminobutyric acid loses a carboxyl group, releasing a CO_2-molecule, and producing 1,3-diaminopropane. SidB is annotated as, and has homology with L-2,4-diaminobutyrate decarboxylases (DABA decarboxylases) of other organisms, which have been shown to catalyze this reaction in other species (Nakao et al. 1990).

3. A hydroxyl-group is incorporated onto one of the amine groups of 1,3-diaminopropane, resulting in N^4-hydroxy-1-aminopropane. This reaction is presumably catalyzed by SidE, which is annotated as an N-monooxygenase.
4. An acetyl-group from acetyl-CoA is incorporated into the hydroxygenated amine group of N^4-hydroxy-1-aminopropane, resulting in N^4-acetyl-N^4-hydroxy-1-aminopropane. This reaction is catalyzed by SidD. SidD has a conserved AlcB-domain, present in a wide range of proteins predicted to have acetyl-transferase-activity.
5. One N^4-acetyl-N^4-hydroxy-1-aminopropane binds to citrate, replacing one of the two hydroxyl-moieties of the citrate molecule.
6. Another N^4-acetyl-N^4-hydroxy-1-aminopropane binds to the citrate molecule, replacing the remaining hydroxyl-moiety. This creates the molecule known as schizokinen, which is used as a siderophore in other bacteria. Mass spectrometry has shown low concentrations of schizokinen in *Synechococcus 7002* in early growth phases, indicating that it is indeed part of the pathway (Boiteau and Repeta 2015). It is possible that step 5 and 6 is catalyzed by SidG and SidC. SidC has a IucA/IucC-domain, while SidG is annotated as a IucA- /IucC-family protein. The proteins IucA and IucC has been shown to catalyze the incorporation of N-acetyl-N-hydroxylysine to citrate in aerobactin synthesis (de Lorenzo and Neilands 1986). Lynch et al. (2001) hypothesize that a similar process could work for incorporation of N^4-acetyl-N^4-hydroxy-1-aminopropane in production of rhizobactin 1021 in *Sinorhizobium Meliloti*.
7. By an unknown reaction mechanism, non-specific fatty acid residues are added, to form synechobactin A, B or C, respectively. I hypothesize that this reaction is catalyzed by SidH, an esterase/lipase, which I will detail in chapter 3.2.2.

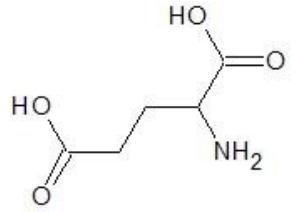

Glutamic acid

+

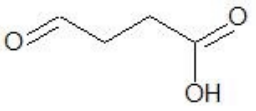

L-aspartic B-semialdehyde

1. SidA - 2,4-diaminobutyrate 4-transaminase → α-Ketoglutaric acid

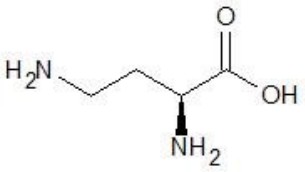

L-2,4-diaminobutyrate

2.SidB - L-2,4-diaminobutyrate decarboxylase → CO_2

1,3-diaminopropane

3. SidE - N-monooxygenase ← 1/2 O_2

N^4-hydroxy-aminopropane

4. SidD - Acetyl Transferase

Acetyl-CoA

CoA

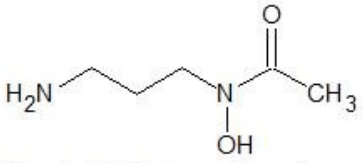

N^4Acetyl-N^4-hydroxy-1-aminopropane

+

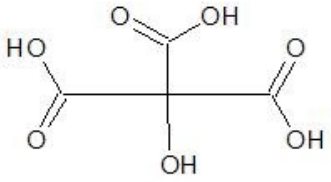

Citrate

5. SidC/SidG

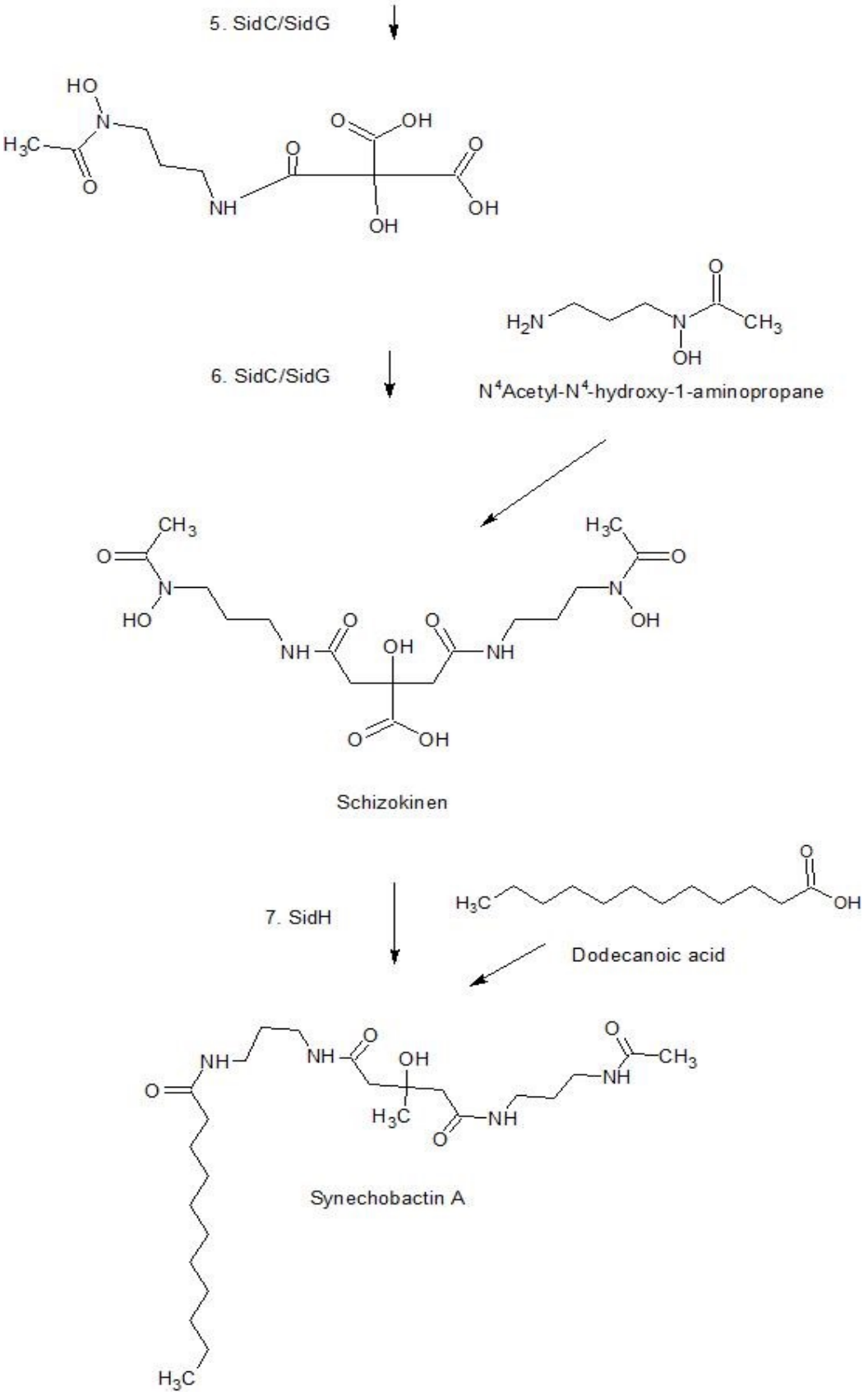

Figure 2: Schematic of hypothesized biosynthesis pathway for synechobactin A, with enzymes marked. Two molecules of *N^4-acetyl-N^4-hydroxy-1-aminopropane are made, and attach to citrate to create schizokinen, before a fatty acid tail is added.* Note that the fatty acid used in step 7 varies, resulting in the other synechobactin variants.

3.2.1 The SidF-transporter

An experimental study of all the genes of the siderophore operon is beyond the scope of this master thesis. Instead, I focus on the genes *SidF* and *SidH*. The predicted siderophore transport protein SidF is a 405 amino acid protein of the mayor facilitator transport protein (MFS) family. The sequence is predicted by Phobius (Käll, Krogh, and Sonnhammer 2004) to contain 12 transmembrane helical regions. MFS-proteins have been shown to be involved in siderophore transport in other organisms, including *Erwinia chrysanthemi, Legionella pneumophila* and *Vibrio parahaemolyticus.* For the most part, MFS's are dependent on *Fur* for regulation, and do not share a high degree of protein sequence identity, at below 20%. This is explained by the rather distant phylogenetic relationships of the proteins, in addition to the large structural differences between the siderophores transported (Miethke and Marahiel 2007).

The best explored siderophore exporter is the entS-protein (previously P43) in *Escherichia coli,* which shows some similarities with SidF. Like SidF, it has 12 transmembrane helical regions. Deletion mutants of *entS* excrete enterobactin at minimal rates, but show high levels of hydrolysis products of enterobactin being exported from the cytosol. This finding show the role of entS in siderophore transport, but also the importance of siderophore breakdown and export to prevent cell toxicity (Furrer et al. 2002). Transporters like entS, transporting charged molecules, typically require two additional components: A membrane fusion protein that links the transporter and the outer membrane, and an outer membrane channel for release of the molecule. Often, the genes for the additional component proteins are located in the same operon as the transporter. If these components exist for the SidF transporter, the lack of a suitable candidate in the siderophore operon indicates that they are located elsewhere in the genome. As SidF is expected to be the mayor transport protein for siderophores in *Synechococcus 7002*, it is a promising target for deletion. As the role of SidF has not been shown experimentally, the primary hypothesis to test is whether SidF works as an siderophore transporter. The expected result of *sidF*-deletion would be that the whole siderophore system for iron uptake is disabled, leading to decreased ability to utilize iron.

3.2.2 SidH

The biosynthetic pathway of rhizobactin 1021 does not identify a protein that adds the fatty acid moiety to the siderophore. However, for synechobactin, SidH appears to be a suitable candidate for this role. The parallel to rhizobactin 1021 assigns role to the genes *sidA* to *sidG* in the synechobactin operon. As *sidH* is the only gene in the operon remaining without an assigned function, it is an ideal candidate for this process. Secondly, the *sidH* codes for a 325 amino acid protein that the Uniprot database categorizes as an esterase/lipase, based on automatic annotation of the amino acid sequence (The UniProt Consortium 2015). Lipases catalyze the hydrolysis or formation of lipids (Svendsen 2000). The enzyme that catalyzes the addition of a fatty acid moiety onto schizokinen, creating synechobactin, would be a lipase. As such, the automatic annotation of the *sidH* based on sequence is a strong piece of evidence for its involvement in the process of adding fatty acid tails to the siderophores.

4 Experimental research goals

In addition to the bioinformatic work done above, four genes described in the foregoing chapters were chosen for further investigation through the approach shown in figure 3.

4.1 FutB

It is known that this protein functions as part of a Fe(III)-transporter, FutABC, in *Synechocystis 6803.* However, it is not highly upregulated during iron limitation in *Synechococcus 7002*. A comparison of growth rates under iron limitation between the deletion mutant ΔFutB and the WT will reveal if FutB has any significant role in iron uptake. These growth experiments will be performed with both ferric and ferrous iron. Since the FutABC-transporter is believed to be a Fe(III)-transporter, I hypothesize that it should only impact growth when the cells are grown on sources of Fe(III), and not on Fe(II).

4.2 Cytochrome C_M

C_M is hypothesized to be part of an electron transport pathway eventually leading to reduction of iron. Deletion of C_M should lead to limited iron uptake, and thus to slower growth under iron limitation. Comparing growth rates and absorption spectra of the deletion mutant ΔC_M against wild type cells under iron limitation should give some indication of whether it is involved in iron reduction.

4.3 SidF

The SidF-gene is hypothesized to transport siderophores out of the cells. The overlay chrome azurol S-assay (O-CAS), which indicates the presence of siderophores, will be used to test this. If no siderophores are exported from the cell, the CAS-assay should give a negative result. This experiment should thus determine whether ΔSidF has limited siderophore export abilities. Additional growth experiments and whole cell absorption spectra should give information on the physiological response of the deletion mutant under different iron availabilities.

4.4 SidH

To test whether SidH is responsible for adding fatty acid tails on the siderophores, a CAS-assay in solid medium will be performed. Since the fatty acid-tail is believed to anchor the siderophores to the membrane, the siderophores produced by ΔSidH should be able to move more freely, and give a larger positive assay result. Growth experiments and whole cell absorption spectra should give information on the physiological response of the deletion mutant.

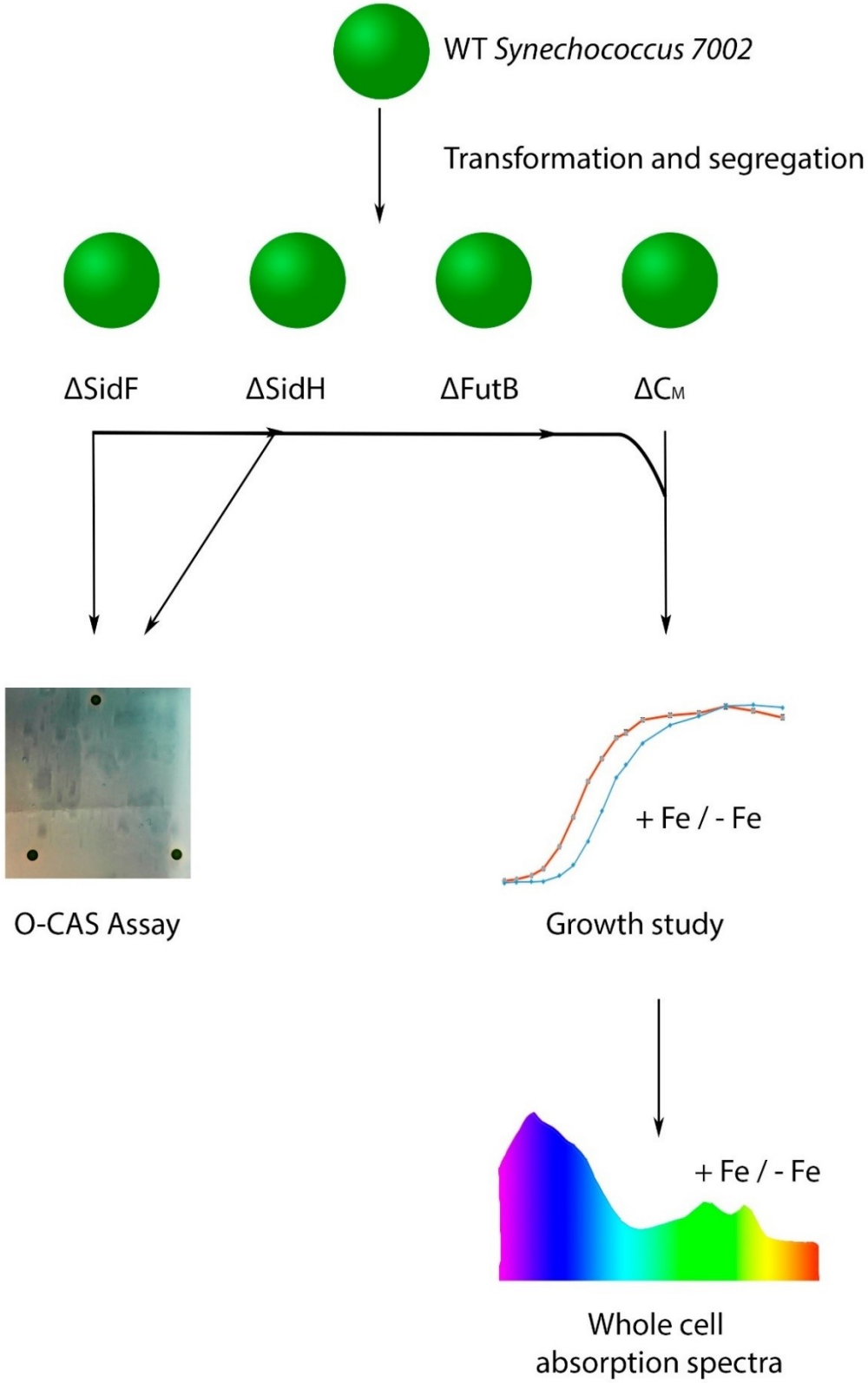

Figure 3: Schematic of experimental approach of this thesis. After creation of four mutants, all of them are tested through growth studies and whole cell absorption spectra. The siderophore mutants are additionally explored through the O-CAS assay. Note that the creation of the ΔC_M-mutant was done by another member of the lab group.

5 Materials and Methods

In this chapter I will first describe the methodology behind growing, transforming and segregating *Synechococcus 7002* mutants. I will then go through the methodology behind the growth experiments, including the necessary data processing. Finally, the methods used for absorption spectra and the O-CAS assay will be detailed.

5.1 Medium and growth conditions

The standard conditions for *Synechococcus 7002* used in this thesis were growth in AA+-medium, at 33°C with lighting conditions of roughly 73 photosynthetically active radiation (PAR). Liquid cultures were grown in either vented 50 ml tissue culture flasks under constant shaking, or in bubbling flasks. Bubbling flasks were set up with continuous filtered air flow from an aquarium pump. The air from the pump was passed through a bottle of water and through a filter before reaching the culture.

The AA+-medium is a defined medium based on Ludwig and Bryant (2011), with composition shown in table 3. For solid medium 15g/l of agar agar was added. Growth experiments were run without glycerol in the medium, as having an abundant carbon source might interfere with the iron-uptake response.

Table 3: Overview over concentrations for AA+ medium. All dilutions were done with autoclaved milliQ-water.

Compound	**Final dilution**	**Comment**
H_3BO_3	2.86 mg/l	Autoclaved or filter sterilized together in 1000X-solution.
$MnCl_2 \cdot 4\ H_2O$	1.81 mg/l	
$ZnSO_4 \cdot 7\ H_2O$	0.222 mg/l	
$Na_2MoO_4 \cdot 2\ H_2O$	0.39 mg/l	
$CuSO_4 \cdot 5\ H_2O$	0.079 mg/l	
$Co(NoO_3)_2 \cdot 6\ H_2O$	0.0494 mg/l	
KH_2PO_4	25 mg/l	Filter sterilized together in 100X-solution.
Na_2-EDTA $\cdot 2\ H_2O$	30 mg/l	
KCl	600 mg/l	
$NaNO_3$	1 g/l	
$CaCl_2$	133 mg/l	
NaCl	9 g/l	Autoclaved together in 1X-solution
$MgSO_4 \bullet 7\ H_2O$	5 g/l	
Glycerol 99.5 %	1.1ml/l	
Tris (pH 8.2)	0.99 g/l	pH adjusted by HCl, made in 100x
$FeCl_3$ x 6H2O	14.28 µM	Filter sterilized in 1000x-solution
Vitamin B_{12}	4 µg/l	

5.2 Design of deletion sequences

Three linear DNA sequences were designed using Benchling (www.benchling.com) to create deletion mutants for FutB, SidF and SidH.

For the FutB-mutant, a linear sequence containing 200bp each of the flanking region was designed and ordered, with 10 bp of in-gene context added for each flank. Between the flanking regions, an antibiotic resistance cassette for Kanamycin was inserted, in addition to Biobrick restriction sites on each side of the cassette.

Similar designs to the FutB-deletion sequences were made for deletion of SidH and SidF, but could not be used to successfully create deletion mutants. New designs were made with 500bp flanking regions for each side of the respective genes, separated by a NotI-restriction side, as seen in figure 4 and table 4. For financial reasons, this design meant that the kanamycin resistance-cassette was inserted after the sequence had been synthesized.

5.2.1 Cloning of knockout constructs

SidF and *SidH* deletion sequences were ordered as part of the Puc57-plasmid, necessitating a cloning strategy to make usable linear sequences with antibiotic resistance cassettes inserted. The strategy, which is summarized in figure 5, consists of linearizing the plasmids and a kanamycin restriction cassette with the *NotI* restriction enzyme. The plasmids and the resistance cassette were ligated before being heat-shock transformed into competent *Escherichia coli* cells. Growth on selective medium allowed selection for transformants. After isolation of the plasmids, PCR using Q5 polymerase was used to create linear fragments for use in transformation of *Synechococcus 7002.*

Table 4: Flanking sequence length and antibiotic cassettes for each designed sequence.

Target gene	Flanking sequence length	Antibiotic cassette
SidF	500	Kanamycin
SidH	500	Kanamycin
FutB	200	Kanamycin

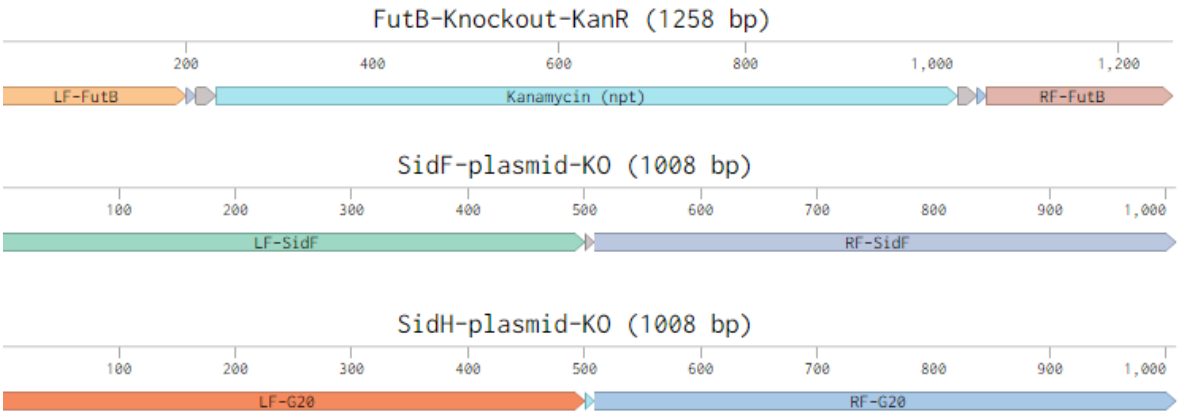

Figure 4: Design of sequences for deletion of FutB, SidF and SidH through homologous recombination. Each sequence has flanking region matching the genomic context of the gene in question. The kanamycin antibiotic resistance cassette was part of the design for the FutB-deletion sequence, but this approach was not successful for the other constructs. Larger overlap sequences without a resistance cassette was therefore used for sidF and sidH.

5.2.2 Restriction digest

The plasmids and a kanamycin resistance cassette were linearized using *NotI*-HF with conditions as shown in table 5. The reaction was run at 37 °C for 10 minutes, before the desired fragments were purified with the QIAGEN PCR purification kit. Concentrations were measured using a Nanodrop spectrophotometer.

Table 5: Reaction conditions for restriction digest by NotI of the plasmids containing the deletion sequences for sidH and sidF, in addition to the kanamycin resistance cassette.

Component	Amount
NotI-HF	1 µl
10x Cutsmart buffer	5 µl
DNA-sequence	500ng (≈5 µl)
Nuclease free water	To 50 ul

5.2.3 Ligation reaction

Two ligation reactions, one for the ΔSidF-Kan construct and one for the ΔSidH-Kan construct, were set up using the reaction shown in table 6. The reaction was incubated at room temperature for 10 minutes.

Table 6: Reaction conditions for two different ligations of plasmids containing deletion sequencese for sidF and sidH, with a kanamycin resistance cassette insert. The molar ratio of vector backbone and insert was set up in a 1:3 relationship.

Component	Amount
10X T4 DNA ligase buffer	4 µl
Vector DNA (SidF-plasmid or SidH-plasmid)	50ng
Insert (KanamycinR)	50ng
T4 DNA ligase	1 µl
Nuclease free water	To 40 µl

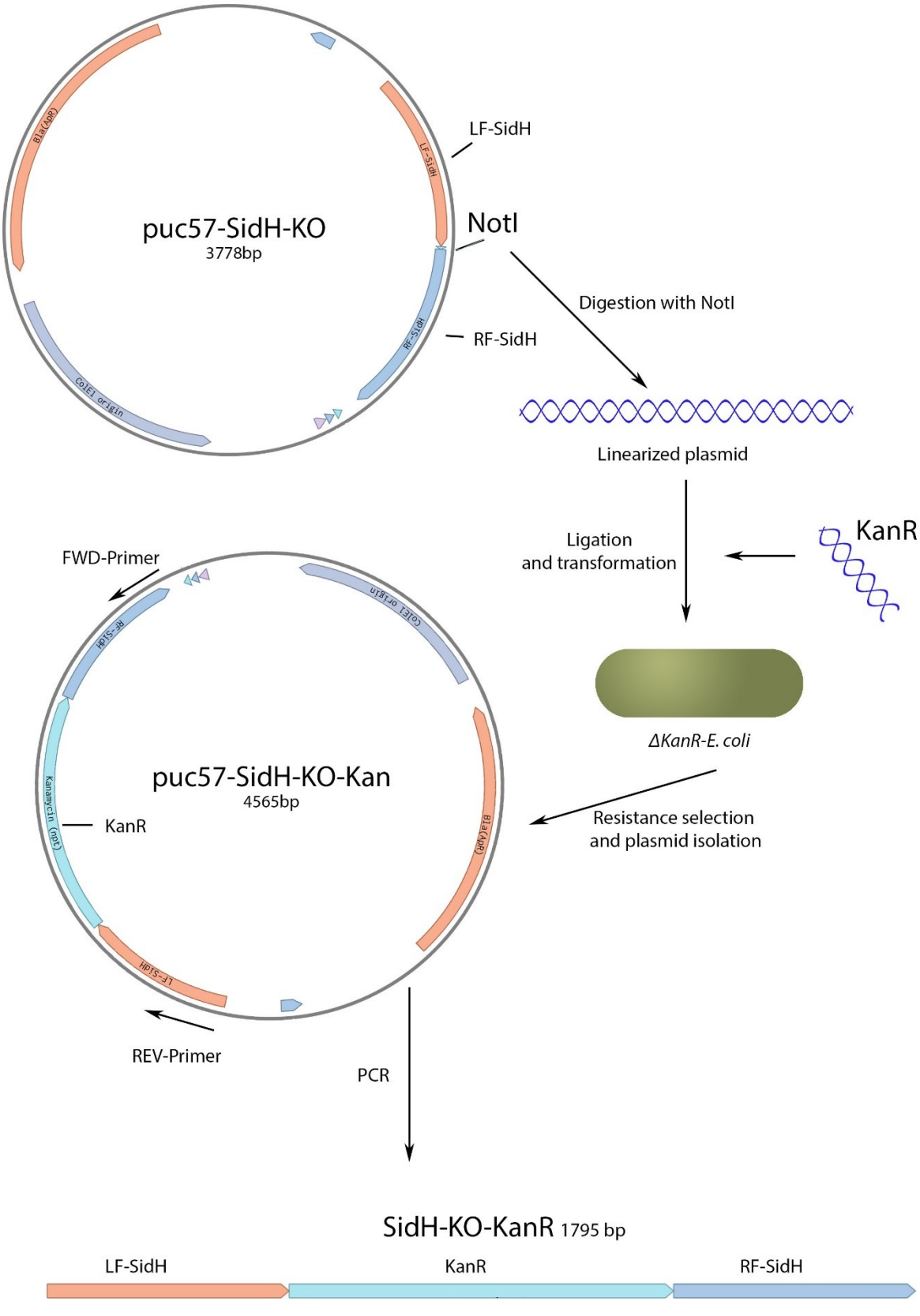

Figure 5: Cloning strategy used for generating knockout-sequences for sidH and sidF. The plasmid is linearized and ligated along with a kanamycin resistance cassette, before being transformed into E.coli. After kanamycin selection, the plasmid is isolated, and a linear knockout-fragment is PCR-amplified.

5.2.4 Heat-shock transformation with ligated plasmids

Both plasmids were transformed to *e. coli*-cells in the same fashion. An aliquot of 0.3 ml of competent DH5α *e. coli*-cells was thawed on ice for 10 minutes, before 30 µl of the ligation mixture was added. The mixture was then incubated on ice for 30 minutes. The cells were heat shocked at 37˚C for 2 minutes, and incubated on ice for 3 minutes. The cells were transferred to 2 ml of LB medium, and incubated at 37˚ C for 90 minutes. A volume of 100 µl cells were added to LB plates with kanamycin, and incubated at 37˚ C overnight. Transformants for each plasmid type were picked from the plates, and grown in selective LB medium overnight. The plasmids were then isolated from the cell culture with the Wizard® Plus SV Miniprep kit.

5.2.5 PCR for sequence construction

The PCR-steps used for sequence construction was done using the high fidelity Q5 polymerase system by New England Biolabs (NEB). Each reaction was set up in the matter described in table 7. After mixing, reaction mixtures were set up in a PCR thermocycler using the parameters described in table 8. Annealing temperatures were calculated by using the NEB T_m calculator (http://tmcalculator.neb.com). Gel electrophoresis was used to verify the product, before purification with the QIAquick PCR Purification Kit.

Table 7: Components for two Q5 PCR-reactions of linear deletion sequence from puc57-plasmids containing resistance cassettes and deletion sequences for either sidF or sidH. The primers used can be found in appendix B.

Component	**Amount**
5X Q5 reaction buffer	10 µl
10 mM dNTPs	1 µl
10 µM Forward Primer	2.5 µl
10 µM Reverse Primer	2.5 µl
Template DNA	Variable volume (100ng)
Nuclease free H_2O	To 50 µl

Table 8: PCR-cycling setup for use of Q5-polymerase to amplify deletion sequences with kanamycin resistance cassette insertion.

Step	**Time**	**Temperature**	**Cycle**
Initial denaturation	30s	98 °C	
Denaturation	10s	98 °C	25X
Annealing	20s	50–72 °C	
Extenstion	25s/kb	72 °C	
Final extension	120s	72 °C	

5.3 Creation of deletion mutants for *Synechococcus 7002*

5.3.1 Transformation protocol

Transformation by homologous recombination was performed to create deletion mutants for ΔFutB, ΔSidH and ΔSidF. The protocol used is derived from a protocol used for *Synechocystis 6803* (Zang et al. 2007). The ΔC_M-strain was supplied by another member of the lab group.

A starter cell culture of WT *Synechococcus 7002* was grown under standard conditions to $OD_{730} > 1$. Wild type-cells were then inoculated from the starter culture, and grown overnight in liquid culture to an OD_{730} of 0.2-0.4 under standard conditions. From this culture, 100 ml of cells was centrifuged for 8 minutes at 2500g. The supernatant was discarded, and the cells re-suspended in AA+-medium to an OD_{730} of roughly 8. A volume of 100-500 µl of this high-OD culture was placed in sterile test-tubes, and ~1µg of purified, linear DNA was added. The test tubes were placed under low-light conditions at 30°C for 6 hours. The full volume of the test tubes was spotted onto sterile filters on prewarmed non-selective AA+-agar plates. After growing overnight in low-light conditions on the nonselective agar-plates, the sterile filters were moved over to prewarmed selective medium (25 µg/ml kanamycin), and grown under the same conditions for two more days. The plates were then moved over to the high-light-incubator (73 PAR) at 33°C, and grown until colonies appeared. This takes 5 to 7 days.

5.3.2 Colony PCR

To verify complete segregation of transformed *Synechococcus 7002,* colony PCR was performed to check for the presence of nonmutant-genetic material. After transformation, colonies were streaked out on new selective plates. New colonies were picked, and diluted in 30 µl of nuclease free H_2O. This solution was used as the source of the template DNA in the colony PCR setup shown in table 9 and table 10. Annealing temperatures for the primers (Appendix B) were found using the NEB T_m calculator (http://tmcalculator.neb.com). Wild type colonies were used as a standard of comparison. The PCR-products were tested by gel electrophoresis, running at 70-100V and 45-120mins depending on the size differential between the WT and mutant sequence. If segregation could be verified, the remaining colony-solution was used to inoculate liquid culture for -80°C storage and later use.

Table 9: Components used for colony PCR of Synechococcus 7002 cells with Taq polymerase, with 20 µl total volume.

Component	Amount
10x Taq Buffer	2 µl
10 mM dNTPs	0.5 µl
10 µM Forward Primer	0.5 µl
10 µM Reverse Primer	0.5 µl
Colony-solution	1 µl
Nuclease free H_2O	17.4 µl
Taq polymerase	0.125 µl

Table 10: Cycling set up used for colony PCR of Synechococcus 7002 cells using Taq polymerase.

Step	Time	Temperature	Repetition
Breaking cell walls	6min	95 °C	
Denaturation	30s	95 °C	
Annealing	30s	45-68 °C	30X
Extension	1min/kb	68 °C	
Final extension	5min	68 °C	

5.4 Growth experiments

To study the impact of iron concentration on the mutant strains, growth experiments for all mutants and the wild type were made by growing cells on solid media with different iron concentrations, and imaging them at regular intervals. In addition to varying concentrations of $FeCl_3$ and FeO, the iron chelator desferroxamine B (DFB) was used to further limit iron concentrations. Two separate experiments were set up, one for ΔFutB and the wild type, with iron concentrations shown in table 11. A later experiment, with different iron concentrations (table 12), was made for ΔC_M, ΔSidH and ΔSidF. The two experiments were run in a nearly identical fashion, with minor differences noted in the text.

Table 11: Iron sources and concentrations for growth experiments on ΔFutB and the wild type.

Iron source	Concentration (nM)	Additive
$FeCl_3$	1400 (iron-replete)	
$Fecl_3$	14	
$FeCl_3$	14	28 nM DFB
$FeCl_3$	1.4	28 nM DFB
FeO	1.4	
FeO	1.4	

Table 12: Iron availabilities and concentrations for growth experiments on ΔC_M, ΔSidH, ΔSidF and the wild type.

Iron source	Concentration (nM)	Additive
$FeCl_3$	1400 (iron-replete)	
$FeCl_3$	14	
$FeCl_3$	14	28 nM DFB
FeO	14	
FeO	14	28 nM DFB

5.4.1 Preparation, washing and spotting

Inoculating from cultures ($OD_{730} > 1$), mutant and wild type *Synechococcus 7002*-cultures were grown in A++-medium without glycerol to an $OD_{730} = 0.4 – 0.6$. The cultures were centrifuged for 10 minutes at 2700g. The supernatant was discarded, before the cells were resuspended in 25 ml AA+-medium without iron. This process of centrifugation and resuspension was repeated two more times, before the cells were resuspended into a dilution series. For the experiment on ΔFutB, a dilution series of $OD_{730} = 1$, 0.1 and 0.01 was made. The $OD_{730} = 0.01$-dilution was not for the experiment on the other mutants.

Three drops of 3 µl from each dilution of the mutants and wild type *Synechococcus 7002* were spotted onto the AA+-plates with different iron concentrations using a multipipette in the manner shown in figure 6. The drops were air-dried, before being grown in high-light-conditions (77PAR) at 33 °C for ten days. To avoid minor differences in light intensity influencing results, plates were placed so that lines of spots of the same density were the same distance from the lighting source. Images were taken after 24 hours, and then every 12 hours for 96 hours. An image was then taken every 24 hours until the cultures had grown for 10 days.

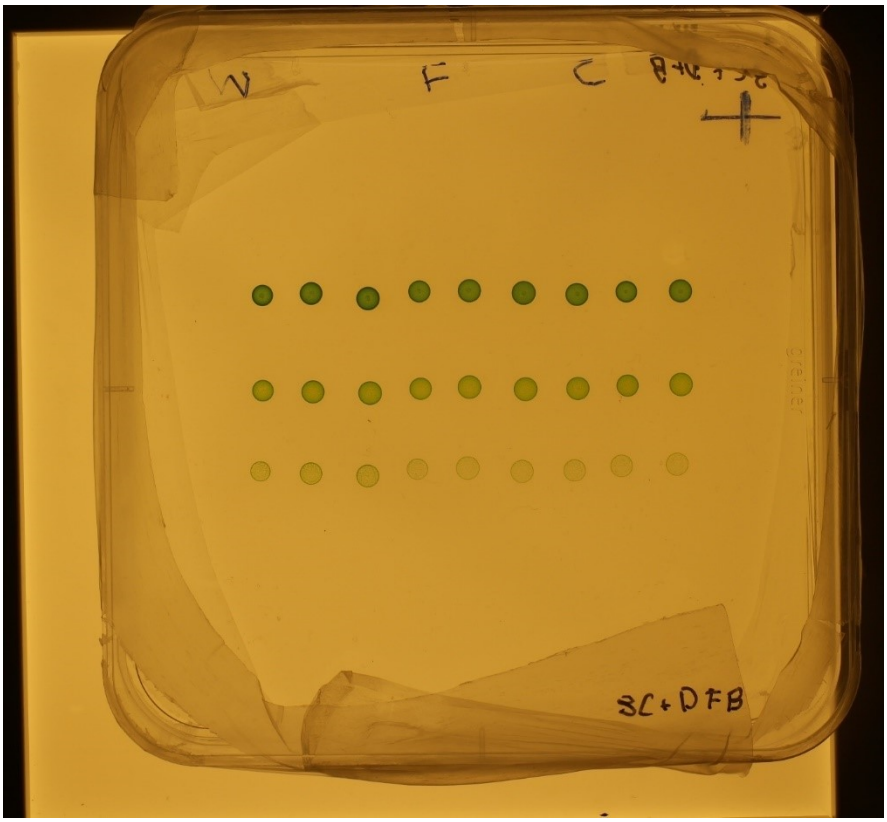

Figure 6: Example picture from picture taking setup, showing colonies from the first experiment grown for four days on 14 nM $FeCl_3$ and 28nM DFB. The 3 WT colonies are on the left, with ΔFutB in the middle. The rightmost 3x3-colonies show an attempted growth experiment on ΔC_M that was abandoned due likely culture contamination by the wild type. The "+" in the upper rightmost corner is used to simplify alignment of the picture series.

5.4.2 Image acquisition and processing

All images of the plates were taken in a novel camera based plate imaging setup (manuscript in preparation, see also Lamb (2016)). The system enables measurements of relative cell densities for each colony by using a light-closed box with a camera at a fixed distance from the plates and constant lighting conditions from a white LED diffused by a plastic film. An in-lab developed script has been written to measure colony density. The script is written in Python 2.73, and consists of the following steps:

1. Consecutive RAW-images are converted into an MRC-format stack.
2. All images are hand aligned using the Midas software, making an aligned stack.
3. The position of each colony is manually assigned in the stack.
4. Cell densities are calculated automatically and compared to background density level of the surrounding agar plate.
5. Density-data for each colony at each point in time is compiled into a data-file, and can be further analyzed.

5.4.3 Grofit analysis of growth data

Calculation of growth rate from the density series was done using the grofit-package for R (Kahm et al. 2010). Due to the large amount of data from both this and other similar experiments in the lab group, a script was developed for calculating standard deviation and average growth rate for each triplicate (appendix A). To make the growth rates between different picture series comparable, all data points were adjusted by the factor needed to equalize the maximum density for each picture stack. All model fits were done using a logistic growth model.

The quality of the model fit for the growth curve was evaluated for each colony. The ratio of the growth rate divided by the standard error of the calculated growth rate was used as a standard of quality. If one of the growth rates calculated in a set of three parallels had a ratio of 12 or lower, the data for the whole triplicate was discarded.

5.5 Whole cell room temperature absorption spectra

To check for signs of iron stress, whole cell absorption spectra were taken of ΔFutB, ΔC_M, ΔSidF, ΔSidH and the wild type. Colonies were picked from solid medium and grown in both iron-replete liquid culture, and in culture with 7 nM $FeCl_3$ and 14 nM of the iron chelator DFB. The cultures were grown to an OD_{730} = 0.2-0.4, before being resuspended to OD_{730} = 0.3. Absorption was measured in triplicate using a Hitach U-3010 Spectrophotometer with an integrating sphere accessory from 400nm to 800nm at a scan speed of 600nm/min. All spectra were baseline subtracted at 800 nm.

5.6 Overlay-CAS-assay of siderophore mutants

5.6.1 Cell culture preparation

For the overlay-chrome azurol S assay (O-CAS) experiment, AA+ agar plates without glycerol and with iron concentrations of 1.4 nM goethite, 1.4 nM FeO or iron-replete (1400 nM $FeCl_3$) were prepared.

Cultures with WT, ΔSidH and ΔSidF *Synechococcus 7002* were grown in iron-replete liquid culture to an OD_{730} = 0.3. After washing (see chapter 5.4.1), the cells were diluted to an OD_{730} = 1. For each strain, three spots of 5 µl of culture were spotted onto each AA+ plate at

equidistant locations from the center of the plate. The cultures were grown under standard conditions for 120 hours before the CAS-assay was started.

5.6.2 Dye-medium preparation

The O-CAS assay mixture was based on Pérez-Miranda et al. (2007). 0.25 l of agar dye-medium was prepared by mixing 15 mg of Chrome azurol S (CAS), 18mg of hexadecyltrimetyl ammonium bromide (HDTMA) and 2.5 ml of 1 mM $FeCl_3 \cdot 6H_2O$ in 10 mM HCl. 0.9% (w/v) agarose was dissolved in ddH_2O by microwave-heating, and the dye-mixtures was added. The pH was adjusted to 6 by adding 1 M NaOH, before gradually adding 7.5 g of Piperazine-1,4-bis(2-ethanesulfonic acid) (PIPES). As adding PIPES drops the pH of the solution, 1 M NaOH was supplied to keep pH > 5. After the PIPES had been added, the pH was adjusted to 6,6.

5.6.3 O-CAS assay observation

The O-CAS-agar was cooled to roughly 50 °C before 20 ml of the O-CAS-agar was applied on top of each agar plate under sterile conditions. The plates were incubated at room temperature, and the assay results were noted after 16 and 72 hours.

6 Results

6.1 Verification of segregation by colony PCR

Colony PCR and gel electrophoresis was performed to confirm complete segregation of the mutant strains ΔFutB, ΔC_M ΔSidF and ΔSidH, the results of which can be seen in figure 7, figure 8, figure 9 and figure 10, respectively. Due to the small difference in length between the PCR-product of the WT and ΔSidH in figure 10, the gel electrophoresis was run for an additional time to ensure a consistent result (data not shown).

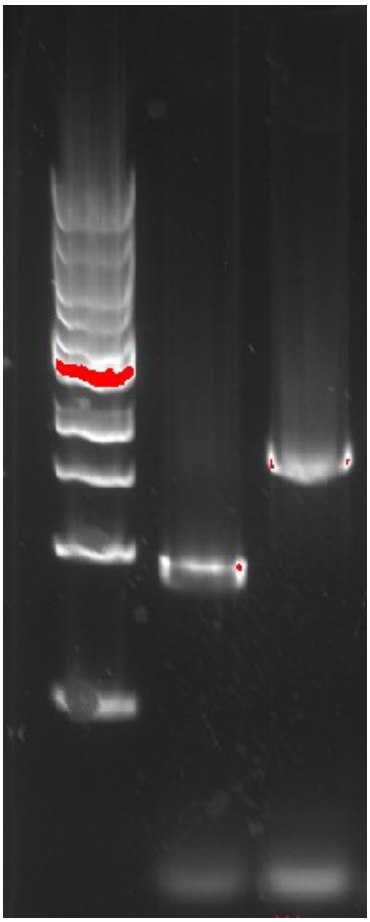

Figure 7: Gel electrophoresis of the colony PCR for ΔFutB and WT, with 1kb Generuler as ladder in lane 1. The PCR product for ΔFutB is in lane 2, with an expected length of 949bp. Lane 3 shows the band for the WT, which has an expected length of roughly 1700bp.

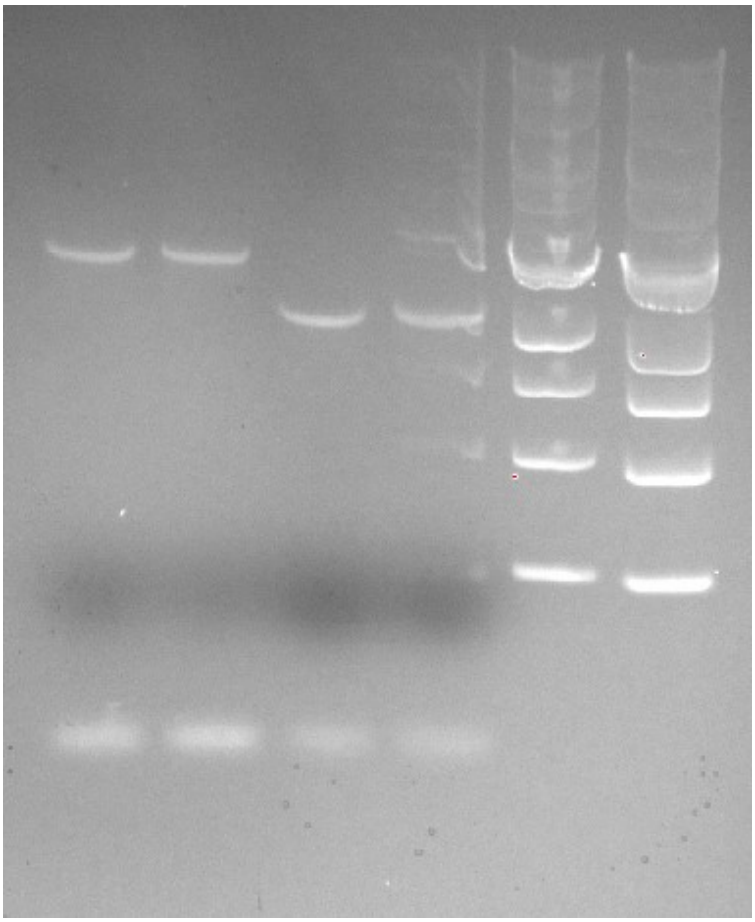

Figure 8: Gel electrophoresis of colony-PCR for ΔC_M and WT, with 1kb Generuler as ladder (lane 5+6). Lane 1 and 2 show the amplified mutant sequence, with an expected length of 2438, while lane 3 and 4 show the WT with an expected length of 1975 basepairs.

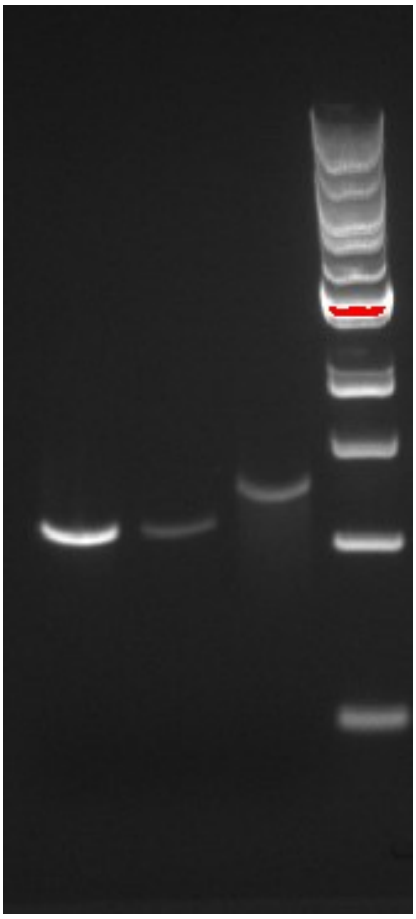

Figure 9: Gel electrophoresis of colony PCR of ΔSidF and the WT, with 1kb Generuler as ladder in lane 4. The mutant DNA is in lane 1 and 2, with an expected length of 950bp. The WT DNA is in lane 3, and has an expected length of 1347bp.

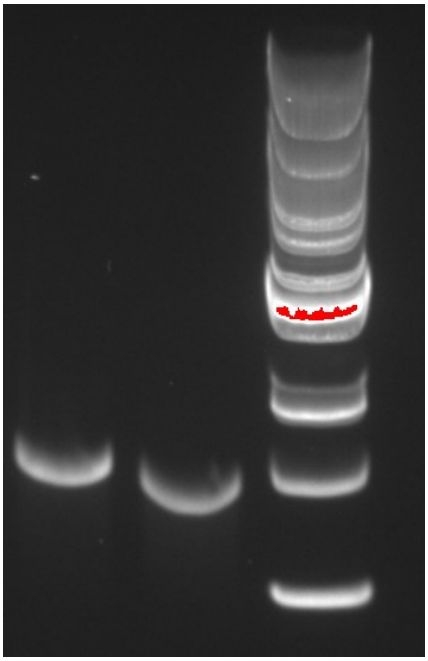

Figure 10: Gel electrophoresis of colony PCR products for WT (lane 1) and ΔSidH (lane 2) , with 1kb Generuler as ladder in lane 3. The expected length of the wild type product is 1450, while the ΔSidH product has an expected PCR-product length of 1300bp. Note that the three shortest fragments of the ladder have run out of the gel, and cannot be seen in the picture.

6.2 Growth experiments

The growth experiments investigated the growth rates and growth curves for different cell strains under various iron availabilities. Each iron availability variation included colonies spotted from a dilution series of both mutant and wild type cells, resulting in a large amount of data. As showing the growth curves for every single experimental variation would be excessive, care has been taken to show data that are representative for growth on each iron availability variation. In general, the OD the colonies were started at did not significantly impact the difference in calculated growth rate between the mutant and the wild type.

In addition to the data shown, analysis was performed on ΔFutB and WT grown on 1.43 nM $FeCl_3$ and 28 nM of the iron chelator DFB. This analysis was hampered by drying out of the solid media, and is therefore not shown. The limited data that was obtained from this plates indicates that *Synechococcus 7002* has limited growth capacity under conditions where the DFB is present in much higher concentrations than the available iron.

6.2.1 ΔFutB under different iron concentrations

Figure 11 shows calculated relative growth rates for the wild type and ΔFutB on different growth conditions, with WT-growth under iron-replete-conditions set as 100. Cells grown on $OD_{730} = 0.1$ generally appear to grow slower than cells grown from $OD_{730} = 1$ spotted cells. While there is variation in growth rates depending on the OD used for spotting, the difference between WT and ΔFutB appear to depend on iron availability, and not on OD. A possible exception to this trend is cells grown on ferrous oxide, where the $OD_{730} = 1$ cultures show a larger difference between mutant and wild type cells than the $OD_{730} = 0.1$ cultures.

Table 13 shows a summary of the growth rate data, with calculated p-values for each comparison between the wild type and ΔFutB. Iron-replete conditions and 1.4nM $FeCl_3$ show no statistically significant difference between WT and ΔFutB, while cultures grown on 14nM $FeCl_3$ with 28nM DFB and on 1.4nm ferrous oxide show the WT growing significantly faster than ΔFutB.

The growth curve of ΔFutB under iron-replete conditions (1400nM $FeCl_3$) show no clear difference from the wild type, as evidenced in figure 12. The calculated growth rates in table 13 reflect this, as the p-values are close to 0.5. Note that the error bars are rather large in the case of the WT, owing to imprecision in spotting one of the colonies.

The growth curves for ΔFutB vs WT on 1.4nM $FeCl_3$ are close to each other, but with ΔFutB growing slightly slower and to a lower density stationary phase (figure 13). A comparison of growth rates in table 14 indicate slower growth for ΔFutB than WT under these conditions, but this difference is not statistically significant.

The growth curves for ΔFutB show slower growth than the WT when grown on 14.28 nM $FeCl_3$ with 28 nM DFB added, as can be seen in figure 14. The growth curve deviates slightly from a standard logistic curve, with growth tapering off before reaching the stationary phase. The calculated growth rates in table 14 indicate a statistically significant difference between the strains.

The growth curve of ΔFutB on Fe(II) oxide show slower growth than the wild type in the exponential phase, but approaches the same relative density in the stationary phase. An example of this growth curve is shown in figure 15. As Table 13 indicates, both cultures started at $OD_{730} = 1$ and $OD_{730} = 0.1$ have a difference in growth rate between WT and mutant cells, but the magnitude of difference is larger for $OD_{730} = 1$.

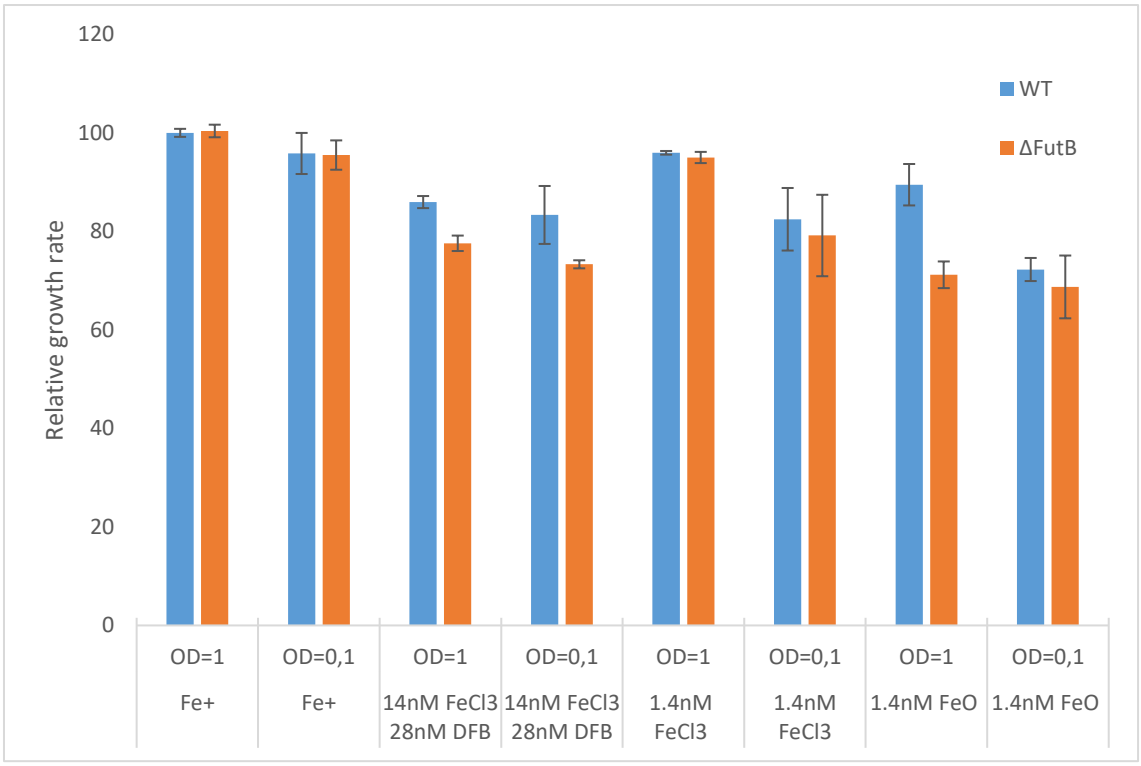

Figure 11: Averaged relative growth rates for WT and ΔFutB, with the growth rate of WT on iron-replete media set as 100. Cells are grown on solid media under different iron concentrations, and different starting OD_{730}. "Fe+" signifies iron-replete conditions (1400nm $FeCl_3$). Standard error for each average is shown.

Table 13: Relative growth-rate values for each experimental condition of wild type and ΔFutB. p-values were calculated for the differences between mutant and wild-type growth rates, using a one-tailed, independent two-sample t-test that assumes equal variances for the two sample sets. Conditions that returned $p < 0.05$ have been bolded.

Iron source	OD	WT-growth rate	ΔFutB-growth rate	p-value
Fe+	1	100.00	100.38	0.407
Fe+	0.1	95.82	95.49	0.476
1.4nM $FeCl_3$	1	95.95	95.00	0.218
1.4nM $FeCl_3$	0.1	82.46	79.16	0.355
14nM $FeCl_3$ 28nM DFB	**1**	**85.95**	**77.58**	**0.003**
14nM $FeCl_3$ 28nM DFB	**0.1**	**83.33**	**73.31**	**0.049**
1.4nM FeO	**1**	**89.47**	**71.19**	**0.007**
1.4nM FeO	0.1	72.26	68.72	0.298

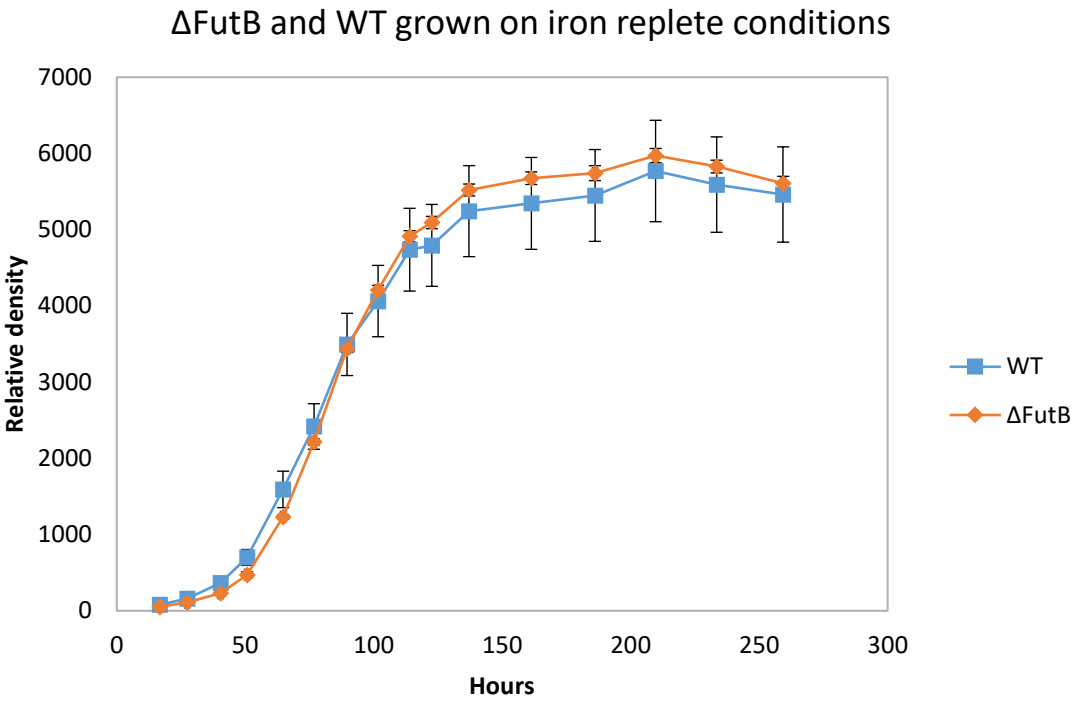

Figure 12: Averaged growth curves for triplicates of ΔFutB and WT cells, grown from OD_{730}=0.1, under iron-replete conditions (1400nm $FeCl_3$). Standard error for each data point shown.

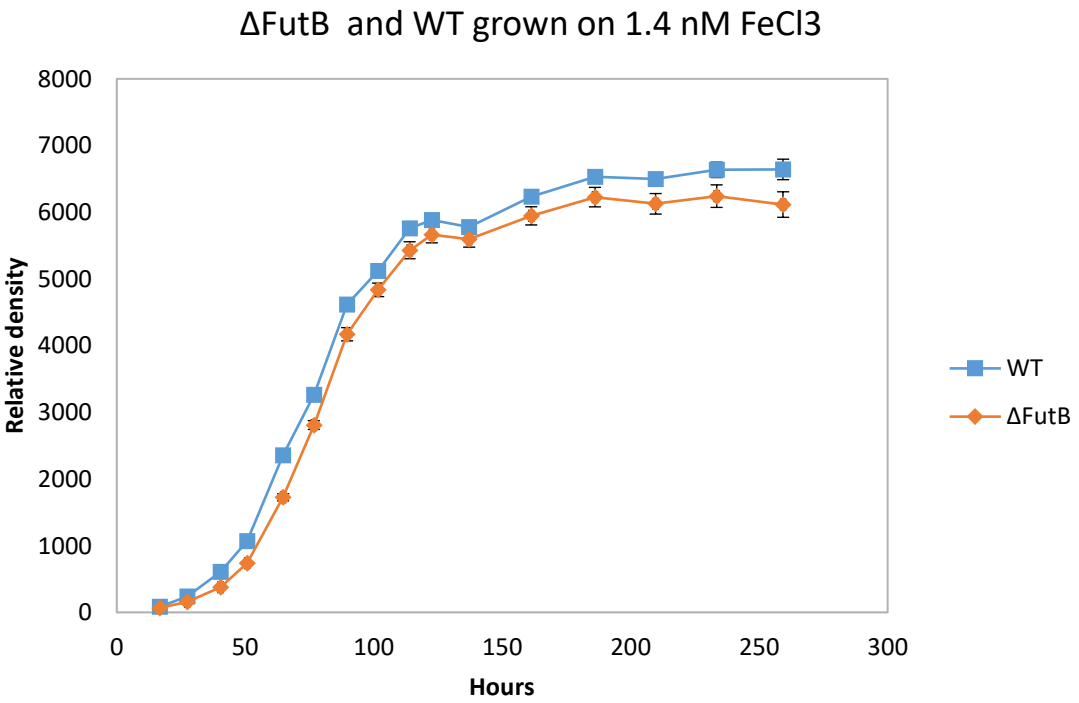

Figure 13: Averaged growth rates for triplicates of ΔFutB and WT cells grown with 1.4nM of $FeCl_3$, starting from OD_{730} = 0.1. Standard error for each data point shown.

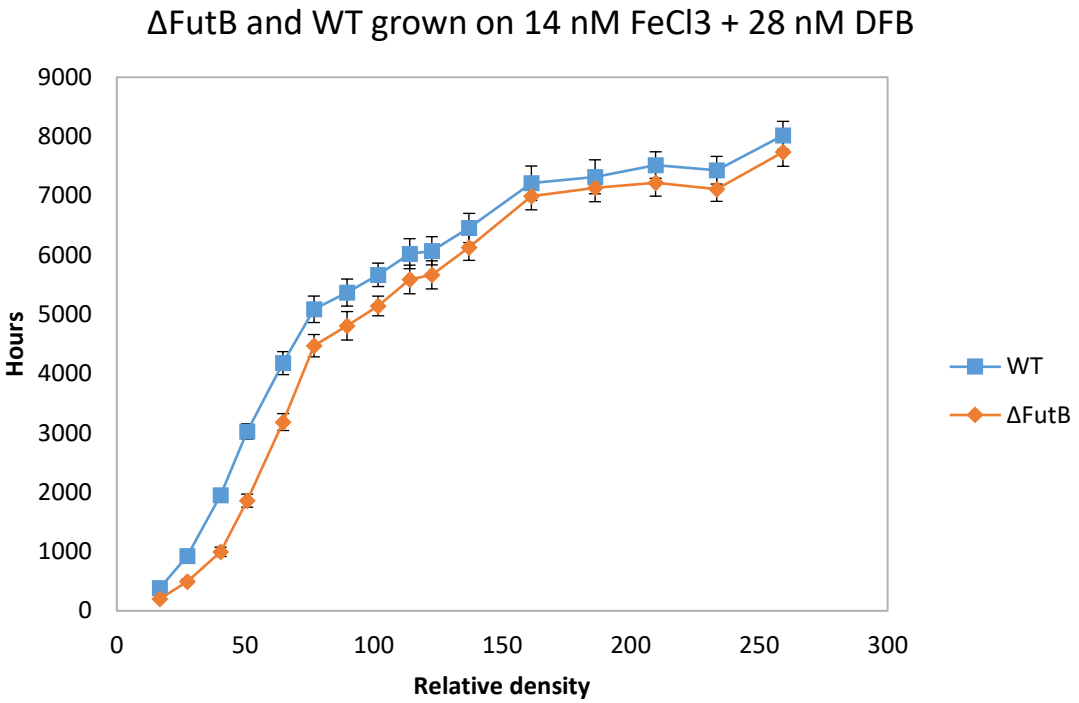

Figure 14: Averaged growth rates for triplicates of ΔFutB and WT grown with 14 nM $FeCl_3$ + 28 nM DFB, grown from culture of OD730 = 1. Standard error for each data point shown.

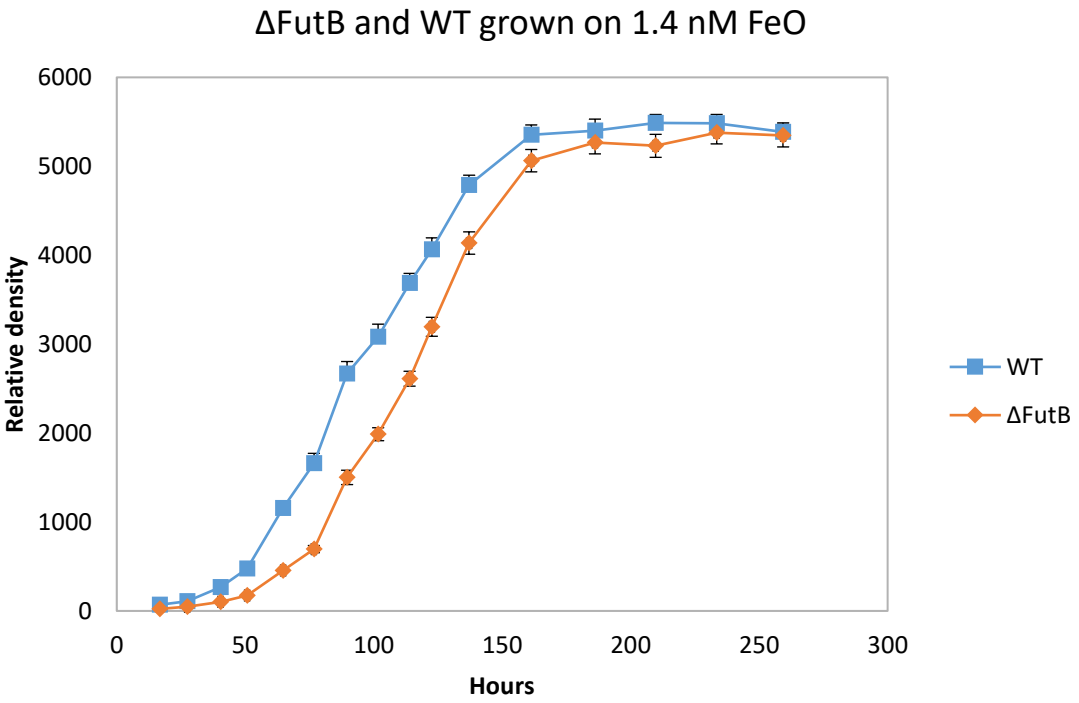

Figure 15: Averaged growth rates for triplicates of ΔFutB and WT cells grown with 1.4nM of FeO, grown from spots of OD_{730} = 0.1. Standard error for each data point shown.

6.2.2 Growth of ΔC_M under different iron concentrations

Growth of the cytochrome C_M-deletion mutant was compared to the wild type *Synechococcus 7002* under a range of different iron availabilities. The average growth rate was calculated for each experimental condition, the results of which can be seen in figure 16, and numerically in table 14, along with p-calculations for the difference in growth rate between ΔC_M and WT. The growth rate is significantly different from WT when ΔC_M is grown under iron-replete conditions. The iron-depleted conditions generally show growth rate differences between mutant and WT within the standard error, and are not statistically significant. An exception is for the OD_{730} = 1 cultures grown on 14 nM FeO, where ΔC_M has statistically significantly slower growth. However, the OD_{730} = 0.1 cultures grown on 14 nM FeO show the opposite result, with WT growing faster than ΔC_M.

Figure 17 to figure 21 show the averaged growth curves for ΔC_M and WT under different iron availabilities. For each experimental condition, either the curve from cultures starting at OD_{730} = 1 or OD_{730} = 0.1 is shown. In general, both OD-conditions show the same pattern for each iron availability, so the graph shown is based mostly on the standard error of the data sets.

While the growth rate between ΔC_M and WT differs only for the iron-replete conditions, figure 17 to figure 21 show that the mutant colonies do not approach the same density as the WT, even after longer periods of growth. This is particularly apparent in cells grown on 14 nM $FeCl_3$ (Figure 18), where the mutant cells grow to a stationary phase 30% lower in relative density than the WT.

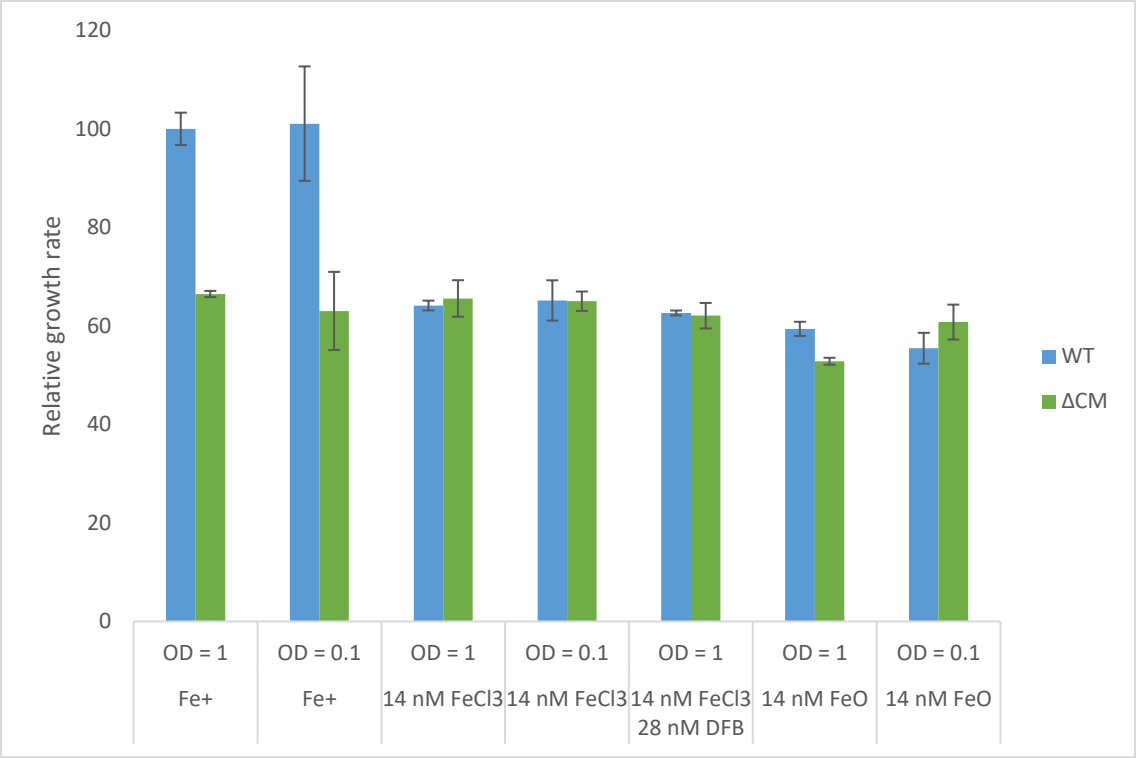

Figure 16: Averaged relative growth rates for WT and ΔC_M, with the growth rate of WT on iron-replete media set as 100. Cells are grown on solid media under different iron concentrations, and different starting OD_{730}. "Fe+" signifies iron-replete conditions (1400nm $FeCl_3$). Calculations are made by Grofit. Standard error for each average is shown.

Table 14: Relative growth-rate values for each experimental condition of wild type and ΔC_M, with the growth rate for iron-replete conditions set as 100. p-values were calculated for the differences between mutant and wild-type growth rates, using a one-tailed, independent two-sample t-test that assumes equal variances for the two sample sets. Conditions that returned $p < 0.05$ have been bolded.

Iron source	OD	WT-growth rate	ΔC_M-growth rate	p-value
Fe+	**1**	**100.00**	**66.47**	**0.0003**
Fe+	**0.1**	**101.06**	**63.04**	**0.0270**
14 nM $FeCl_3$	1	64.14	65.57	0.3645
14 nM $FeCl_3$	0.1	65.16	65.01	0.4873
14 nM $FeCl_3$ 28nM DFB	1	62.62	62.07	0.4226
14 nM FeO	**1**	**59.40**	**52.83**	**0.0074**
14 nM FeO	0.1	55.46	60.77	0.1619

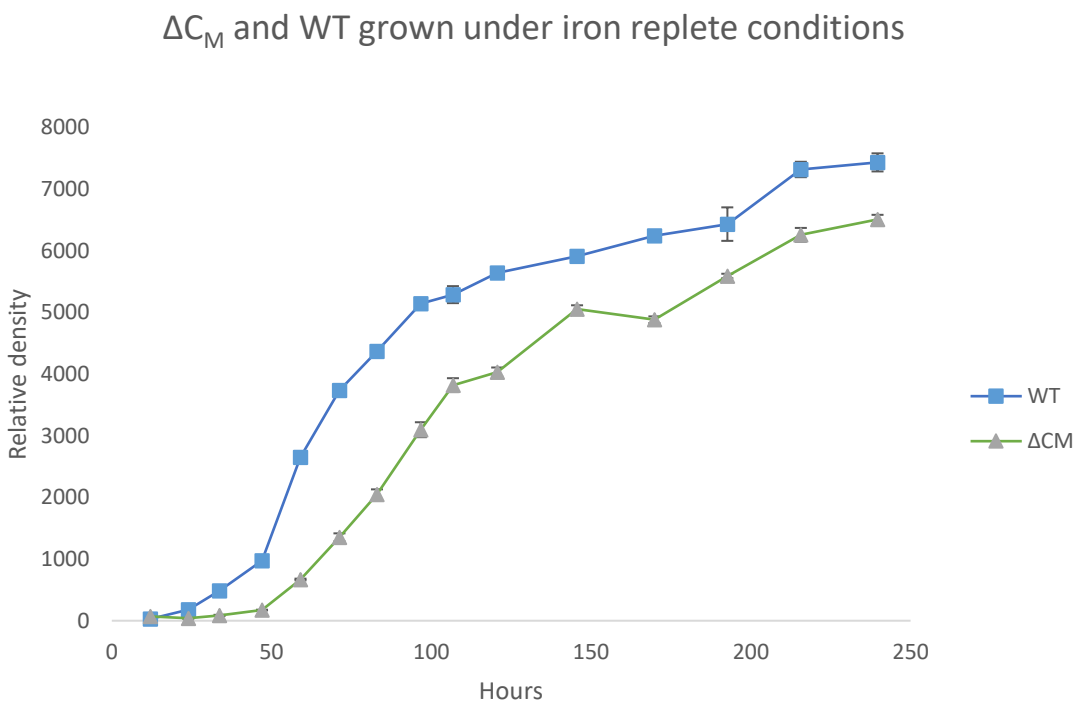

Figure 17: Averaged growth curves for triplicates of ΔC_M and WT cells, grown from cultures of OD_{730} = 0.1, under iron-replete conditions (1400nM $Fecl_3$). Standard error for each data point shown.

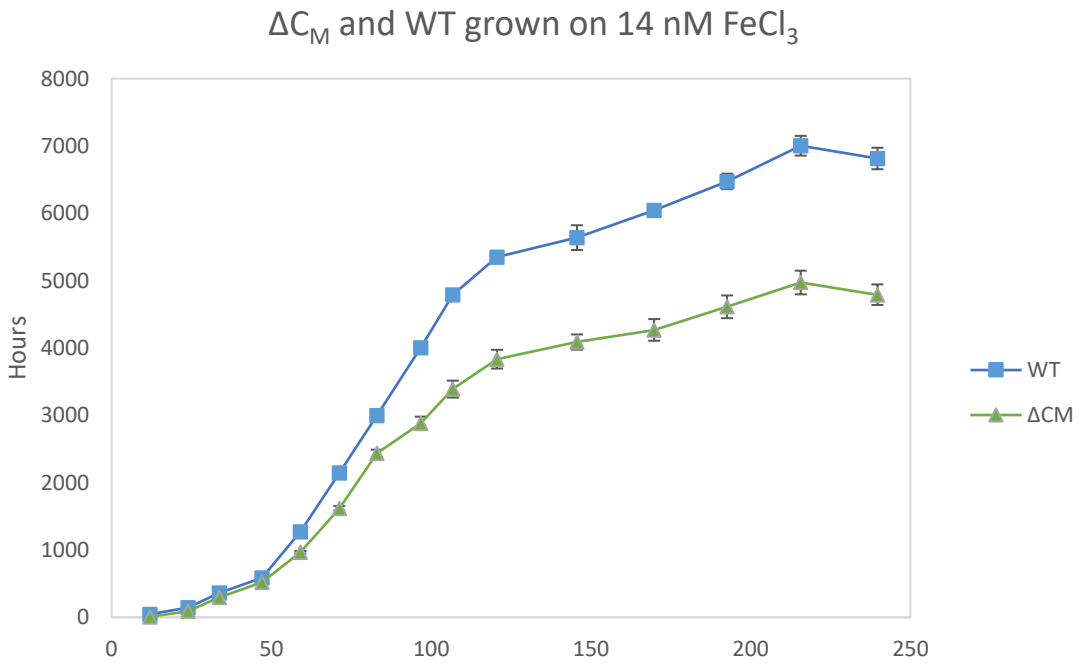

Figure 18: Averaged growth curves for triplicates of ΔCM and WT cells, grown from cultures of OD_{730} = 0.1, under iron concentrations of 14 nM FeO. Standard error for each data point shown.

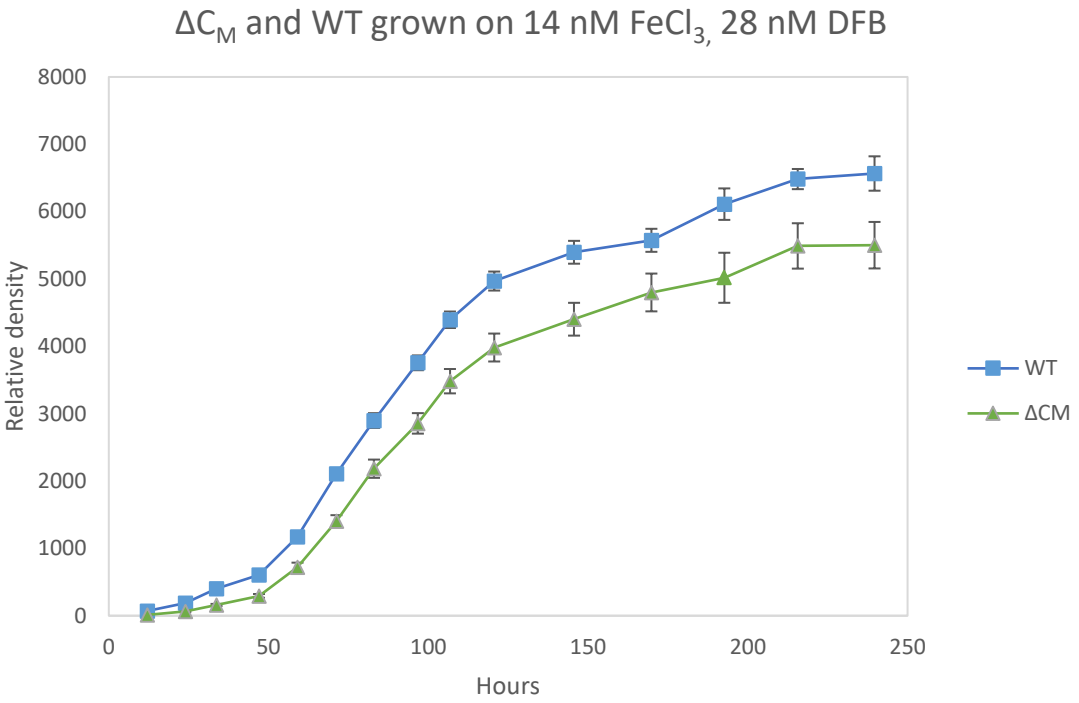

Figure 19: Averaged growth curves for triplicates of ΔC_M and WT cells, grown from cultures of OD_{730}=0.1, under iron concentrations of 14 nM $FeCl_3$ and 28 nM DFB. Standard error for each data point shown.

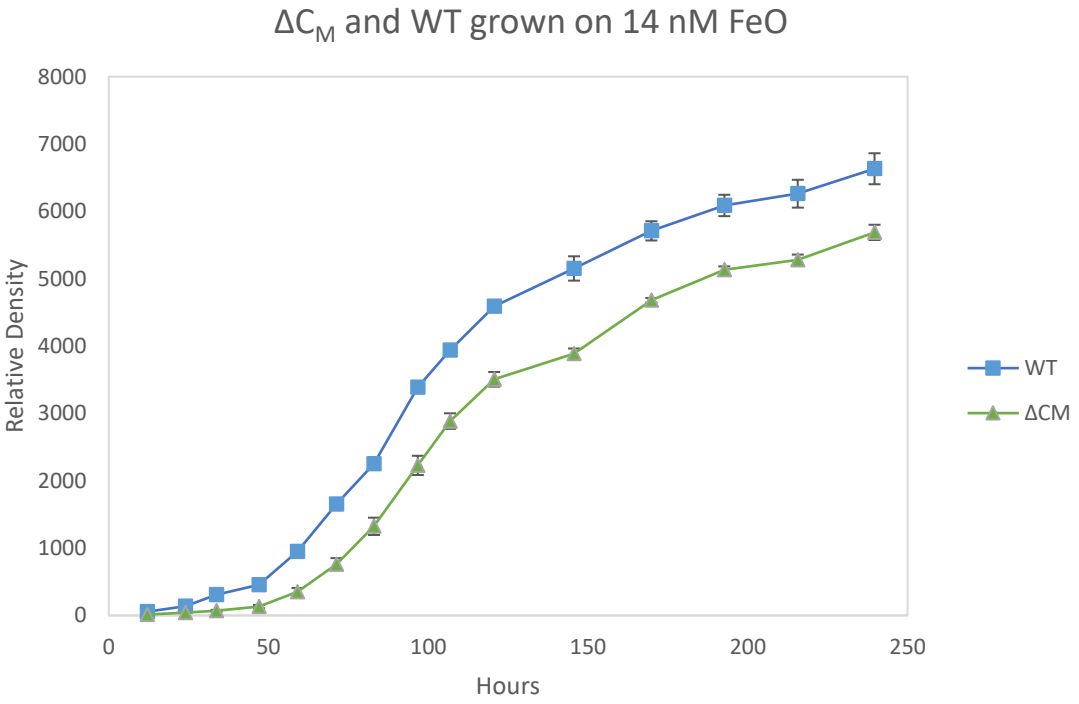

Figure 20: Averaged growth curves for triplicates of ΔCM and WT cells, grown from cultures of OD_{730} =0.1, under iron concentrations of 14 nM FeO. Standard error for each data point shown.

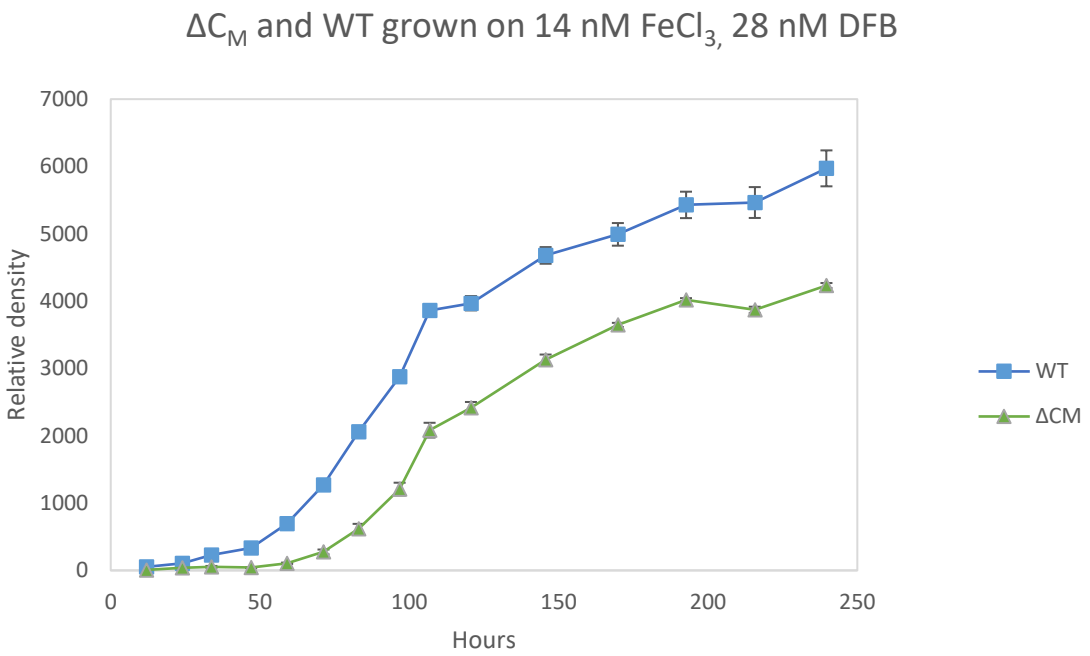

Figure 21: Averaged growth curves for triplicates of ΔCM and WT cells, grown from cultures of OD_{730}=0.1, under iron concentrations of 14 nM FeO and 28 nM DFB. Standard error for each data point shown.

6.2.3 Growth of siderophore mutants under different iron concentrations

Growth of the two siderophore deletion mutants ΔSidF and ΔSidH was compared to the wild type *Synehococcus 7002* under a range of different iron availabilities. The average growth rate was calculated for both mutants and the wild type for each experimental condition, the results of which is shown in figure 22. Table 15 displays the results numerically, with p-calculations for the difference in growth rate between ΔSidF and the WT, and for ΔSidF and the WT.

Figure 22 and table 15 show that there is a difference in calculated growth rate between WT and ΔSidH when grown under different iron limitations. These differences are either statistically significant ($p < 0.05$) or close to statistical significance. When grown under iron-replete conditions, the growth rates of WT and ΔSidH are similar, and the differences is not statistically significant.

For ΔSidF, no statistically significant difference between mutant and WT can be seen for either iron-replete or iron limited conditions. The standard error of the average growth rate is in general larger for ΔSidF than it is for the WT or ΔSidH, making it difficult to see any clear patterns.

Figure 23 to figure 27 show the averaged growth curves for WT, ΔSidF and ΔSidH under both iron-replete conditions, as well as different iron limitations. Figure 23, showing growth under iron-replete conditions, indicates no difference between the mutants and the WT. For the different iron limitations, the trend is that both ΔSidF and ΔSidH grow to lower densities than the WT. The general trend of this does not appear to be influenced by the degree of iron limitation. For instance, the growth curve for 14 nM $FeCl_3$ (figure 24) appear to follow the same pattern as cells grown on 14 nM FeO and 28nM DFB (figure 27).

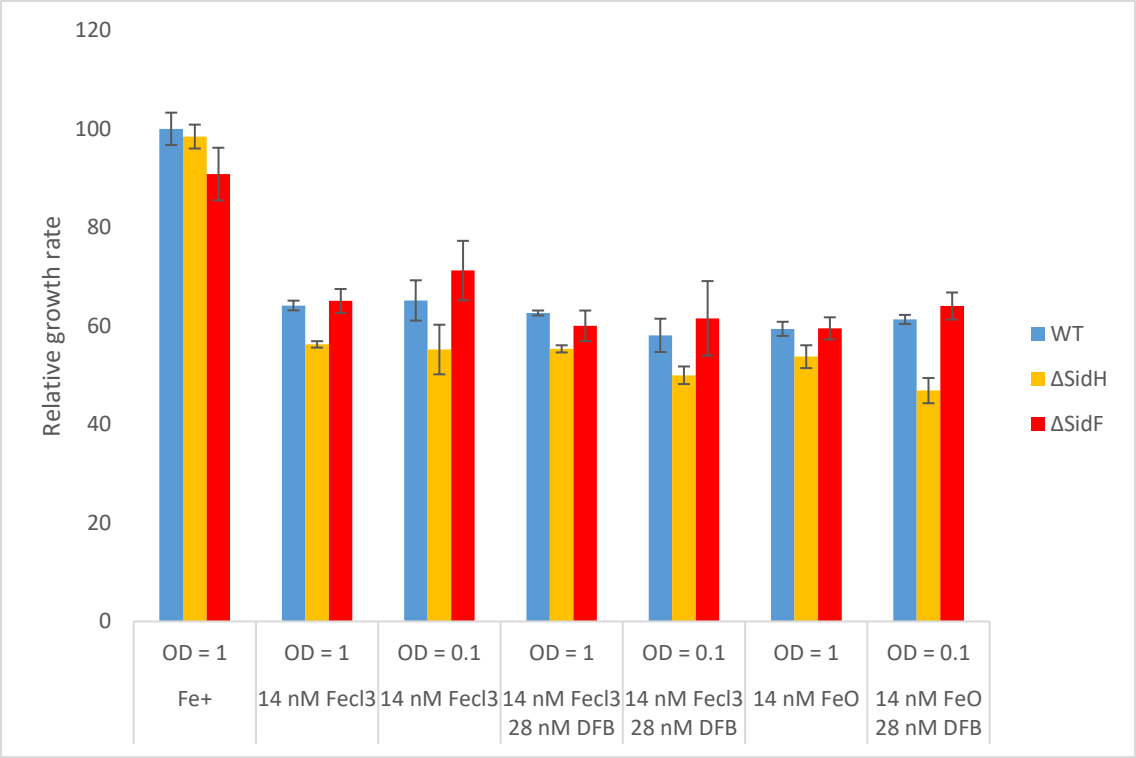

Figure 22: Averaged relative growth rates for WT and the siderophore mutants ΔSidF and ΔSidH. The growth rate of WT on iron-replete media has been set as 100. "Fe+" signifies iron-replete conditions (1400nM $FeCl_3$). *Cells are grown on solid media under different iron concentrations, and different starting* OD_{730}. *Calculations are made by Grofit.*

Table 15: Relative growth-rate values for each iron availability condition of wild type and the siderophore mutants ΔSidF and ΔSidH. The growth rate for the wild type under iron-replete conditions has been set as 100. p-values were calculated for the differences between mutant and wild-type growth rates, using a one-tailed, independent two-sample t-test that assumes equal variances for the two sample sets. Growth rates that differ from the wild type under that condition with $p < 0.05$ have been bolded.

Iron source	**OD**	**WT growth rate**	**ΔSidH growth rate**	**ΔSidH p-value**	**ΔSidF growth rate**	**ΔSidF p-value**
Fe+	1	100.00	98.44	0.361	90.83	0.109
14 nM $FeCl_3$	1	64.14	**56.24**	**0.001**	65.07	0.371
14 nM $FeCl_3$	0.1	65.16	55.20	0.100	71.23	0.226
14nM $FeCl_3$ 28 nM DFB	1	62.62	**55.34**	**0.001**	60.01	0.227
14 nM $FeCl_3$ 28 nM DFB	0.1	58.08	49.98	0.051	61.54	0.349
14 nM FeO	1	59.40	53.75	0.053	59.50	0.486
14 nM FeO 28 nM DFB	1	61.31	**46.86**	**0.024**	64.04	0.166

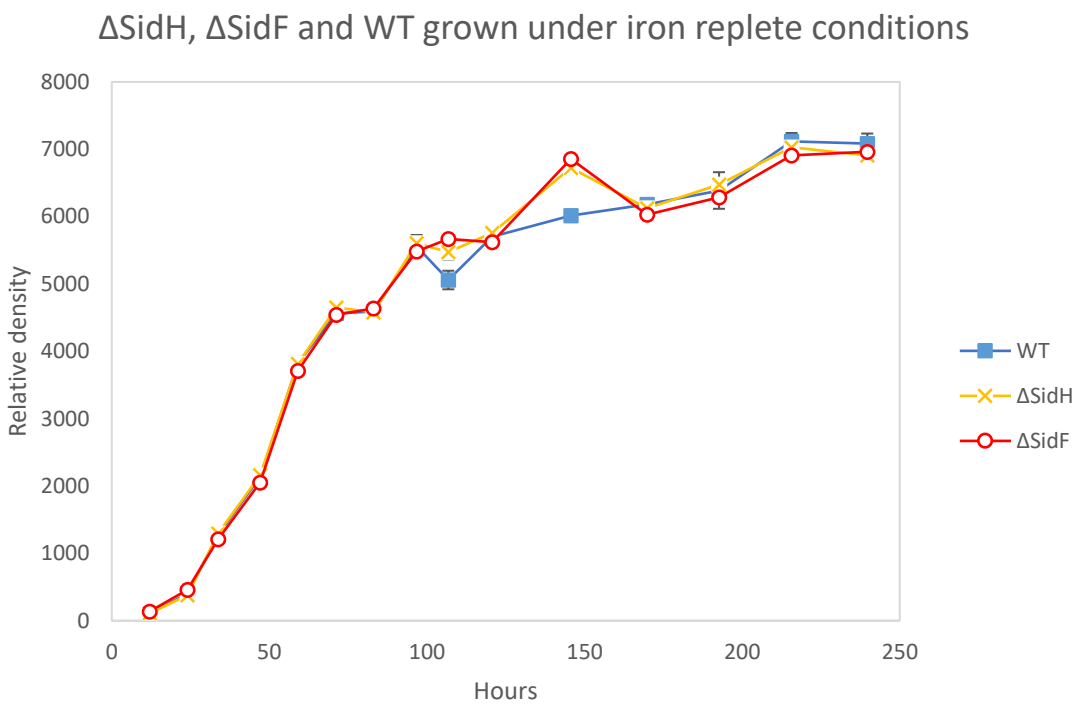

Figure 23: Averaged growth curves for triplicates of WT and the siderophore mutants ΔSidF and ΔSidH. Grown from cultures of OD_{730} = 1, under iron-replete conditions (1400nM $FeCl_3$). Standard error for each data point shown.

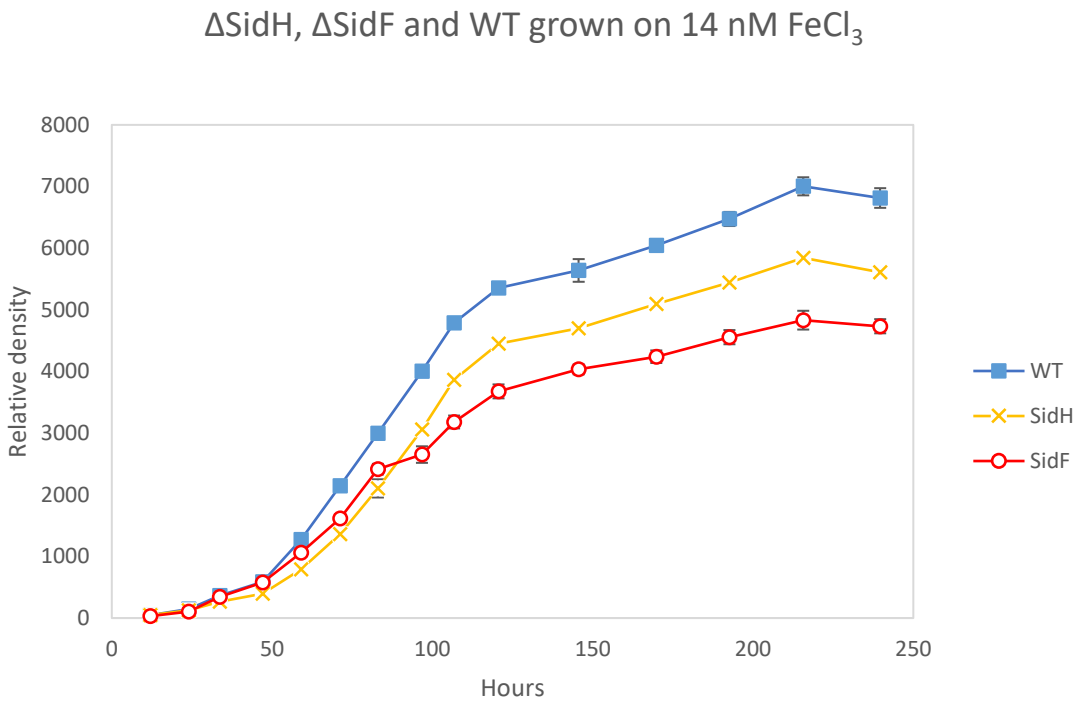

Figure 24: Averaged growth curves for triplicates of WT and the siderophore mutants ΔSidF and ΔSidH. Grown from cultures of OD_{730} = 0.1, on iron concentrations of 14nM $FeCl_3$. Standard error for each data point shown.

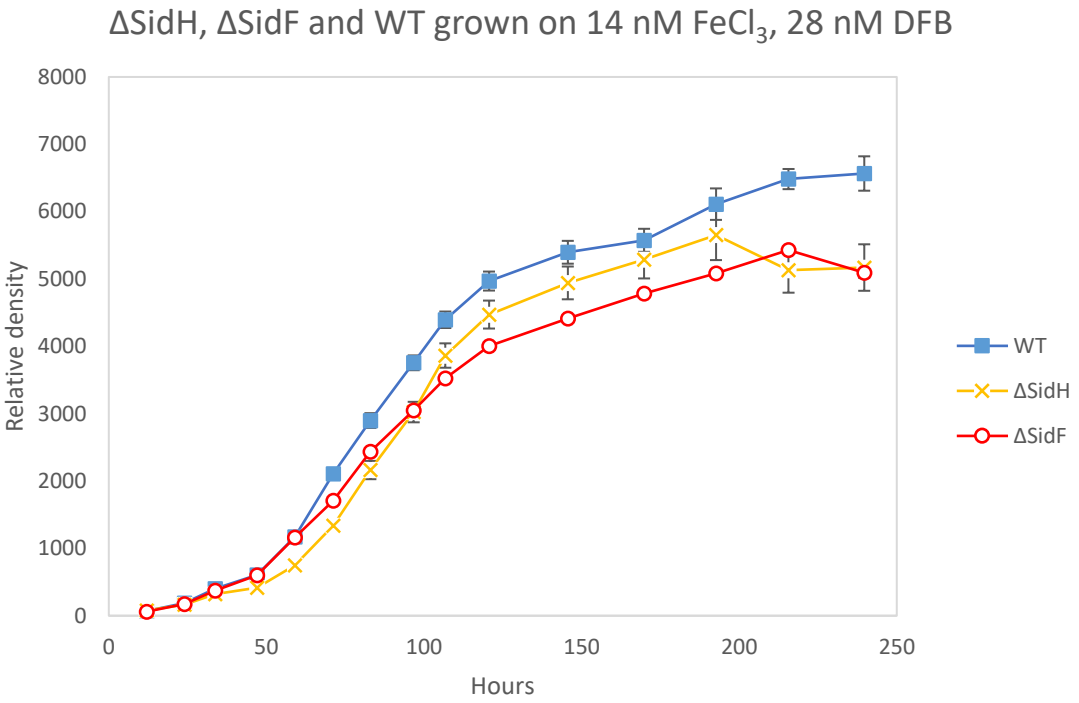

Figure 25: Averaged growth curves for triplicates of WT and the siderophore mutants ΔSidF and ΔSidH. Grown from cultures of OD_{730} = 0.1, on iron concentrations of 14nM $FeCl_3$ with 28nM DFB. Standard error for each data point shown.

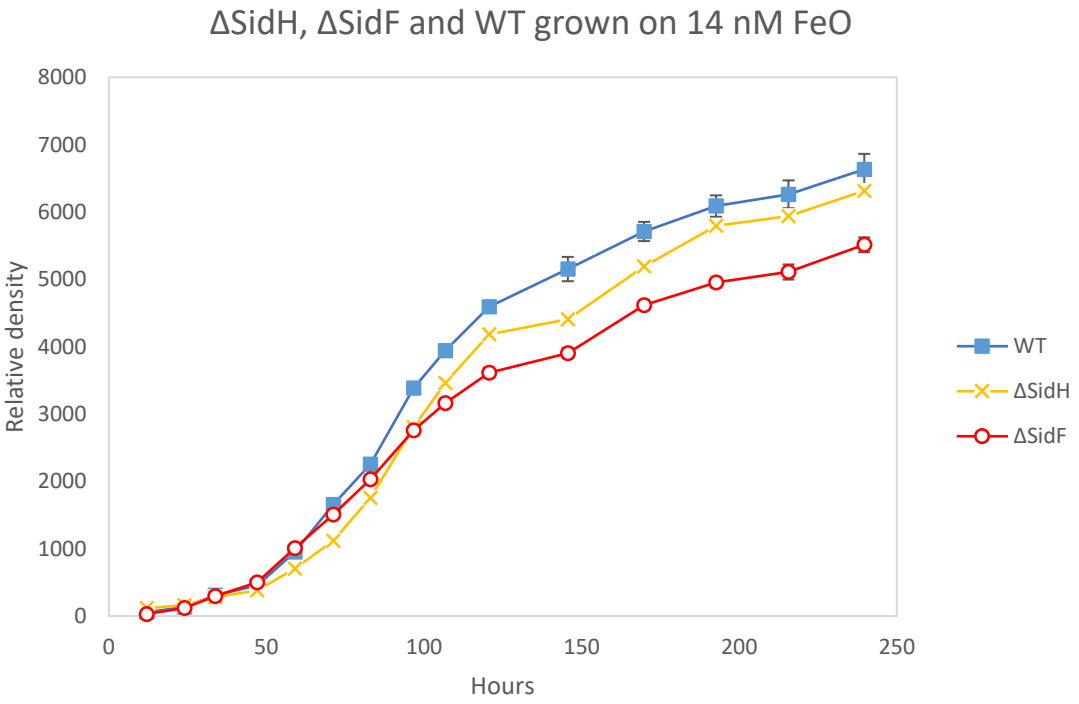

Figure 26: Averaged growth curves for triplicates of WT and the siderophore mutants ΔSidF and ΔSidH. Grown from cultures of OD_{730} = 0.1, on iron concentrations of 14nM FeO. Standard error for each data point shown.

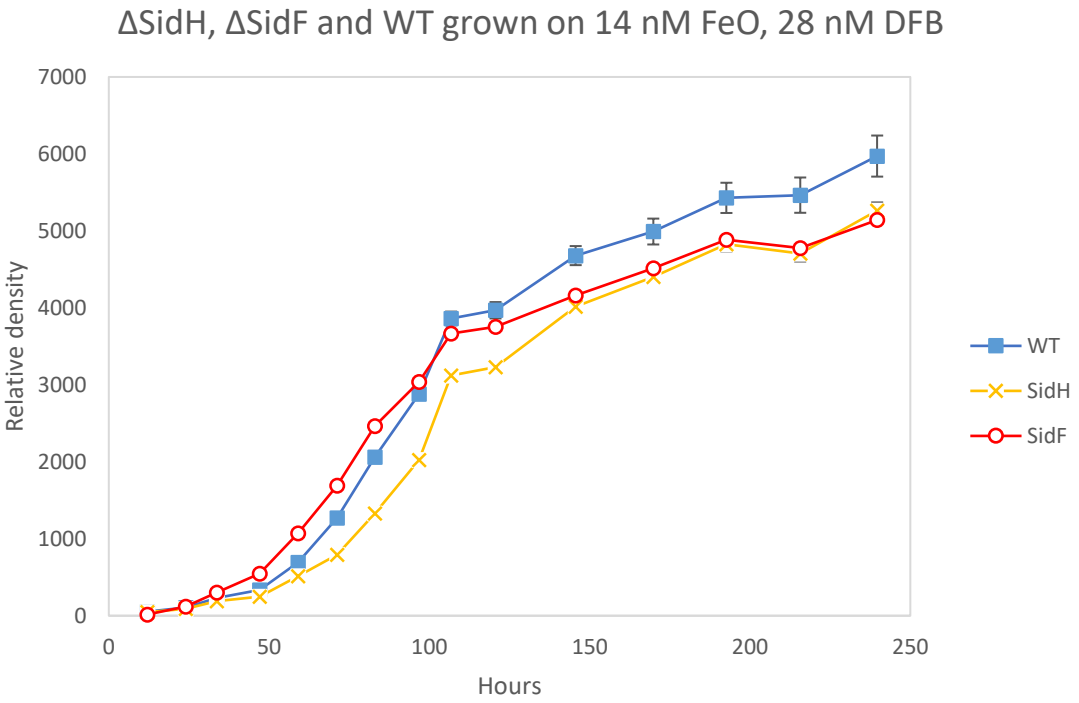

Figure 27: Averaged growth curves for triplicates of WT and the siderophore mutants ΔSidF and ΔSidH. Grown from cultures of OD_{730} = 0.1, on iron concentrations of 14nM FeOwith 28nM DFB. Standard error for each data point shown.

6.3 Results of whole cell absorption spectra

To evaluate the response to iron stress, whole cell absorption spectra were recorded for all deletion mutants and the wild type under both iron deprivation (7 nM $FeCl_3$, 14 nM DFB) and iron-replete conditions (1400nm $FeCl_3$).

For the iron-replete conditions, ΔC_M shows lower pigment production than the WT, as seen in figure 28. The spectra are essentially identical between the wild type, ΔFutB, ΔSidF and ΔSidH, as can be seen in figure 29 and figure 30. While the spectra measurements were made in triplicate, one representative spectra is shown for each strain.

The relative amount of carotenoids to chlorophyll is an indicator of cell stress, and is calculated from the 435nm/680nm absorbance ratio. This ratio was calculated for each strain under iron-replete conditions, and is shown with standard errors in figure 31. WT, ΔFutB, ΔSidF and ΔSidH all have a ratio of around 1.9. ΔC_M has a ratio of 1.8.

For the iron depleted conditions, sample spectra are shown in figure 32 to figure 34. The mutants general show lower pigment production than the WT. This effect is more pronounced in ΔFutB and ΔC_M (figure 32 and figure 33) than it is for the siderophore mutants (figure 34) The carotenoids/chlorophyll ratio is shown in figure 35, where all strains show higher ratios in iron restricted conditions compared to iron-replete conditions. The deletion mutants all show higher 435nm/680nm absorbance ratio than the WT. The difference is within standard error for ΔSidF and ΔSidH, while both ΔFutB and ΔC_M show significant deviations from the ratio of the WT.

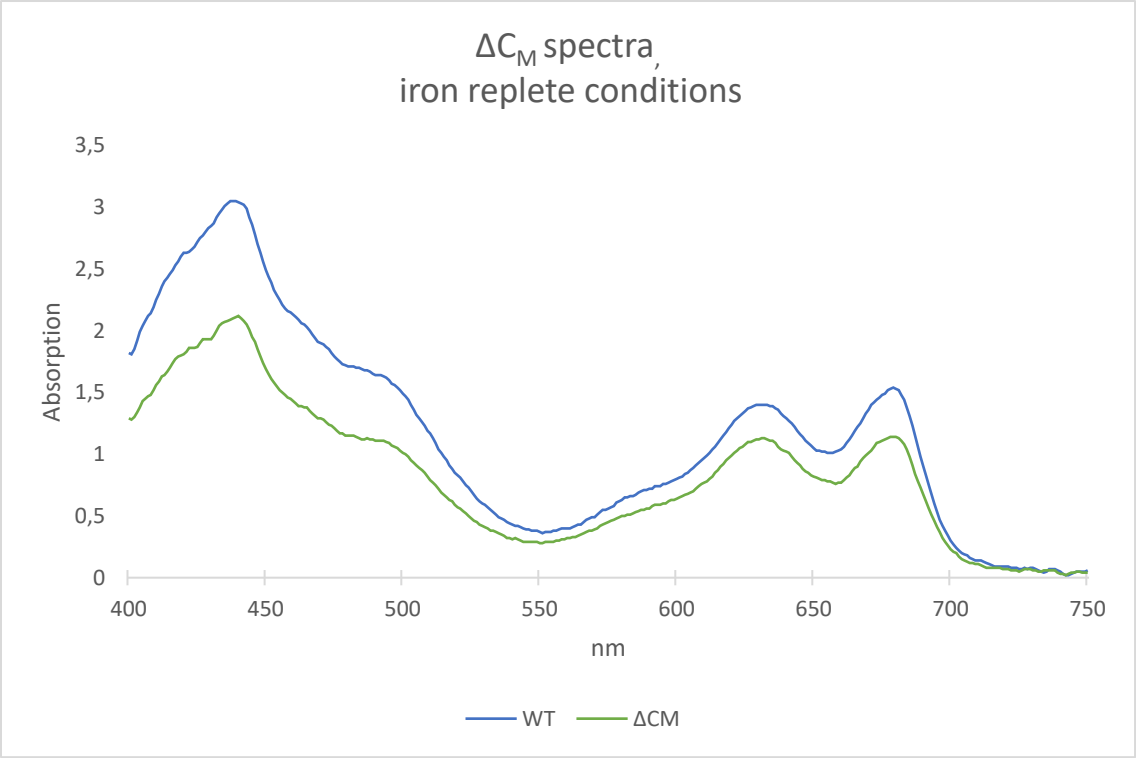

Figure 28: Absorption spectra for ΔC_M and WT grown under iron-replete conditions (1400nM $FeCl_3$). Measurements were made at OD_{730} = 0.3, and have been baseline subtracted at 800nm. Note the lower pigment production of ΔC_M compared to WT.

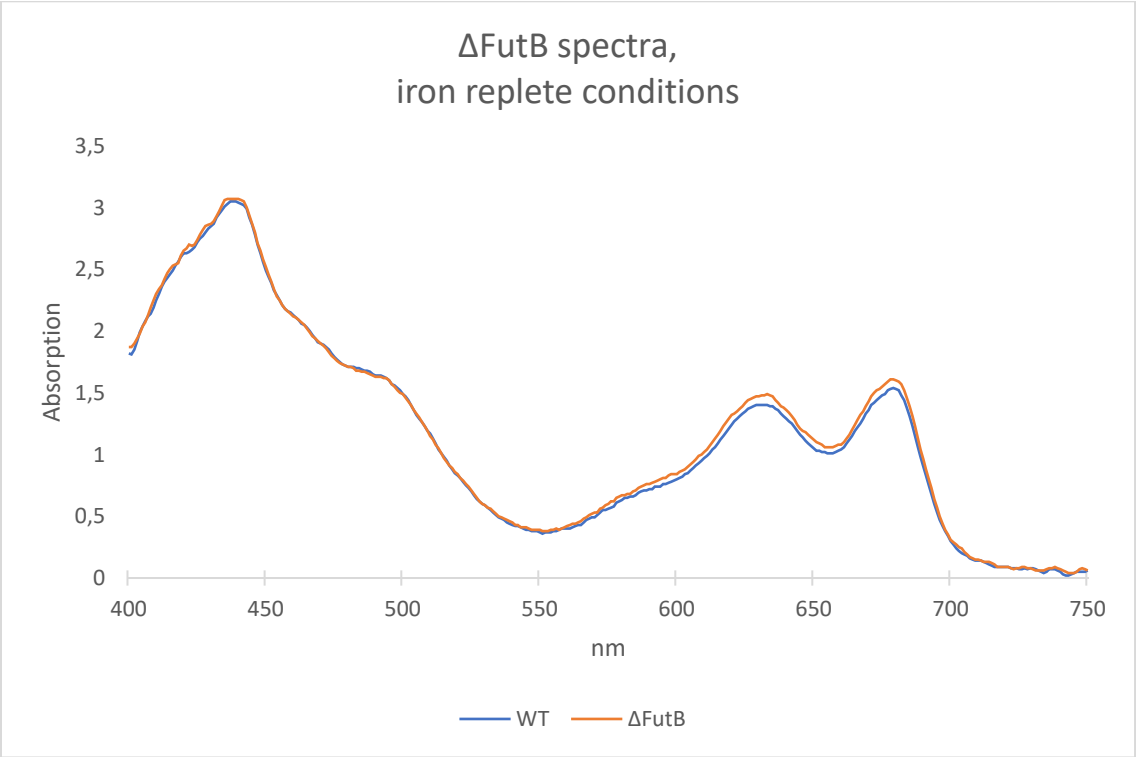

Figure 29: Absorption spectra for ΔFutB and WT grown under iron-replete conditions(1400nM $FeCl_3$). Measurements were made at OD_{730} = 0.3, and have been baseline subtracted at 800nm. The two spectra are essentially identical.

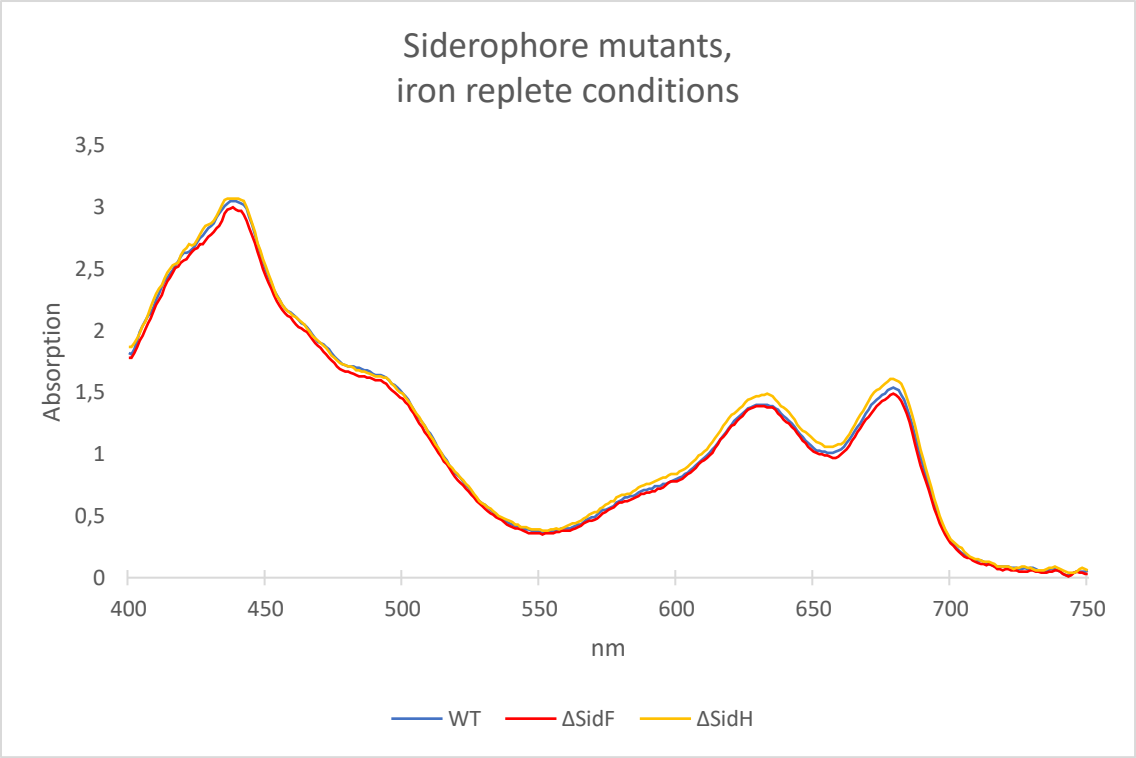

Figure 30: Absorption spectra for ΔSidF, ΔSidH and WT grown under iron-replete conditions (1400nM $FeCl_3$). Measurements were made at OD_{730} = 0.3, and have been baseline subtracted at 800nm. The three spectra are essentially identical.

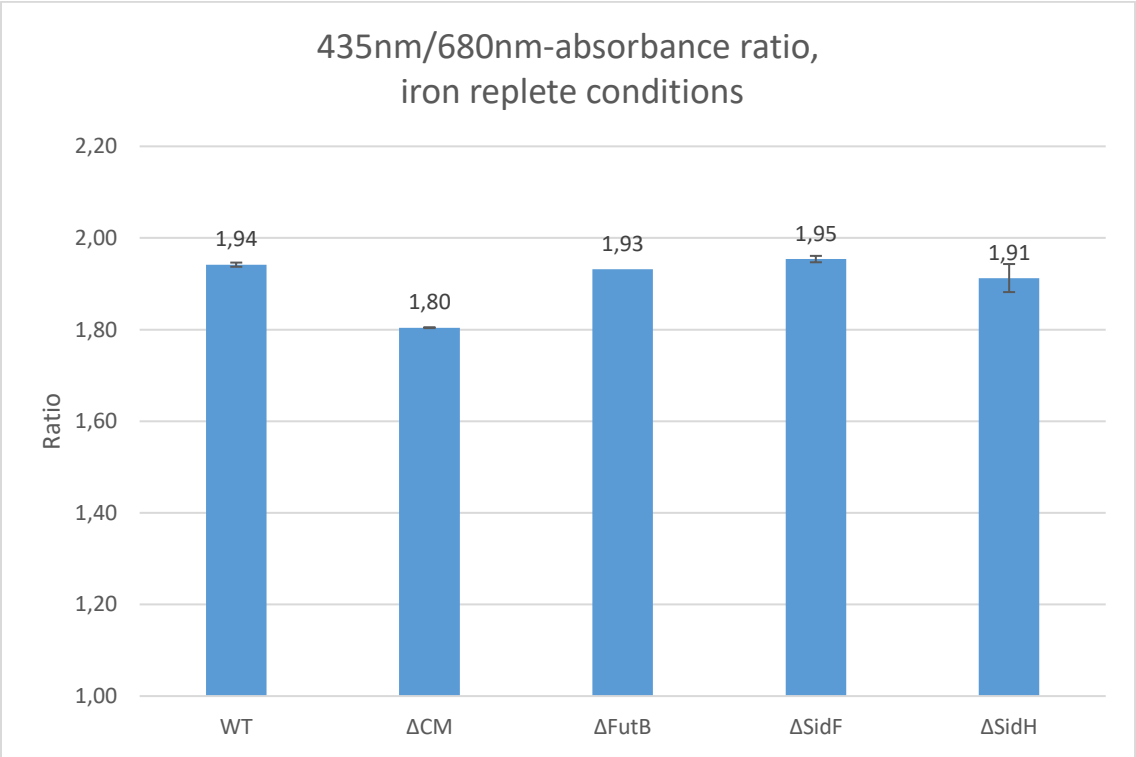

Figure 31: Relative carotenoid/chlorophyll ratio for all deletion mutants and WT grown under iron-replete conditions. Cultures were measured at OD730 = 0.3, and baseline subtracted at 800nm. Standard error of triplicate measurements shown. Only one measurement was made for ΔFutB.

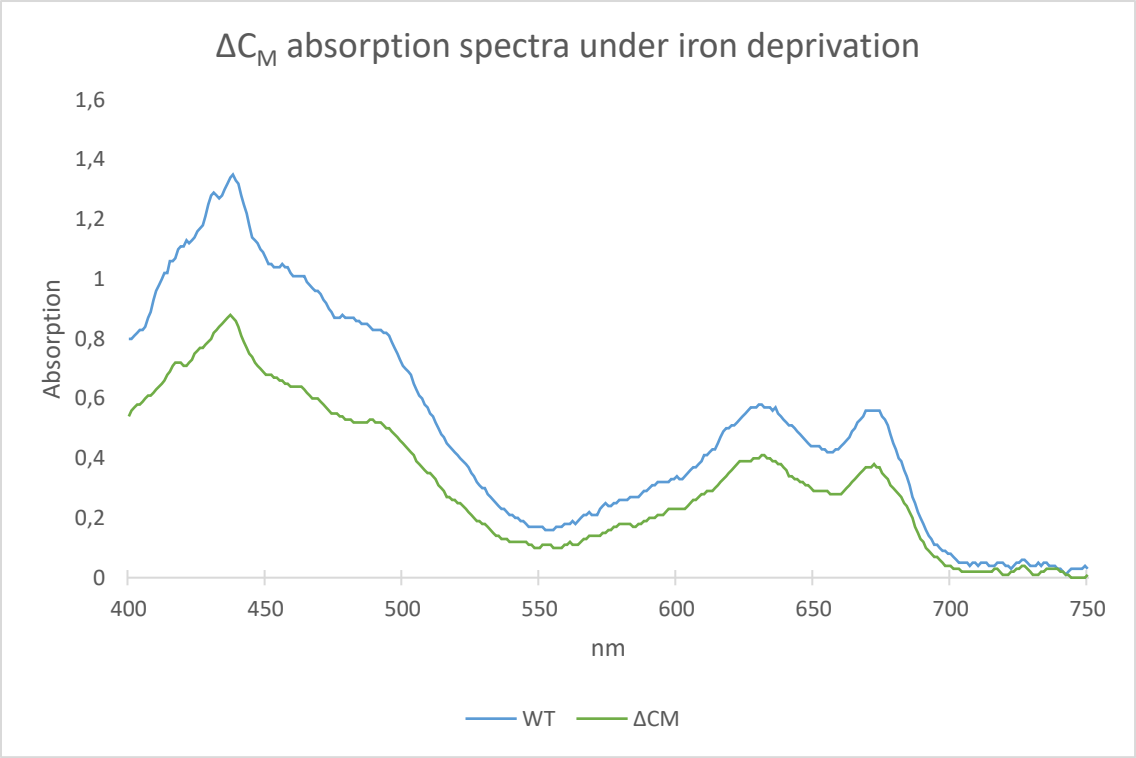

Figure 32: Absorption spectra for ΔC_M and WT grown under iron-deprived conditions (7 nM $FeCl_3$, 14 nM DFB). Measurements were made at OD_{730} = 0.3, and have been baseline subtracted at 800nm. Note the lower pigment production of ΔC_M compared to WT, as well as the difference in relative peak height between 435nm and 680nm.

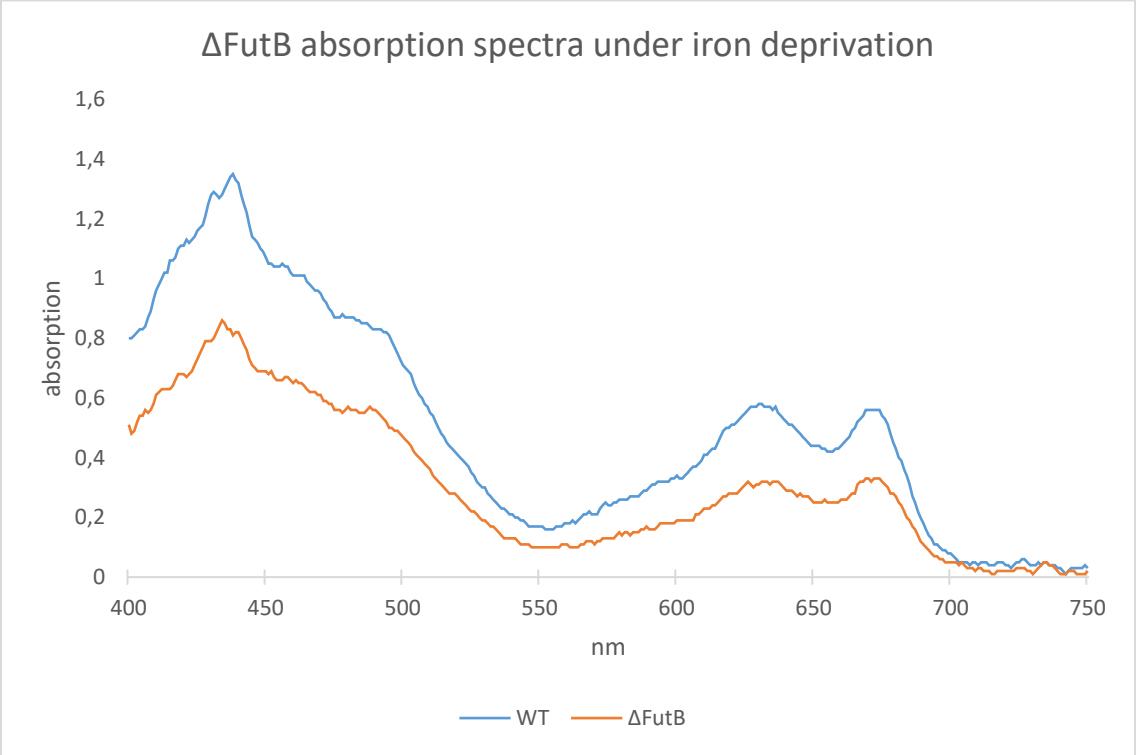

Figure 33: Absorption spectra for ΔFutB and WT grown under iron-deprived conditions (7 nM $FeCl_3$, 14 nM DFB). Measurements were made at OD_{730} = 0.3, and have been baseline subtracted at 800nm. ΔFutB shows lower pigment production than the WT, and higher relative difference between the peak at 435nm and 680nm.

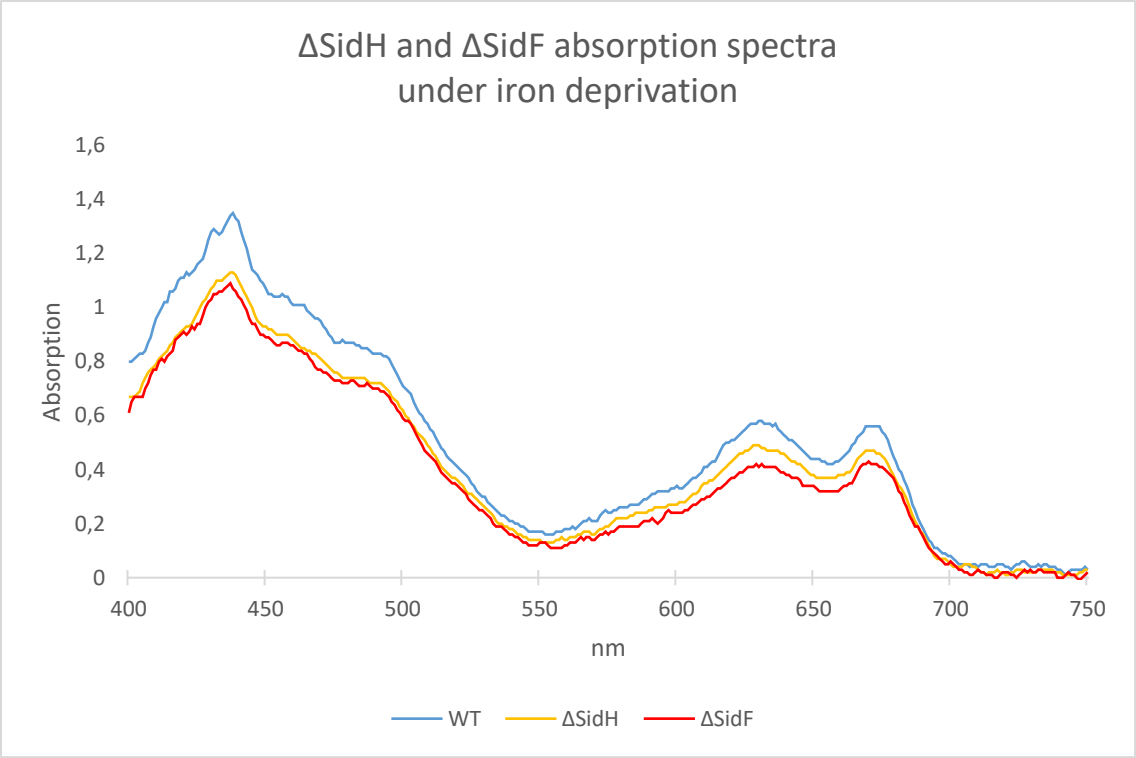

Figure 34: Absorption spectra for ΔSidF ΔSidH and WT grown under iron-deprived conditions (7 nM $FeCl_3$, 14 nM DFB). Measurements were made at OD_{730} = 0.3, and have been baseline subtracted at 800nm. The siderophore mutants exhibit generally lower pigment production than the WT.

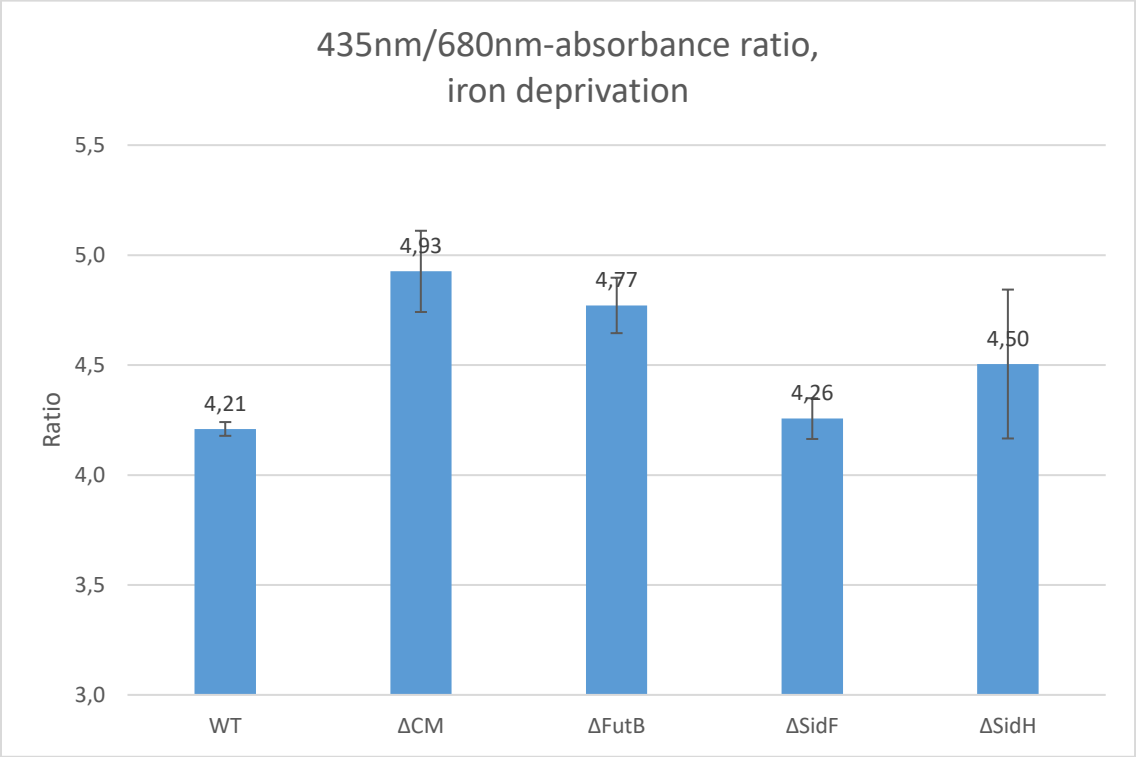

Figure 35: Relative carotenoid/chlorophyll ratio for all deletion mutants and WT when grown under iron deprivation (7 nM $FeCl_3$, 14 nM DFB). Cultures were measured at OD730 = 0.3, and baseline subtracted at 800nm. Standard error of triplicate measurements shown

6.4 O-CAS assay

Results for the O-CAS assay, which indicates the presence of siderophores, are shown in table 16 for the WT and the two siderophore mutants ΔSidF and ΔSidH. Two different runs of medium were made for the experiment, one for the plates containing 1.4nM ferrous oxide, and one for the iron-replete (1400nM $FeCl_3$) and 1.4 nM goethite. In general, the results were clearer for the ferrous oxide-plates. Because of this, pictures from this run is shown in figure 36, figure 37 and figure 38. Note that the positive assay-result might be difficult to spot in the assay for the WT in figure 38.

Table 16: Overview of O-CAS assay result for different mutants and iron conditions. The plates were evaluated qualitatively, with "0" indicating no visible assay result, "+" a small positive assay result, and "++" a larger circle around the colony.

Strain	Iron condition	Assay after 16 hours	Assay after 72 hours
WT	Fe+	0	+
WT	1.4 nM goethite	+	+
WT	1.4 nM ferrous oxide	+	+
ΔSidF	Fe+	0	+
ΔSidF	1.4 nM goethite	++	++
ΔSidF	1.4 nM ferrous oxide	++	++
ΔSidH	Fe+	0	+
ΔSidH	1.4 nM goethite	++	++
ΔSidH	1.4 nM ferrous oxide	++	++

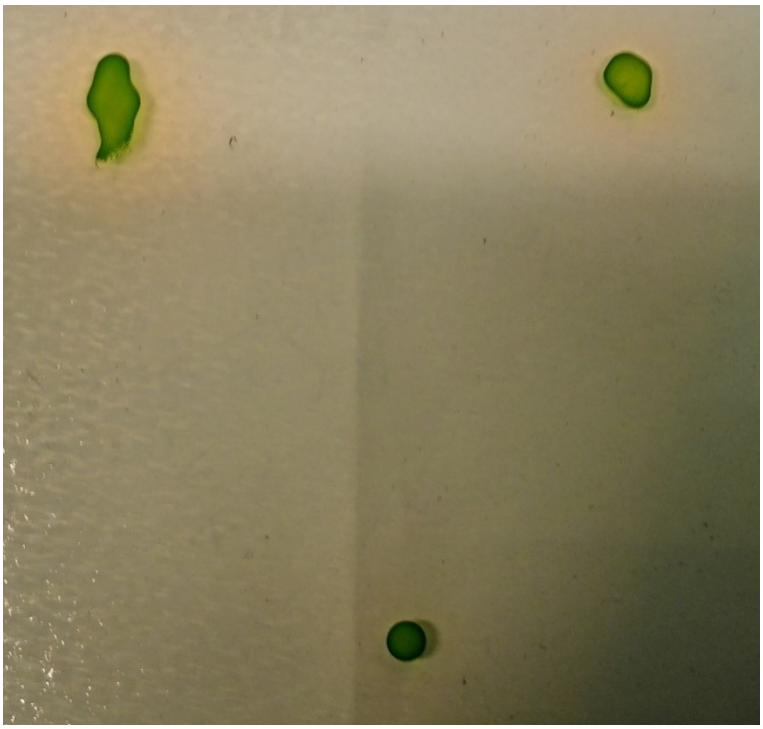

Figure 36: Positive assay-indication for ΔSidF grown on 1.4 nM FeO, shown as yellow circles surrounding the colonies. Note the disproportionally larger assay indication in the top two colonies, where the cells have been slightly misspotted.

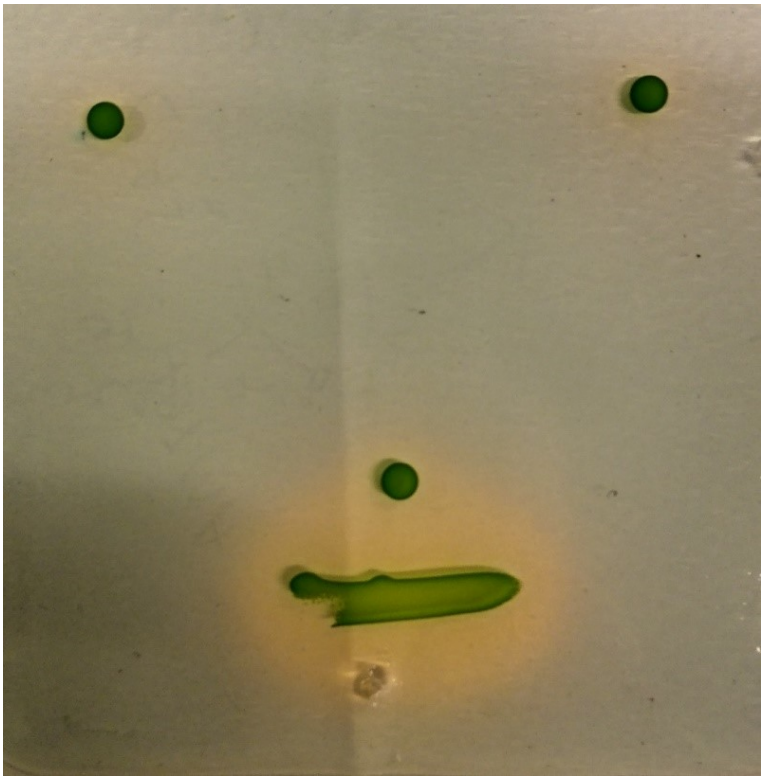

Figure 37: Positive CAS-assay-indication for ΔSidH grown on 1.4 nM FeO, shown as yellow circles surrounding the colonies.

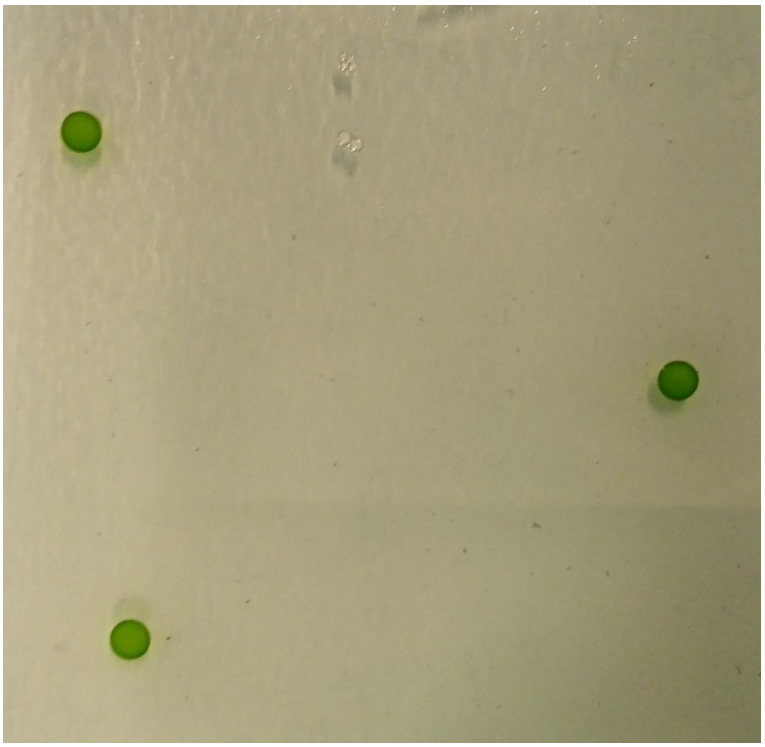

Figure 38: WT grown on 1.4 FeO showing small siderophore indication on O-CAS-assay. It is possible to see faint yellow outlines surrounding the colonies, particularly the lower left colony.

7 Discussion

7.1 Creation and verification of deletion mutants

7.1.1 Transformation by homologous recombination

The transformation protocol used in chapter 5.3.1 relies on creating deletion mutations by homologous recombination. Linear DNA sequences were designed that contain antibiotic resistance cassettes flanked by the DNA sequences directly upstream and downstream from the gene of interest. When these sequences are applied to WT cells, the antibiotic resistance cassette and the gene of interest can change places through the process of homologous recombination, resulting in a cell losing the gene of interest, and gaining antibiotic resistance.

For *Synechococcus 7002*, natural transformation is used, with a protocol similar to what has been found to be optimal in *Synechocystis 6803* (Zang et al. 2007) . However, this protocol has not been optimized for *Synechococcus 7002*, and it is possible other transformation methods could work better. Changing factors such as DNA concentrations, overlapping sequence length, incubation times temperatures, or pretreatment with chemicals could lead to higher transformation efficiency.

While the protocol as described works well for most transformations, it was difficult to obtain transformants for the siderophore gene deletions. After four failed transformation attempts using a deletion sequence with 200bp overlaps upstream and downstream from the gene of interest, new sequences were ordered with 500bp overlaps. Transformation was successful with these sequences, but the transformation efficiency was orders of magnitude lower than for the ΔFutB-transformation. The most likely explanation for this difficulty appears to be that the siderophore genes are located on the pAQ7-plasmid, which in an intractable way impacts the transformation process negatively compared to deletions of genes located on the chromosome. Experimental error or the fitness of the deletion mutants are other possible reasons for this difficulty, but the number of attempts made and the behavior of the siderophore mutants in the later experiments weaken the credibility of such explanations. As *Synechococcus 7002* contains seven plasmids with roughly 400kbp of genetic material in total, note of this difficulty should be taken for future work.

7.1.2 Modification of transformation protocol

A possible refinement of the protocol involves skipping the step where the volume of cells is transferred first to nonselective AA+ plates, and grown on these for one day before moving the colonies to selective AA+ plates. Instead choosing to grow the cells directly on selective plates lowers the transformation efficiency significantly, but saves time and money, as there is no need for expensive sterile filters to enable transfer of colonies from non-selective to selective plates. For many applications, this adjusted protocol has sufficient transformation efficiency.

7.1.3 Verification of transformants

As bacteria can have multiple copies of their bacterial chromosome and plasmids, it is necessary to verify that the deletion mutation has been implemented in all copies of the gene in question. Colony PCR can be used to check whether there still exist copies of the WT gene, either as extra copies in transformed bacteria, or as contamination with WT cells. The method relies on using primers outside of the area affected by the transformation, enabling amplification regardless of whether an antibiotic resistance cassette insertion was made or not. By checking with gel electrophoresis whether colony PCR results in two products (antibiotic resistance + original gene) or just one (antibiotic resistance), one can verify complete segregation.

As can be seen in figure 7, figure 8, figure 9 and figure 10, complete segregation was achieved for ΔFutB, ΔC_M, ΔSidF and ΔSidH. In addition to being necessary for further experiments, the possibility of achieving complete segregation shows that none of the genes are necessary for survival under the iron-replete growth conditions used.

7.2 Discussion of growth experiments

7.2.1 Experimental issues

Originally, several more plates containing different iron sources and concentrations were made than the ones shown in table 11 for ΔFutB. However, a problem with tearing of the parafilm used to seal the plates caused some the plates to dry out. It is not clear what caused this issue, as the tearing was experienced by other members of the lab as well. The result was that several of the plates had to be discarded, including plates using goethite as an iron source, and plates without any iron added.

7.2.2 Data processing

The grofit package allows fitting growth curves data to a variety of different models. It automatically chooses whatever growth model fits best for the given dataset, including gompertz' and Richards' growth models. For fitting a single dataset this flexibility would be ideal. However, if the intention is to compare growth rates between many growth series, using a different model for each fit would introduce unwanted inconsistency. Inspection of the model fits and the standard error for each growth curve revealed that the logistic model in general gave the best fit for most models. This was therefore chosen as the model to be applied to all data series.

The standard errors of the mean for the growth rates shown in the results section gives an indication of the variability within each triplicate. However, it does not indicate how good each model fit is. Theoretically, all three models for a triplicate could be poor fits with the data, but still return growth rates that are relatively close to each other. The resulting low standard error would conceal that the underlying data is of low quality. To alleviate this problem, the quality of each model was evaluated individually, using the ratio of the growth rate/model standard error as a measure of quality. If one of the models in a triplicate had a ratio of 12 or lower, the whole triplicate was left out of the results. The choice of a ratio of 12 as the cutoff is arbitrary. The models which returned clearly poor fits, based on inspection of model graphs, had ratios between 5 and 10. As the individual models which had low ratios tended to group together, changing the ratio had limited impact: Most values close to the cutoff were neighbored by models with lower ratios. It is worth noting that the growth curves made from spots starting at $OD_{730} = 0.01$ were universally of poor quality, and were not used for further analysis. The reason for this effect is not clear, but latter experiments did not use this dilution.

As the methodology for data processing adopted in this thesis might appear needlessly complicated, it is worth commenting on the reasoning for creating a separate model to calculate growth rate for every colony. A more intuitive approach would have been to average the density of the three parallel colonies at each timepoint, and to calculate the growth rate from the average growth-curve. This procedure would have lowered the amount of data processing dramatically. The problem with this simplified approach is that small variations in the amount of lag before the exponential phase starts would artificially lower the growth rate calculated. If two logistic curves that do not undergo exponential growth at the same time is averaged, the result is a logistic curve with a lower growth rate than each curve calculated individually. This artifact is avoided by calculating growth rates for individual colonies. The average of the three colonies is shown in the growth curves, which therefore are influenced by this effect on the steepness of the exponential phase. However, the effect is relatively minor, and do not make a difference in the qualitative assessment of the growth curves.

Instead of using the calculated growth rates or doubling times, the results section indicates growth as a percentage of the growth rate of WT colonies grown under iron-replete conditions. The main reason for this choice is that the methodology used appears to give some variability in the numerical growth rate calculations. The radius of the circles designated as colony and background when making the image-series impacts the relative density measured for each colony at a given time point. This effect has close to no impact on the growth curves, as one only compares growth curves of colonies grown on the same plate, and thus the same image series. However, when using grofit to calculate the growth-rates, the absolute numbers supplied to the script appears to have some effect on the growth rate calculated. To make growth rate numbers comparable between image stacks, the densities were normalized by the factor between maximum density of the given image stack and the maximum density of the WT colonies grown under iron-replete conditions. This method ensures that the numbers are comparable to each other, but they do not reflect any objective growth rate, as the normalization standard is arbitrary. While the outputted growth rate numbers appear reasonable, giving doubling times in the scale of roughly 8 to 11 hours, using these numbers would be misleading.

To show statistical significance for the difference in growth-rates between WT and mutants, p-values were calculated. As it seems unreasonable to expect higher growth in the mutant cells than in the WT, a one-tailed calculation was used. The variance between samples is assumed to stem from the methodology of the experiment, leading to equal variance between

the WT and mutant sets. In sum, the p-values were calculated using a one-tailed, unpaired samples t-test that assumes equal variances for the two sample sets.

7.2.3 Iron contamination as an error source

Controlling iron concentration to a high degree of precision requires a clean room environment. This was not available for the experiments conducted in this thesis. It is therefore likely that trace amounts of iron have been introduced into the growth medium. Previous experience in the lab group has shown that it is possible for *Synechococcus 7002* to grow without any iron added to the medium, presumably due to some degree of contamination. Possible sources for contamination includes lab equipment and trace iron found in the compounds used to make growth medium. It is also possible that the washing process used when moving cells from iron-replete medium to the experimental conditions is not sufficient to remove excess iron. The cells are washed in an iron-free medium three times before transfer, but how effective this process is have to my knowledge not been tested. In addition, the washing process only removes iron in the medium, presumably leaving intracellular iron intact.

If iron contamination made the iron amounts added insignificant, one would expect that no clear difference could be shown in growth between different iron sources. Essentially, all growth conditions would be equal to the iron-replete conditions. This is not the case, as clear differences in growth between the different iron sources can be seen. While this indicates that iron contamination is not an issue that invalidates the data, it remains unclear to what degree iron contamination impacts the results found.

The difference in growth rates between the WT under iron limitation and iron-replete conditions give a possible indication of the degree of contamination of different iron sources with other iron species and contamination of iron contained in the trace minerals that are part of all growth media. Comparing the growth rates calculated for the WT in the ΔFutB growth experiment (figure 11) to the growth rates calculated for the ΔC_M growth experiment (figure 16) reveal large differences. While the difference between iron limited and iron-replete is relatively small for the ΔFutB-experiment, the iron limited WT has roughly 40% lower growth rate in the ΔC_M-experiment. The implication is that there is a larger amount of iron contamination in the ΔFutB-experiment than there is in the ΔC_M growth experiment.

The addition of the iron chelator desferroxamine B (DFB) to the medium is a way to limit the concentration of available iron. This would also effectively remove portions of the iron added

through contamination. DFB was added in two of the experimental conditions, both indicating through slower growth that *Synechococcus 7002* cannot make use of iron chelated to DFB. Preliminary experiments also revealed that *Synechococcus 7002* cannot grow on high concentrations of DFB (100nM), indicating that some availability of iron is indeed necessary for growth (data not shown).

7.2.4 Implications of ΔFutB results

The results for the growth experiments on ΔFutB (chapter 6.2.1) indicate some role for *futB* in regulation of iron uptake, showing a clear difference between ΔFutB and WT when grown under iron limitation. However, unexpected results regarding cells grown on Fe(II) oxide makes verifiying the exact function of *futB* difficult.

For cells grown under iron-replete conditions, the growth rates of the wild type and ΔFutB are less than half a percentage point apart, showing no statistically significant difference, as can be seen in figure 11. The lack of a phenotypical difference under these conditions can also be seen in the growth curve in figure 12. In the context of the results under other iron concentrations, this result implies that FutB has some role in iron uptake. If all experimental conditions revealed growth differences between WT and ΔFutB, non-iron-related functions of FutB could not be ruled out. The implication of this result is that any iron-uptake role FutB might have is redundant under iron-replete conditions, as other uptake mechanisms are presumably able to ensure sufficient iron uptake. As the iron concentration used, 1400 nM $FeCl_3$, is between 1000-10 000 times higher than what can be found in the ocean, this result is as expected.

There is a small difference in growth rates for cells grown on 1,4 nM $FeCl_3$, as the mutant cells grow slightly slower. The difference is not statistically significant for cells grown from OD_{730} = 1 nor OD_{730} = 0,1, as can be seen in table 13. Given that both ODs show a difference between ΔFutB and WT, and that both strains grow more slowly than under iron-replete conditions, it is likely that this effect is due to ΔFutB having some impact on growth under iron limitation. However, due to the size of the standard error compared to the relatively small difference in growth, this result cannot be used to confirm any hypothesis on the role of ΔFutB.

Cells grown on 14 nM $FeCl_3$ supplied with 28 nM DFB show a clear and statistically significant difference in growth rate between WT and mutant cells (table 13). WT and mutant cells grow between 13% - 27% slower than cells grown under iron-replete conditions,

indicating the impact of iron limitation on growth for both strains. The negative impact on growth rates is 6-8 percentage points larger ΔFutB than the WT, indicating that the loss of function of this gene impacts the cells ability acquire iron. The growth curve shown in figure 14 does not follow a clear logarithmic pattern, with one phase of exponential growth. Instead, there appears to be two phases of growth: One phase of rapid growth from 12 to 76 hours, and a second phase of slightly slower growth from 76 to 160 hours, before reaching the stationary phase. The explanation for this growth curve is not clear. A possible explanation is that the cells are using two different sources of iron. After making use of all the easily available iron, the cells must make use of more difficultly available iron sources, causing slower growth.

A difference between WT and ΔFutB can also be seen when cells are grown on 1.4 nM Fe(II) oxide. Both cells grown from OD_{730} = 1 and OD_{730} = 0.1 show slower growth for the ΔFutB , but this result is only statistically significant for the cells grown from OD_{730} = 1 (table 13, figure 15). As the FutB-protein is expected to work as a Fe(III)-transporter, it is unexpected that there would be any difference between the WT and ΔFutB when cells are grown on Fe(II). There are two possible explanations for this discrepancy. The most likely explanation appears to be iron contamination. Prior experience in the lab indicate that cells grow slowly when supplied Fe(II) oxide as an iron source. As such, it might be that much of the iron used by the cells stem from contamination, where the ability to transport Fe(III) would be important. The other explanation is that FutB can transport both Fe(II) and Fe(III). The results obtained here cannot distinguish between these two explanations. A possible way to test this would be to grow WT and ΔFutB on Fe(II) oxide supplied with large amounts of DFB. As an iron chelator, DFB binds only Fe(III), ensuring that the only iron uptake available to the cells would be Fe(II).

In conclusion, the results confirm a role for *futB* in iron uptake. The decreased growth rate when grown on Fe(II) might imply a slightly different function than in *Synechocystis 6803*, where it functions as a Fe(III)-transporter. However, possible residual contamination of iron make this result uncertain.

7.2.5 Implications of ΔC_M growth study results

The results of the growth study on ΔC_M (chapter 6.2.2) compared to the WT reveal some unexpected results. The calculated growth rate of ΔC_M is shown to be 33-35% lower than the growth rate of the WT when grown under iron-replete conditions, a statistically significant result (table 14).

When the cells are grown under different iron limitation conditions, WT and ΔC_M are close to each other in terms of growth rate, with differences generally statistically insignificant.

Since C_M was hypothesized to be part of pili-mediated iron reduction, the expected result of the growth experiment was that the deletion of C_M would have little impact on cells grown under iron-replete conditions, but retard growth when cells are grown under iron limitation. The actual results come close to a full reversal of the expected results. It appears that C_M has a phenotypic effect when cells are not under iron deprivation, where it enables higher growth. For iron deprived cultures, the effect of C_M is more limited. While iron deprived ΔC_M appears to have the same growth rate as the WT, the strain does not grow to the same density as the WT, as can be seen in Figure 18 to figure 21.

Strains grown from $OD_{730} = 1$ on 14 nM FeO show a statistically significant lower growth rate for ΔC_M than the WT. This result is an interesting outlier. The same iron availability reveal the opposite result when $OD_{730} = 0.1$-cultures were used, although this result is not statistically significant. One could argue that denser colonies use more iron, thereby decreasing the iron available to each cell. However, it is not possible to see this effect in the other variations of the experiment. The incongruence of the two results limits the importance one can attach to them.

It is difficult explain the result of the experiment in a convincing fashion. Metaphorically, C_M appears to be a fair-weather friend, enabling faster growth under favorable iron conditions, but with limited effect under iron deprivation. Deleting C_M results in a strain that has a growth pattern under iron-replete conditions similar to the WT under iron limitation. This result is incongruous with the regulatory pattern of C_M, as the gene is upregulated under iron limitation (Ludwig and Bryant 2012a). It is also unexpected that the growth patterns for ΔC_M appear to be similar to WT for cultures grown on $FeCl_3$ (Figure 18 and figure 19) and FeO (figure 20 and figure 21.). If C_M works to reduce Fe(III) to Fe(II), one would expect the impact of a deletion to be larger on cells grown on the Fe(III) present in $FeCl_3$, than on the Fe(II) in FeO.

It is possible that the lack of a difference between iron sources can be ascribed to iron contamination.

7.2.6 Implications of siderophore growth study results

Growth characteristics of the siderophore deletion mutants compared to the wild type (chapter 6.2.3) reveals an effect on the growth rate under iron limitation, but only for ΔSidH. ΔSidH has roughly 15% lower growth rate than the WT across the four different iron limitation conditions (table 15, figure 23). The effect size varies to some extent, but not in a consistent fashion along iron source or whether iron availability is further reduced by the iron chelator DFB. When ΔSidH is grown under iron-replete conditions, the growth rate is similar to the WT.

For ΔSidF, there is no statistically significant difference in growth rate compared to WT under any iron availability. There is no clear pattern in the small deviations the ΔSidF-growth rates makes from the WT growth rates.

The growth curves shown in figure 24 to figure 27 reveal that both siderophore mutants grow to slightly lower densities than the WT colonies when grown under iron limitation. The difference between mutant and WT is slightly larger for ΔSidF than for ΔSidH. It is not possible to distinguish any significant difference in growth patterns when considering iron source or the presence of the iron chelator DFB. Under iron-replete conditions, the growth curves are essentially identical for all three strains (figure 23).

The results of the growth study support that *sidH* has some role in iron uptake, even if the difference in growth rate between mutant and WT is small. As *sidH* is hypothesized to have a role in anchoring the siderophores to the cells, it is as expected that a deletion mutant for this gene would be limited in iron uptake, as siderophores would be spread further out into the solid medium, and thus not be as easily available for the colonies.

The similar growth characteristics of ΔSidF and WT in terms of growth rate is unexpected. The gene *sidF* is hypothesized to code from a siderophore transporter, but the lack of an effect for the *sidF* deletion mutation does not lend support to this hypothesis. Additionally, possible downstream deletion effects (discussed further in chapter 7.4.2) would imply that the phenotypic effect of the *sidF* deletion should be at least as strong as the *sidH*-deletion.

While it is possible that the hypothesis regarding *sidF* is wrong, experimental error could also have disrupted the results. As using antibiotics during the preparation for the experiment

could affect the results, all culture growth and washing steps are done without antibiotics in the media. Considering that all cultures are dealt with in succession when preparing the experiment, it is difficult to discount the possibility of cross-contamination. The risk of this error was demonstrated when preparing the growth experiment for ΔFutB. Originally, ΔC_M was also spotted onto the plates, but these colonies were later found by colony-PCR to have been contaminated by WT cells, rendering the results unusable. However, it is not clear how such an error could account for the lower density to which the ΔSidF colonies grow to compared to WT.

7.3 Discussion of absorption spectra

Whole cell absorption spectra give information about pigment content, an important physiological response in photosynthetic organisms. While whole cell absorption spectra can be used to reveal a plethora of information about a multitude of different pigments, in this thesis only two measures will be discussed. The first is the relative ratio of carotenoid to chlorophyll a, as measured by 435nm/680nm absorbance ratio, where a higher ratio can be taken as an indicator of iron stress or cell stress in general (see chapter 2.3.4). The other measure will be general pigment production, as indicated by the absorbance over the whole spectrum. The samples used in this experiment were normalized to $OD_{730} = 0.3$, ensuring that the intensity of absorption reflect general pigment production.

7.3.1 Implications of absorption spectra for ΔC_M

The ΔC_M absorption spectra for cells grown under iron-replete conditions shows lowered pigment production compared to the WT (figure 28). Lower pigment production can be taken as a sign of cell stress, as cells under stress are unlikely to be able to produce as many pigments as healthy cells. This result thus aligns well with the results for the ΔC_M growth study, which indicated lowered growth of ΔC_M compared to the WT under iron-replete conditions.

It is unexpected that the carotenoid/chlorophyll ratio is somewhat lower for ΔC_M than it is for the WT, as shown in figure 31. Cell stress is normally associated with increased carotenoid production, rendering this result incongruent with the generally lower pigment levels. As the difference between the ratio for WT (1.94) and ΔC_M (1.80) is quite small, it is not clear how much significance should be attached to this result.

A clear physiological response could be seen when ΔC_M and WT were grown under iron limitation, as seen in figure 32. Both strains show lower pigment production than under iron-replete conditions, with ΔC_M producing less pigments than the WT. Figure 35 shows that the carotenoid/chlorophyll ratio is significantly higher for ΔC_M (4.93) than the WT (4.21), indicating a larger degree of cell stress.

The implications of the absorption spectra for ΔC_M is not clear. Cytochrome C_M clearly plays some role under both iron-replete and iron-replete conditions. The results are aligned with the results for the growth study (chapter 6.2.2). While the larger difference between ΔC_M and WT under iron limitation implies some role under iron limitation, it is possible that ΔC_M functions in an entirely unrelated cellular process. The additional stress response from ΔC_M seen under iron limitation could thus be related to the cells being stressed in general, and not due the deletion mutation interfering with iron uptake.

7.3.2 Implications of absorption spectra for ΔFutB

ΔFutB and WT have identical spectra under iron-replete conditions, as shown in figure 29. This indicates that there is no growth enhancing function for the FutABC-complex when cells are grown under iron-replete conditions, as other iron uptake mechanisms presumably give a layer of redundancy under iron-replete conditions. While user error caused only one of the three spectra taken to be saved for analysis, the close alignment between mutant and WT spectra gives confidence in the result for iron-replete conditions.

When ΔFutB was grown under iron-deprived conditions, two primary differences from the WT spectra could be seen. Pigment production in general is lower (figure 33), and the carotenoid/chlorophyll ratio is significantly higher for ΔFutB (4.77) than for the WT (4.21), as seen in figure 35. Both are indications that the degree of cell stress is larger for ΔFutB than it is for the WT. The results are for *futB's* involvement in iron uptake, but it does not give any information about the exact role of *futB* in *Synechococcus 7002.*

7.3.3 Implications of absorption spectra for siderophore mutants

When the absorption spectra were taken on cultures grown under iron-replete condition, it was in general not possible to differentiate between ΔSidF, ΔSidH and the WT. The three spectra shown in figure 30 overlap to a very large degree. This indicates that there is no physiological response to the deletion mutations under iron-replete growth conditions. Considering their high degree of upregulation under iron depletion, the siderophore genes *sidF* and *sidH* are likely not to be expressed at high levels when under iron-replete conditions.

Thus, it is as expected that deleting these genes would not create a physiological response under iron-replete conditions. Other iron uptake mechanisms are likely sufficient to ensure adequate iron levels for optimal growth.

When the mutant strains are grown under iron limitation, the physiological response of ΔSidF and ΔSidH differs from the WT. Pigment production is lower (figure 34), and the carotenoid/chlorophyll ratio (figure 35) is somewhat higher for ΔSidF (4.5) and ΔSidH (4.25) compared to the WT (4.21). However, the difference is minimal in the case of ΔSidF, and the standard error of ΔSidH is too high to conclude definitely.

In summation, the absorbance spectra for the siderophore mutants give further support for their role in iron uptake, primarily due to their lower pigment production indicating cell stress.

7.4 Discussion of O-CAS-assay

7.4.1 Experimental issues

The chrome azurol S-assay (CAS-assay) first described by Schwyn and Neilands (1987) is used to detect the presence of strong iron chelators such as siderophores. In the absence of strong iron chelators, the combination of CAS and hexadecyltrimethylammonium bromide (HDTMA) complexes with iron, resulting in a blue color. If there are siderophores or other strong iron chelators present, the CAS-HDTMA-complex dissociates from the iron, giving an orange or yellow color. As the color change is independent of the structure of the iron chelator, the test is used as an universal assay for siderophores. Variations of the CAS-assay can be made for agar plates or liquid medium.

To my knowledge, whether *Synechococcus 7002* can be grown in the CAS-agar described by Schwyn and Neilands (1987) has not been tested. As CAS-agar for growth is at any rate cumbersome and fickle to make, the alternative overlay-CAS (O-CAS) method proposed by Pérez-Miranda et al. (2007) was chosen. This involves pouring a liquid agar-solution with the CAS-dye over colonies grown on the preferred medium of the cells.

Numerous attempts to get this assay to work during this thesis indicates that the O-CAS-overlay-solution is more difficult to make than described by Pérez-Miranda et al. (2007). Making the overlay as described, by mixing all components, resulted in a red or purple solution. pH-adjustments revealed that this color change related to the pH in the medium. While the issue of pH-sensitivity is discussed in the original CAS-assay, little mention of it is

made in literature where the O-CAS-assay is used. Numerous attempts were made to alleviate the pH-problem, with the PIPES buffer appearing to cause the color change when added. Not adding the PIPES resulted in the correct blue color, but did not work consistently in preliminary tests of the assay solution, likely due to the pH-sensitivity of the unbuffered medium. In the end, PIPES was added in accordance with the procedure described by Louden, Haarmann, and Lynne (2011) for making regular CAS-agar. This involves adjusting the pH of the CAS-solution to 6 by adding 1M NaOH, and gradually adding PIPES under stirring. As addition of PIPES causes the pH to drop, care is taken to keep pH over 5, as lower pH makes PIPES insoluble. After all PIPES has been added, the pH was adjusted to 6.6, which appears to be within the working range of the CAS-HDTMA-complex. Even with using this method, consistently getting the same color for the medium was difficult.

Pérez-Miranda et al. (2007) describe being able to produce a positive assay-result in 15 minutes after the CAS-overlay has been applied. The results obtained in chapter 6.4 shows that such speed could not consistently be replicated, as a clear indication of a positive result necessitated incubating the plates overnight. Other experiments using the same method indicate that this is not just an issue for the experimental design used in this thesis (Simonetti et al. 2015; Oulkadi et al. 2014). It is possible that the assay speed issue is a matter of siderophore concentration, as some researchers appear to get assay results quickly. Informal experiments support this hypothesis: Application of grains of the siderophore DFB to the assay-solution gave a positive assay indication in a matter of seconds.

Obtaining precise results with O-CAS method was more difficult than anticipated. The CAS-agar was difficult to pour evenly, as irregularities in the thickness of the original solid AA+ medium caused significant differences in overlay thickness. A possible fix for this issue would be to use circular conventionally sized petri-dishes, and taking more care with regards to evenness when pouring. Due to time limitations, the experiment was not repeated.

7.4.2 Implications of O-CAS-results

The original goal for the experiment was to measure the radius of the positive assay-indication of the colonies, and using this data to compare mutant cells to the wild type. As the figures in chapter 6.4 shows, this method would be impractical due to the relatively small size of the positive assay-indication zone around the cells compared to the size of the colonies. A more qualitative approach has therefore been used, resulting in table 16 showing assay results for each experimental condition with the different categorizations “++”, “+” and “-“,

indicating a large assay result, a small one, or no assay indication of siderophores, respectively. CAS-agar was produced twice, once used for the plates containing 1.4 nM ferrous (II) oxide, and once for the plates with iron-replete conditions and 1.4 nM goethite. Even though the production method was the same, the color of the medium was significantly different. The medium used for FeO had a weaker blue color, and in general gave clearer results. Because of this, the following discussion will mainly use the results obtained from those plates.

The results indicate that the WT strain of *Synechococcus 7002* produces siderophores when under iron stress, but the radius of the yellow area is generally small, as seen in figure 38, showing growth on 1,4 nM FeO. The yellow tint is barely visible around the colonies, and is difficult to capture in photographs in a way that makes the result clear. Since the fatty-acid tail of synechobactin is thought to anchor the siderophores to the cell membrane, the small radius of the positive assay-result is as expected.

For the first 16 hours, it was not possible to see signs of a positive assay-result on WT cells grown under iron-replete conditions, indicating that no siderophores are produced. As the siderophore operon has been shown to be induced by the Fur-protein when the cells are under iron stress, it is expected that cells grown under iron-replete conditions would not produce siderophores in large quantities.

Figure 36 and figure 37 show that the positive assay-radius is larger for ΔSidH and ΔSidF than the WT shown in figure 38. This indicates that the mutant cells spread siderophores further into the solid medium than the WT. This result is consistent with the hypothesis for the function of SidH. If SidH is responsible for adding the fatty-acid tail to synechobactin, one would expect that interrupting this function would lead to unanchored siderophores that would travel further from the colonies than the siderophores from the WT.

That ΔSidF-cells (figure 37) give a clear and relatively large positive assay-result is not consistent with the hypothesis that ΔSidF is a siderophore transporter. The expected result would be that no siderophores would be detectable outside of the cells, resulting in a negative assay-result. Neither the cells grown on goethite or on ferrous oxide support the hypothesis, both showing larger siderophore-zones than the WT. This result does not rule out the possibility of SidF being a siderophore transporter, as it is possible that multiple proteins are capable of exporting siderophores. Accounting for this, that the ΔSidF-mutant spreads siderophores further than the WT is unexpected. A possible explanation is that the creation of

the deletion mutant for ΔSidF also abolished the expression of *sidH*. Due to the lack of clear promoters between the genes, it is reasonable to assume that the siderophore operon is polycistronic. Interrupting *sidF* by inserting an antibiotic resistance cassette is thus likely to interfere with the downstream genes in the operon, *sidG* and *sidH*. If this is the case, then it might be that deleting *sidF* has no phenotypical effect under the tested conditions, but that the phenotype observed stems from the incidental interruption of *sidH and/or sidG.* Whether the interruption of *SidG* would have any effect is unclear. The biosynthetic role of this gene is not certain in the proposed pathway for siderophore production in chapter 3.2. Another possible explanation for the result is that the phenotypical effect of ΔSidF mirrors that of the *entS*-deletion mutant for *E. coli* described in chapter 3.2.1. In this case, hydrolysis products of siderophores could be excreted into the environment. It is possible that some of these excretion products could cause a positive assay result. In particular, citrate, a likely hydrolysis product, has been shown to act as a siderophore in other organisms (Guerinot, Meidl, and Plessner 1990).

Both figure 36 and figure 37, showing ΔSidH and ΔSidF grown on FeO have cases where the spotting of cells onto the solid medium has been done with some imprecision. This leads to areas where there is cells spread over a greater area than the other colonies in the experiment. Compared to the properly spotted colonies, the relative increase in the area of positive assay result is clearly larger than the increased colony area would lead one to expect. The reason for this mismatch is not clear. One explanation would be physiological response that depends on a quorum sensing ability. Another possible explanation would be that some of the cells in these miss-spotted colonies are still in the logarithmic phase, as their lower cell density indicates. It is likely that siderophore production is higher in this phase than the maintenance phase exhibited by the correctly spotted colonies. If there is some breakdown of siderophores over time, it appears likely that cells that are still in logarithmic growth would give rise to a larger assay result.

For all experimental conditions, all strains and iron availabilities, give a positive assay result after incubation for 72 hours, indicating that siderophore production still happens at low levels, even under iron-replete conditions.

In summary, the results from the O-CAS assay give some indication that the hypothesis regarding the function of *sidH* is correct, showing further siderophore spread than the WT. The same cannot be said for *sidF*, where the implications of the observed phenotype are unclear. A clear assessment is hampered by the low quality data obtained from the plates with

iron-replete conditions and 1.4 nM goethite. Further data could be added by attempting to grow *Synechococcus 7002* on the CAS-assay-plates described by Schwyn and Neilands (1987). As the results obtained from the O-CAS-assay were inconsistent, further attempts to achieve consistently high quality O-CAS assays could also improve the reliability of the results.

8 Conclusion

In this thesis I have considered four different genes that based on previous studies are involved in iron uptake in *Synechococcus 7002*. The function of these genes has been examined by creating deletion mutants, and performing growth studies and absorption spectra under various iron availabilities.

FutB is thought to be part of the FutABC-transporter, which transports Fe(III) across the cytoplasmic membraine in *Synechocystis 6803* (Katoh et al. 2001). Growth studies and absorption spectra support the role of *futB* in iron uptake. However, the growth study did not show a clear difference between growth on Fe(III) and Fe(II) for the deletion mutant. This is unexpected, as growth on Fe(II) would presumably be independent of FutABC. It is at this stage not possible to tell whether this effect is because of iron contamination, or due to an unknown function of FutABC.

The cytochrome C_M has sequence homology and midpoint potential that makes it potentially suitable for involvement in pili-mediated iron uptake. The deletion mutant showed a clear physiological difference from WT in growth studies and absorption spectra under iron depleted conditions. However, there was significant physiological differences between mutant and WT even under iron-replete conditions, leading to two possibilities that can explain the results:

1. Cytochrome C_M is so essential for iron uptake that the deletion mutant elicits a physiological response akin to WT under iron limitation, even when ΔC_M is grown under iron-replete conditions. When ΔC_M is grown under actual iron limitation, the physiological effects are further compounded.
2. Cytochrome C_M has no specific role in iron uptake, but plays an important role in other cell functions. The additional signs of cell stress when ΔC_M is grown under iron limitation compared to WT stems from two separate stress factors compounding, not from cytochrome C_M's role in iron uptake.

While the regulatory pattern of C_M, sequence similarity and physical properties give strong support to possibility number one, it is at this point not possible to conclude definitely.

From a bioinformatic analysis, the genes *sidF* and *sidH* were chosen as likely to be involved in siderophore transport and siderophore biosynthesis, respectively. Siderophore indication by the overlay chrome azurol S assay supports the hypothesis that *sidH* adds fatty acid anchors to

the siderophores, as the deletion mutant spread siderophore mutants further into the medium than the WT. No definite conclusion could be reached for *sidF*, most likely due to downstream effects of the deletion mutation. In absorption spectra comparisons to the WT, the deletion strains show signs of cell stress when grown under iron limitation, primarily through lower pigment production. This is not the case under iron-replete conditions. The growth study results show slower growth than the WT for ΔSidH under iron limitation. This is not the case for ΔSidF, potentially due to experimental error. In sum, the results support the role of both genes in iron uptake, but support for the specific hypothesized role can only be found for *sidH*.

While the experiments in this thesis yielded usable data, there is room for improvement in certain areas. Potential iron contamination causes some results to be somewhat uncertain. Access to a clean room environment is being worked on in the lab group, so this issue could potentially be rectified in the future. Further experimentation with the O-CAS assay could improve the reliability of the results. The work described was the first attempt at using this assay in the lab group. Additional practical experience could improve the reliability of the results.

As the thesis concerns itself with several different iron uptake systems, further work could go in a number of different directions. Experimental validation of the proposed biosynthetic pathway for siderophores in *Synechococcus 7002* could yield interesting results applicable to cyanobacteria iron uptake more generally. The deletion of cytochrome C_M showed that it has an important role in *Synechococcus 7002.* Cytochrome C_M thus warrants further exploration both for its function in iron uptake, and for the potential practical applications of nanowires in novel conducive materials.

The work in this thesis are but a small part of the required to fully understand iron uptake in *Synechococcus 7002* and cyanobacteria more generally. This important topic has implications both ecologically, industrially and for potential geoengineering of marine oceans. While John Martin in 1988 stated that he could start another ice age with a tanker of iron (Blaustein 2011), I hope that this work will instead heat up the discussion on iron uptake.

9 Appendices

9.1 Appendix A – R script for mass Grofit

The R script below, referenced in chapter 5.4.3 calculates growth rates for many density-time series from a .csv-file. The number of data points in the time series and the number of columns in the experimental information columns need to be assigned in the script. The "triplicate"-column needs to be the rightmost metadata-column, and indicates which data series that are parallels of each other. An example csv-table is shown in table 17. The script uses the grofit-package, which can be found at https://cran.r-project.org/web/packages/grofit/index.html

Table 17: Example setup for time-series analysis. Each row represents a time series, with experiment data in the first columns. Each "triplicate" represents the time series that are parallels of each other.

Ironsource	Dilution	OD	Type	Triplicate						
FeCl3	4	1	WT	1	171	700	990	1655	2313	3178
FeCl3	4	1	WT	1	110	665	980	1589	2377	3285
FeCl3	4	1	WT	1	58	501	845	1326	1973	2827
FeCl3	4	1	FutB	2	73	528	779	1237	1775	2580
FeCl3	4	1	FutB	2	96	562	863	1410	2035	2984
FeCl3	4	1	FutB	2	120	613	908	1459	2054	3003

```
#Mass grofit, by Erland Årstøl
#Script takes a dataset containing growth series and metadata
from experiment set up in a csv.file, and runs the grofit
module to estimate growth rates.
# It returns two files, "mydata" with growth rates and
modelerrors for each parallel, and "summary" which shows means
and std.dev for each parallel.
# Time series supplied seperately. Datasetup should be in a
certain fashion, with triplicate number indicating
# which which experiments should be averaged and run together.
Se example data-file for setup.

###VARIABLES TO SET BEFORE RUNNING SCRIPT
Time = c(16.75, 27.40,40.41,50.74,
64.75,76.72,89.64,101.72,113.97,122.64,137.14,161.31,186.12,20
9.73,233.46,259.33) ##Insert times for each picture taken,
normally in hours.
ser.pos = 5:20 ###Insert the column positions where the time
series is located in your CSV.file.
meta.pos = 1:4 ###Insert the column positions for your
metadata, (OD,iron source, etc.)
```

```
tri.pos = 4 ###Insert the column position for your triplicate
indicator (all three triplicates gets the same integer
number.) This assumes that you are using triplicates.
mod.use = c("logistic") ##Indicates which models you want
Grofit to fit models to. Logistic is recommended, but other
models can be used, see grofit-documentation. Delete line for
default.
mydata = read.csv2("alldata.csv") #Importing data from your
file.
####

###Initializing and importing
library(grofit)
tempsubset = subset(mydata, mydata[tri.pos] == 1) #Creates a
temporary subset for each triplicate
summarydataset = tempsubset[1,meta.pos-1] ##Initializing
summary dataset (The triplicate number is excluded.)
growthratemeans = numeric(length = max(mydata[tri.pos])) ##
Creating empty vectors
sd = numeric(length = max(mydata[tri.pos]))
growthrates =  vector(mode="numeric", length=(nrow(mydata)))
modelerror =  vector(mode="numeric", length=(nrow(mydata)))

#For each colony time-series, applies grofit, and adds all
growthrates to vector.
for (i in 1:(nrow(mydata)))
{
  modeldata = gcFitModel(Time, (mydata[i,ser.pos]), control =
grofit.control(suppress.messages = TRUE, model.type = mod.use,
log.y.gc = TRUE)) ### The messages
  #from this is excessive if you are running many models, but
consider switching message suppression off for error
searching.
  growthrates[i] = modeldata$parameters$mu[1]
  modelerror[i] = modeldata$parameters$mu[2]
}

##Updates original dataframe with growthrates and standard
errors for each model.
mydata[,"growthrates"] = growthrates
mydata[,"modelstderror"] = modelerror

##Populates a temporary dataframe for each triplicate,
calculates mean and standard deviation between them.
for (i in 1:max(mydata[tri.pos]))
{
  tempsubset = subset(mydata, mydata[tri.pos] == i) #Creates a
temporary subset for each triplicate
  summarydataset[i,] = rbind(tempsubset[1,meta.pos-1])
  growthratemeans[i] = colMeans(tempsubset["growthrates"])
#Populates growthratesmeans-vector.
```

```
  sd[i] = sd(tempsubset[1:nrow(tempsubset),"growthrates"])
#Populates sd-vector.
}

##Making a summary dataset, writing that and "mydata" to
separate files.
summarydataset[,"GR-mean"] = growthratemeans
summarydataset[,"sd"] = sd
write.table(summarydataset,"summary.csv", sep =";", row.names
= FALSE)
write.table(mydata,"mydata.csv", sep =";", row.names = FALSE)
```

9.2 Appendix B: PCR primers

Table 18 shows the different primers used for this project, along with the situation they were used in. Care was taken that most primers should give usable T_m-ranges for both Q5 and Taq polymerase.

Table 18: Primer sequences for PCR-amplification of the sequences used in this project, along with their use case

Primer	Sequence	Use-case
SidF-P-F	TTGGTAATTGCCTCTTT	Amplification of deletion sequence from plasmid.
SidF-P-R	AAAAAATCAAAAATCCAATC	
SidH-P-F	GCTGCAGAATTAATTGCCC	Amplification of deletion sequence from plasmid.
SidH-P-R	TCCAGCTCGGCATAGTTGA	
SidF-C-F	AATGTCTTCCAAAACTTCGGTGTAAGCTGA	Colony PCR
SidF-C-R	TTTCCAGATTTCAGGAGTTAAGGCGGCATT	
SidH-C-F	TCCCTCTTTTAACTAATATGGGTTTTA	Colony PCR
SidH-C-R	ATCTTTGAGATTTCCTTAAAATTAGCA	
FutB-C-F	CCTTCACTCCACAATGGGATTTTGGTACCT	Colony PCR
FutB-C-R	AGAAGTCACCTTACCCATTCTCACCCAGTT	
C_M-F	GCTCAGGAGGACTTTGCCGTTGATGTCGTA	Colony PCR
C_M-R	GACAAATTCTAGACCGATGCCGCGACCAGC	

10 Bibliography

Alvey, Richard M., Avijit Biswas, Wendy M. Schluchter, and Donald A. Bryant. 2011. "Effects of Modified Phycobilin Biosynthesis in the Cyanobacterium Synechococcus Sp. Strain PCC 7002." *Journal of Bacteriology* 193 (7): 1663–71. doi:10.1128/JB.01392-10.

Armstrong, James E., and Chase Van Baalen. 1979. "Iron Transport in Microalgae : The Isolation and Biological Activity of a Hydroxamate Siderophore from the Blue-Green Alga Agmenellum Quadruplicatum." *Journal of General Microbiology* 111: 253–62.

Balasubramanian, Ramakrishnan, Gaozhong Shen, Donald A. Bryant, and John H. Golbeck. 2006. "Regulatory Roles for IscA and SufA in Iron Homeostasis and Redox Stress Responses in the Cyanobacterium Synechococcus Sp. Strain PCC 7002." *Journal of Bacteriology* 188 (9): 3182–91. doi:10.1128/JB.188.9.3182-3191.2006.

Barbeau, Katherine, Guangping Zhang, David H. Live, and Alison Butler. 2002. "Petrobactin, a Photoreactive Siderophore Produced by the Oil-Degrading Marine Bacterium Marinobacter Hydrocarbonoclasticus." *Journal of the American Chemical Society* 124 (3): 378–79. doi:10.1021/ja0119088.

Batterton, John C., and C. Van Baalen. 1971. "Growth Responses of Blue-Green Algae to Sodium Chloride Concentration." *Archiv Für Mikrobiologie* 76 (2): 151–65. doi:10.1007/BF00411789.

Bird, Lina J., Violaine Bonnefoy, and Dianne K. Newman. 2011. "Bioenergetic Challenges of Microbial Iron Metabolisms." *Trends in Microbiology* 19 (7): 330–40. doi:10.1016/j.tim.2011.05.001.

Blaustein, Richard. 2011. "Fertilizing the Seas with Iron." *BioScience* 61 (10): 840–840. doi:10.1525/bio.2011.61.10.21.

Boiteau, Rene M., and Daniel J. Repeta. 2015. "An Extended Siderophore Suite from Synechococcus Sp. PCC 7002 Revealed by LC-ICPMS-ESIMS." *Metallomics* 7: 877–84.

Challis, Gregory L. 2005. "A Widely Distributed Bacterial Pathway for Siderophore Biosynthesis Independent of Nonribosomal Peptide Synthetases." *ChemBioChem* 6 (4): 601–11. doi:10.1002/cbic.200400283.

Cho, Yoon Shin, Himadri B. Pakrasi, and John Whitmarsh. 2000. "Cytochrome cM from Synechocystis 6803." *European Journal of Biochemistry* 267 (4): 1068–74. doi:10.1046/j.1432-1327.2000.01092.x.

Fujisawa, Takatomo, Shinobu Okamoto, Toshiaki Katayama, Mitsuteru Nakao, Hidehisa Yoshimura, Hiromi Kajiya-Kanegae, Sumiko Yamamoto, et al. 2014. "CyanoBase and RhizoBase: Databases of Manually Curated Annotations for Cyanobacterial and Rhizobial Genomes." *Nucleic Acids Research* 42 (D1): D666–70. doi:10.1093/nar/gkt1145.

Furrer, Jason L., Douglas N. Sanders, India G. Hook-Barnard, and Mark A. McIntosh. 2002. "Export of the Siderophore Enterobactin in Escherichia Coli: Involvement of a 43 kDa Membrane Exporter." *Molecular Microbiology* 44 (5): 1225–34. doi:10.1046/j.1365-2958.2002.02885.x.

Guerinot, M L, E J Meidl, and O Plessner. 1990. "Citrate as a Siderophore in Bradyrhizobium Japonicum." *Journal of Bacteriology* 172 (6): 3298–3303.

Hernández-Prieto, Miguel A, Verena Schön, Jens Georg, Luísa Barreira, João Varela, Wolfgang R Hess, and Matthias E Futschik. 2012. "Iron Deprivation in Synechocystis: Inference of Pathways, Non-Coding RNAs, and Regulatory Elements from

Comprehensive Expression Profiling." *G3: Genes|Genomes|Genetics* 2 (12): 1475–95. doi:10.1534/g3.112.003863.
Hunter, K. A., and P. W. Boyd. 2007. "Iron-Binding Ligands and Their Role in the Ocean Biogeochemistry of Iron." *Environmental Chemistry* 4 (4): 221–32.
Ito, Yusai, and Alison Butler. 2005. "Structure of Synechobactins, New Siderophores of the Marine Cyanobacterium Synechococcus Sp. PCC 7002." *Limnology and Oceanography* 50 (6): 1918–23. doi:10.4319/lo.2005.50.6.1918.
Ivanov, Alexander G., Marianna Krol, Eva Selstam, Prafullachandra Vishnu Sane, Dmitry Sveshnikov, Youn-Il Park, Gunnar Öquist, and Norman P.A. Huner. 2007. "The Induction of CP43′ by Iron-Stress in Synechococcus Sp. PCC 7942 Is Associated with Carotenoid Accumulation and Enhanced Fatty Acid Unsaturation." *Structure and Function of Photosystems* 1767 (6): 807–13. doi:10.1016/j.bbabio.2007.02.006.
Kahm, Matthias, Guido Hasenbrink, Hella Lichtenberg-Fraté, Jost Ludwig, and Maik Kschischo. 2010. "Grofit: Fitting Biological Growth Curves with R." *Journal of Statistical Software; Vol 1, Issue 7 (2010)*, February. https://www.jstatsoft.org/index.php/jss/article/view/v033i07.
Käll, Lukas, Anders Krogh, and Erik L.L Sonnhammer. 2004. "A Combined Transmembrane Topology and Signal Peptide Prediction Method." *Journal of Molecular Biology* 338 (5): 1027–36. doi:10.1016/j.jmb.2004.03.016.
Katoh, Hirokazu, Natsu Hagino, Arthur R. Grossman, and Teruo Ogawa. 2001. "Genes Essential to Iron Transport in the Cyanobacterium Synechocystis Sp. Strain PCC 6803." *Journal of Bacteriology* 183 (9): 2779–84. doi:10.1128/JB.183.9.2779-2784.2001.
Kranzler, Chana, Hagar Lis, Omri M Finkel, Georg Schmetterer, Yeala Shaked, and Nir Keren. 2014. "Coordinated Transporter Activity Shapes High-Affinity Iron Acquisition in Cyanobacteria." *ISME J* 8 (2): 409–17.
Kranzler, Chana, Hagar Lis, Yeala Shaked, and Nir Keren. 2011. "The Role of Reduction in Iron Uptake Processes in a Unicellular, Planktonic Cyanobacterium." *Environmental Microbiology* 13 (11): 2990–99. doi:10.1111/j.1462-2920.2011.02572.x.
Kranzler, Chana, Mareike Rudolf, Nir Keren, and Enrico Schlieff. 2012. "Iron in Cyanobacteria." In *Genomics of Cyanobacteria*, edited by F. Chauvat and C. Cassier-Chauvat. Advances in Botanical Research. Elsevier Science. https://books.google.no/books?id=n2SC_1uAVUgC.
La Rocca, Nicoletta, Isabella Moro, and Nicoletta Rascio. 2016. "Excess Light and Limited Carbon: Two Problems with Which Cyanobacteria and Microalgae Cope." In *Handbook of Photosynthesis, Third Edition*, 369–96. Books in Soils, Plants, and the Environment. CRC Press. http://dx.doi.org/10.1201/b19498-28.
Lamb, Jacob J. 2016. "Characterization of Bacterial Electron Transport to Extracellular Electron Acceptors." Doctoral dissertation, Trondheim: NTNU.
Lamb, Jacob J., Ryan E. Hill, Julian J. Eaton-Rye, and Martin F. Hohmann-Marriott. 2014. "Functional Role of PilA in Iron Acquisition in the Cyanobacterium Synechocystis Sp. PCC 6803." *PLoS ONE* 9 (8): e105761. doi:10.1371/journal.pone.0105761.
Lambert, D H, and S E Stevens. 1986. "Photoheterotrophic Growth of Agmenellum Quadruplicatum PR-6." *Journal of Bacteriology* 165 (2): 654–56.
Lau, Nyok-Sean, Minami Matsui, Amirul Al-Ashraf Abdullah, Nyok-Sean Lau, Minami Matsui, and Amirul Al-Ashraf Abdullah. 2015. "Cyanobacteria: Photoautotrophic Microbial Factories for the Sustainable Synthesis of Industrial Products, Cyanobacteria: Photoautotrophic Microbial Factories for the Sustainable Synthesis of

Industrial Products." *BioMed Research International, BioMed Research International* 2015, 2015 (June). doi:10.1155/2015/754934, 10.1155/2015/754934.
Lee, Jin-Won, and John D. Helmann. 2007. "Functional Specialization within the Fur Family of Metalloregulators." *BioMetals* 20 (3): 485–99. doi:10.1007/s10534-006-9070-7.
Lim, Han N., Yeong Lee, and Razika Hussein. 2011. "Fundamental Relationship between Operon Organization and Gene Expression." *Proceedings of the National Academy of Sciences* 108 (26): 10626–31. doi:10.1073/pnas.1105692108.
Liu, Shu-Wen, and Bao-Sheng Qiu. 2012. "Different Responses of Photosynthesis and Flow Cytometric Signals to Iron Limitation and Nitrogen Source in Coastal and Oceanic Synechococcus Strains (Cyanophyceae)." *Marine Biology* 159 (3): 519–32. doi:10.1007/s00227-011-1832-2.
Lorenzo, V de, and J B Neilands. 1986. "Characterization of iucA and iucC Genes of the Aerobactin System of Plasmid ColV-K30 in Escherichia Coli." *Journal of Bacteriology* 167 (1): 350–55.
Louden, Brian C, Daniel Haarmann, and Aaron M Lynne. 2011. "Use of Blue Agar CAS Assay for Siderophore Detection." *Journal of Microbiology & Biology Education : JMBE* 12 (1): 51–53. doi:10.1128/jmbe.v12i1.249.
Ludwig, Marcus, and Donald A Bryant. 2011. "Transcription Profiling of the Model Cyanobacterium Synechococcus Sp. Strain PCC 7002 by Next-Gen (SOLiD™) Sequencing of cDNA." *Frontiers in Microbiology* 2: 41. doi:10.3389/fmicb.2011.00041.
———. 2012a. "Acclimation of the Global Transcriptome of the Cyanobacterium Synechococcus Sp. Strain PCC 7002 to Nutrient Limitations and Different Nitrogen Sources." *Frontiers in Microbiology* 3: 145. doi:10.3389/fmicb.2012.00145.
———. 2012b. "Synechococcus Sp. Strain PCC 7002 Transcriptome: Acclimation to Temperature, Salinity, Oxidative Stress, and Mixotrophic Growth Conditions." *Frontiers in Microbiology* 3: 354. doi:10.3389/fmicb.2012.00354.
Ludwig, Marcus, Tiing Tiing Chua, Chyue Yie Chew, and Donald A Bryant. 2015. "Fur-Type Transcriptional Repressors and Metal Homeostasis in the Cyanobacterium Synechococcus Sp. PCC 7002." *Frontiers in Microbiology* 6: 1217. doi:10.3389/fmicb.2015.01217.
Lynch, Damien, John O'Brien, Timothy Welch, Paul Clarke, Páraic Ó Cuív, Jorge H Crosa, and Michael O'Connell. 2001. "Genetic Organization of the Region Encoding Regulation, Biosynthesis, and Transport of Rhizobactin 1021, a Siderophore Produced by Sinorhizobium Meliloti." *Journal of Bacteriology* 183 (8): 2576–85. doi:10.1128/JB.183.8.2576-2585.2001.
Martin, John H. 1990. "Glacial-Interglacial CO2 Change: The Iron Hypothesis." *Paleoceanography* 5 (1): 1–13. doi:10.1029/PA005i001p00001.
Miethke, Marcus, and Mohamed A Marahiel. 2007. "Siderophore-Based Iron Acquisition and Pathogen Control." *Microbiology and Molecular Biology Reviews : MMBR* 71 (3): 413–51. doi:10.1128/MMBR.00012-07.
Nakao, Hiroshi, Keiko Takeuchi, Sumio Shinoda, and Shigeo Yamamoto. 1990. "L-2,4-Diaminobutyric Acid Decarboxylase Activity Responsible for the Formation of 1,3-Diaminopropane in Enterobacter Aerogenes." *FEMS Microbiology Letters* 70 (1): 61–66. doi:10.1016/0378-1097(90)90104-X.
Nomura, Christopher T., Toshio Sakamoto, and Donald A. Bryant. 2006. "Roles for Heme–copper Oxidases in Extreme High-Light and Oxidative Stress Response in the Cyanobacterium Synechococcus Sp. PCC 7002." *Archives of Microbiology* 185 (6): 471–79. doi:10.1007/s00203-006-0107-7.

Oulkadi, D., C. Balland-Bolou-Bi, L.J. Michot, M. Grybos, P. Billard, C. Mustin, and S. Banon. 2014. “Bioweathering of Nontronite Colloids in Hybrid Silica Gel: Implications for Iron Mobilization.” *Journal of Applied Microbiology* 116 (2): 325–34. doi:10.1111/jam.12361.

Passananti, Monica, Virginie Vinatier, Anne-Marie Delort, Gilles Mailhot, and Marcello Brigante. 2016. “Siderophores in Cloud Waters and Potential Impact on Atmospheric Chemistry: Photoreactivity of Iron Complexes under Sun-Simulated Conditions.” *Environmental Science & Technology* 50 (17): 9324–32. doi:10.1021/acs.est.6b02338.

Pérez-Miranda, S., N. Cabirol, R. George-Téllez, L.S. Zamudio-Rivera, and F.J. Fernández. 2007. “O-CAS, a Fast and Universal Method for Siderophore Detection.” *Journal of Microbiological Methods* 70 (1): 127–31. doi:10.1016/j.mimet.2007.03.023.

Saha, Ratul, Nabaneeta Saha, Robert S. Donofrio, and Lorelle L. Bestervelt. 2013. “Microbial Siderophores: A Mini Review.” *Journal of Basic Microbiology* 53 (4): 303–17. doi:10.1002/jobm.201100552.

Schwyn, Bernhard, and J.B. Neilands. 1987. “Universal Chemical Assay for the Detection and Determination of Siderophores.” *Analytical Biochemistry* 160 (1): 47–56. doi:10.1016/0003-2697(87)90612-9.

Shaked, Yeala, and Hagar Lis. 2012. “Disassembling Iron Availability to Phytoplankton.” *Frontiers in Microbiology* 3: 123. doi:10.3389/fmicb.2012.00123.

Simonetti, Ester, Natalia Pin Viso, Marcela Montecchia, Carla Zilli, Karina Balestrasse, and Marcelo Carmona. 2015. “Evaluation of Native Bacteria and Manganese Phosphite for Alternative Control of Charcoal Root Rot of Soybean.” *Microbiological Research* 180 (November): 40–48. doi:10.1016/j.micres.2015.07.004.

Svendsen, Allan. 2000. “Lipase Protein Engineering.” *Protein Engineering of Enzymes* 1543 (2): 223–38. doi:10.1016/S0167-4838(00)00239-9.

The UniProt Consortium. 2015. “UniProt: A Hub for Protein Information.” *Nucleic Acids Research* 43 (D1): D204–12. doi:10.1093/nar/gku989.

Wilhelm, Steven W., Denis P. Maxwell, and Charles G. Trick. 1996. “Growth, Iron Requirements, and Siderophore Production in Iron-Limited S’nechococczks PCC 7002.” *Limnology and Oceanography* 41 (1): 89–97.

Williamson, Phillip, Douglas W.R. Wallace, Cliff S. Law, Philip W. Boyd, Yves Collos, Peter Croot, Ken Denman, Ulf Riebesell, Shigenobu Takeda, and Chris Vivian. 2012. “Ocean Fertilization for Geoengineering: A Review of Effectiveness, Environmental Impacts and Emerging Governance.” *Special Issue: Negative Emissions Technology* 90 (6): 475–88. doi:10.1016/j.psep.2012.10.007.

Xu, Yu, Richard M. Alvey, Patrick O. Byrne, Joel E. Graham, Gaozhong Shen, and Donald A. Bryant. 2011. “Expression of Genes in Cyanobacteria: Adaptation of Endogenous Plasmids as Platforms for High-Level Gene Expression in Synechococcus Sp. PCC 7002.” In *Photosynthesis Research Protocols*, edited by Robert Carpentier, 273–93. http://dx.doi.org/10.1007/978-1-60761-925-3_21.

Zang, Xiaonan, Bin Liu, Shunmei Liu, K K I U Arunakumara, and Xuecheng Zhang. 2007. “Optimum Conditions for Transformation of Synechocystis Sp. PCC 6803.” *Journal of Microbiology (Seoul, Korea)* 45 (3): 241–45.

Zhu, Yuehui, Joel E. Graham, Marcus Ludwig, Wei Xiong, Richard M. Alvey, Gaozhong Shen, and Donald A. Bryant. 2010. “Roles of Xanthophyll Carotenoids in Protection against Photoinhibition and Oxidative Stress in the Cyanobacterium Synechococcus Sp. Strain PCC 7002.” *Carotenoids* 504 (1): 86–99. doi:10.1016/j.abb.2010.07.007.